Physiological Chemistry and Physics and Medical NMR Volume 36, Number 2, 2004

Addresses of Chief Editor and Editorial College

Toshihiko Ubuka
Department of Clinical Nutrition
Kawasaki University of Medical Welfare
Kurashiki, Okayama, 701-0193, Japan

Denys Wheatley
Department of Pathology
University of Aberdeen
Aberdeen AB9 2ZD, Scotland

EDITORIAL AND BUSINESS OFFICE

Physiological Chemistry and Physics
and Medical NMR
P.O. Box 1452
Melville, New York 11747

Editor In Chief, Dr. Gilbert N. Ling
Managing Editor, Margaret M. Ochsenfeld

SCOPE: PCP provides a forum for the review and publication of reports of original research in a broad range of subjects in biophysics, biochemistry and cellular physiology. Reports of direct applications of basic knowledge to human studies are invited; examples would include the measurements of relaxation times as part of NMR imaging. Single experiments, conclusions based on inadequate statistics, purely speculative papers, and clinical case reports are not accepted.

POLICY: The pages of PCP are accessible to competing viewpoints, interpretations, theories and opinions. Debate is invited via Editorial Comments and Letters to the Editor. Criteria for evaluating submissions include soundness of the study and clarity of presentation, and papers are not rejected on the basis of interpretation or theory, however controversial. PCP believes that scientific issues should be settled by investigation and open debate, not by an appeal to anonymous authority.

PCP attempts to achieve a balance between freedom of expression and constructive peer review. All papers are refereed by reviewers who may remain anonymous, but the Chief Editors make all final decisions, and will handle appeals from authors who feel their papers are unfairly reviewed.

The Editors endeavor to make decisions regarding acceptance or rejection of manuscripts quickly, and have set self-imposed deadlines for doing so. Referees also are given deadlines.

TYPES OF PAPERS: *Regular papers* may be experimental or theoretical. *Short notes, Priority notes* and *Letters* in response to published papers are invited. *Reviews* are desired, but authors are urged to contact an Editor before sending a finished review manuscript. *Symposia* may be published as regular or supplemental issues.

SUBSCRIPTIONS: Price is US$80.00 per volume in the United States and US$87.00 outside the United States. *Physiological Chemistry and Physics and Medical NMR* is published biannually, 2 issues per year, the volume numbered yearly. New subscriptions will start with the first issue of the volume in progress, unless the subscriber directs otherwise. Most back issues are available

Instructions to Authors

SUBMISSIONS: An original and two copies of all material are requested. The original must be typewritten on one side only. Papers should be sent to Dr. Gilbert N. Ling, Editor, P.O. Box 1452, Melville, New York 11747 U.S.A. Manuscripts should be submitted only to this journal and not have been published in part or whole in another publication, except as short preliminary notes, abstracts, or as unpublished work in reviews or symposia. Be sure to keep a copy of your manuscript.

NOTE: Referees will be instructed to destroy their copies of the manuscript after reviewing them. We will return only the original manuscript to you for revision or if rejected.

MANUSCRIPTS: All material should be typed double-spaced with margins at least one inch wide and pages numbered consecutively beginning with the title page. In addition to a paper copy, send an IBM- or Macintosh-compatible file on a floppy disk or CD, in Word or Wordperfect. *Title Page* should include title (of at most 100 characters and spaces), full names of authors as you wish them to be published, names and cities of institutional affiliation(s) of authors and of institution(s) where the studies were performed, and name, full address, telephone number, fax number and e-mail address of the person to whom correspondence, proofs, and reprint requests are to be sent. Four to six *key words* should be listed on the title page. These words will assist indexers. Also, at bottom of title page include a short running title of 40 characters or less.

Abstract should be concise and no longer than 225 words. *Body* may or may not be divided into Introduction, Materials and Methods, Results and Discussion, depending on the length and nature of the paper. Introductory remarks should indicate clearly the significance of the work presented. *References* may be indicated in the text and listed in the reference list in whatever style the author prefers, but we prefer that titles of articles be omitted.

TABLES: Tables should be typewritten on separate sheets and identified by roman numerals (eg. Table III) and titles. Table notes should be keyed by superscript italic lower-case letters (eg. [a]Control). The approximate locations of *tables* and *figures* should be indicated in the margins of the manuscript.

ILLUSTRATIONS: Original artwork or glossy photostatic prints, together with two photocopies (like Xerox copies) should be provided. Each illustration should be numbered on the back in pencil, along with the authors' names. It is preferred that line drawings be made on paper that is not larger than $8\frac{1}{2}$ by 13 inches, and that the drawing be its intended size in the printed paper. Most figures will occupy $\frac{1}{2}$ to full column, that is 5 inches wide. Lines and lettering should be thick enough to allow reduction. A drawing of overall dimension of 8 by 10 inches that will be reduced to $\frac{1}{4}$ of its original size should be lettered with 18-point (capitals 6 mm high, lower-case 4 mm high) or larger lettering. Glossy photostatic prints are acceptable, and should be attached firmly to a sheet of paper the same size as the manuscript. Postacceptance: If possible send figures as an image file using TIFF or JPEG formatting scanned at a resolution of 600 dpi.

PHOTOGRAPHS: High-quality black and white glossy prints should be provided in triplicate, and may be provided as one print plus two photocopies if the photocopies are sufficiently clear to portray the original to referees. Photographs should be attached firmly to a sheet of paper the same size as the manuscript. Photographs that have been scanned and stored as a TIFF file with a resolution of 300 dpi may also be submitted.

REFEREES: Two anonymous referees will be sought for each paper. Authors are encouraged to suggest names and addresses of suitable referees. Referees will be given deadlines for mailing manuscripts back or phoning reviews in, and will be invited to provide editorial statements or Letters that deal with issues raised by submitted papers.

REPRINTS: An order form is enclosed with proofs sent to authors.

PAGE CHARGES: Page charge is $20.00 per published page. It may be waived in the case of severe international exchange difficulties. An additional charge of $15.00 will be levied for photographs that require screening (eg., E.M's, chromatograms, scans).

Physiol. Chem. Phys. & Med. NMR (2004) *36*: 85–94

Molecular Properties and Antibacterial Activity of the Methyl and Ethyl Ester Derivatives of Ampicillin

Ronald Bartzatt[1], Suat L. G. Cirillo[2], Jeffrey D. Cirillo[2]

[1]*University of Nebraska, College of Arts and Sciences, Medicinal Chemistry Laboratory, Omaha, Nebraska 68182 U.S.A., E-mail: bartzatt@mail.unomaha.edu*
[2]*University of Nebraska-Lincoln, Dept. of Veterinary & Biomedical Sciences, Lincoln, Nebraska 68563 U.S.A.*

Abstract: Ampicillin is a β-lactam antibiotic that is effective against gram-negative bacteria. Ampicillin has a single carboxyl group (-C(O)OH) within its structure which is suitable for forming ester compounds. Diazomethane and diazoethane were utilized to react with ampicillin to form the methyl and ethyl esters, respectively. The ester derivatives of ampicillin were solubilized together (mole ratio 1:1) in LB media and penicillin resistant *Escherichia coli* added to measure antibacterial activity. Growth inhibition of bacteria was monitored by optical density after a known time period and with known specific concentrations of the ampicillin esters present. Significant growth inhibition of penicillin resistant bacteria occurred at concentrations of the combined methyl and ethyl ampicillin esters from less than 50 μgram/mL to more than 150 μgram/mL. Molecular properties of the ester compounds were determined. The two ester derivatives showed values of Log BB, Log P, polar surface area, intestinal absorption, and solubility suitable for clinical application. The two ester compounds showed zero violations of the Rule of 5 indicating good bioavailability. The two ester derivatives showed greater intestinal absorbance and greater penetration of the blood brain barrier than the parent ampicillin. Favorable druglikeness was determined for both ester derivatives.

THE β-LACTAM antibiotics include the penicillins, cephalosporins, and cephamycins (1). Ampicillin is one of the most widely utilized members of the penicillin group. The transpeptidase enzyme reacts with the β-lactam ring within the ampicillin structure rather than the bacterial target D-alanyl-D-alanine (the O=C-N group of the lactam ring analogous to a peptide bond), resulting in fatal flaws in the bacterial membrane (2). Ampicillin also has a carboxyl group, primary amine group, and an aromatic ring. Ampicillin is zwitterionic, a trait eliminated by substituting the carboxyl group (-C(O)OH) with an ester group (3). The extent of drug metabolism is dependent on its water solubility and site availability (4). Phase I metabolism includes hydrolysis of ester groups to an acid and alcohol (other

Phase I reactions include N-dealkylation and N- oxidations) (5). It has been shown in previous studies that the methyl ester group is not hydrolyzed (6).

Previous studies have shown that tissue binding and intracellular distribution of ampicillin is limited, however the bioavailability of its ester prodrugs is significantly greater than the parent compound (7). Various other esters have been designed to dramatically increase intracellular accumulation (8), oral availability (9), and simultaneous rise of peaks in serum levels (10). Other ester derivatives of ampicillin have been shown to produce higher blood levels of this antibiotic (11).

Escherichia coli (*E. coli*) is a gram-negative bacilli within the *Enterobacteriaceae* family. *E. coli* is the leading cause of urinary tract infections and is best known for its ability to cause intestinal disorders. *E. coli* proliferates in hospitals due to it's resistance to multiple antibiotics. Other bacterial types appearing in hospitals and resistant to the β-lactam antibiotics include *Staphylococcus aureus* strains (12). The number of pathological *E. coli* strains that are resistant to ampicillin was found to be as high as 76% in The Netherlands (13).

Presented here is an analysis of biological and chemical molecular properties of ampicillin and two derivatives, which comprise a structure property correlation study (14). The results of analysis of molecular properties and *in vitro* testing with *E. coli* bacteria supports the clinical efficacy of the methyl and ethyl ester derivatives of ampicillin.

Materials and Methods

Software

Molecular modeling and molecular properties determined by ChemSketch (ACD, Toronto Ontario, M5H3V9 Canada). Log P and other properties were calculated utilizing Interactive Analysis (IA, Bedford, MA 01730) and Molinspiration (MI Chemoinformatics, SK-841 04 Bratislava, Slovak Republic). CLogP calculated by Daylight (Mission Viejo, CA 92691) and Interactive Analysis. Log Kow, Kp, rate of hydrolysis determined by EpiSuite (U.S. Environmental Protection Agency, Washington D.C.). I. Moriguchi Log P, Ghose-Crippen molar refractivity, and polar surface area determined by Dragon (Milano Chemometrics and QSAR Research Group, Dept. of Environmental Sciences, University of Milano-Bicocca, Milano Italy). Druglikeness and other properties were determined by the methods of Actelion (Actelion, 4123 Allschwil Switzerland) and MolSoft (MolSoft LLC, La Jolla, CA).

Supplies and Instruments

All reagents were obtained from Aldrich Chemical Co., St. Louis MO 63178. Bacterial supplies acquired from DIFCO. Infrared spectra acquired by Galaxy Series FTIR 3000 in dimethylsulfoxide dried over molecular sieves.

Synthesis of Ester Compounds

Approximately 6 milligrams of ampicillin was placed in organic solvent (ethyl acetate, diethyl ether, 1:1 v/v) and diazomethane or diazoethane gas allowed to dissolve into the mixture (reaction runs 1 hour and repeated up to 3X). The appropriate diazoalkane is pre-

pared by placing either 0.15 g of 1-methyl-3-nitro-1-nitrosoguanidine (diazomethane) or 0.15 g of 1-ethyl-3-nitro-1-nitrosogranidine (diazoethane) with 0.35 mL of 5 molar NaOH. After reaction (1 hour) the solvent can be removed under mild vacuum or under nitrogen gas flow. Products are ampicillin ester and N_2. Purity of 100% is confirmed by spotting silica T.L.C. plate and resolving with CH_2Cl_2.

Evaulation of Bacterial Growth Inhibition by Tissue Culture

The methyl ester and ethyl ester of ampicillin were combined in a mole ratio of 1:1. To 4.9 milligrams of methyl ester ampicillin (1.35E-05 moles) was added 5.1 milligrams of ethyl ester ampicillin (1.35E-05 moles). The mixture was solubilized in liquid Luria-Bertani (LB) media and dispensed in known concentrations from 1.563 μgram/mL to 400 μgram/mL, followed by inoculation with penicilllin resistant *Escherichia coli*. Optical densities of cultures were measured at 600 nm after five hours at 37° C to evaluate antibacterial activity.

Results and Discussion

Ampicillin is among the most widely prescribed of the penicillin antibiotics. Ampicillin is considered closely related to amoxicillin, both of which can penetrate and inhibit the growth of gram-negative bacteria. Ampicillin also inhibits gram-positive bacteria, aerobic and anaerobic, and is utilized primarily to treat infections of the sinuses, middle ear, kidney, bladder, meningitis, and gonorrhea. Ampicillin is excreted unchanged in the urine, partially explaining its efficacy in the treatment of bladder infections. The ester forms of ampicillin presented in this work provide additional evidence for beneficial applications of ampicillin derivatives. Ester groups formed to replace the carboxyl group on the parent structure significantly alter the molecular properties. Derivatives of antibiotics that have altered structural properties may be beneficially applied against the growing numbers of resistant bacteria (15–20).

Molecular structures of the ampicillin methyl and ethyl ester derivatives are compared to the parent structure, shown in Figure 1, with ester groups (-C(O)OR) indicated. Other functional groups present in the structures include the β-lactam ring, primary amine, aromatic ring, and secondary amide group. Previous studies have shown that esters of ampicillin have enhanced bioavailability, which can be clinically important (7). A beneficial result of addition of ester groups are higher absorption rates (7). In addition, it has been shown that the methyl ester of ampicillin is not metabolized (6), which will extend the half-life of the drug in the bloodstream while expressing antibacterial activity. The two ampicillin esters shown here formed a yellowish solid that was stable for more than six months at −10° C and sufficiently soluble in aqueous media for tissue culture studies. Infrared spectroscopy was utilized to identify formation of ester groups in place of the initial carboxyl group. The infrared spectra confirmed the presence of the ester groups in place of the carboxyl group. Infrared peaks appeared at 1200 cm^{-1} and 1730 cm^{-1} and are diagnostic of the presence of an ester group.

The synthesis of methyl and ethyl ampicillin esters utilized diazoalkanes which have many advantages over acid or base catalyzed ester formation. Utilizing diazoalkanes for synthesis applications has been well characterized and they are known to alkylate car-

AMPICILLIN

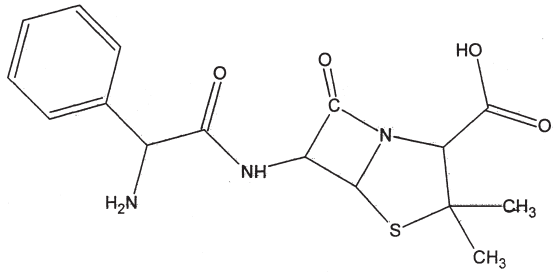

6-{[amino(phenyl)acetyl]amino}-3,3-dimethyl-7-oxo-4-thia-1-azabicyclo[3.2.0]heptane-2-carboxylic acid

METHYL ESTER OF AMPICILLIN

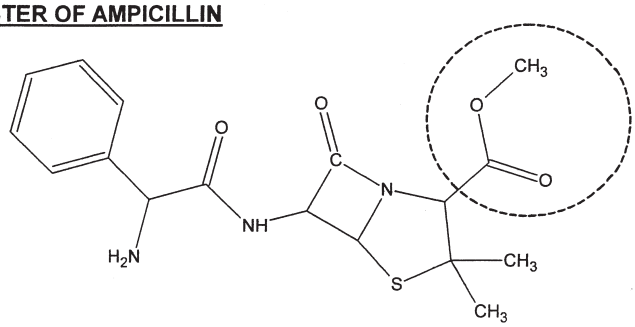

methyl 6-{[amino(phenyl)acetyl]amino}-3,3-dimethyl-7-oxo-4-thia-1-azabicyclo[3.2.0]heptane-2-carboxylate

ETHYL ESTER OF AMPICILLIN

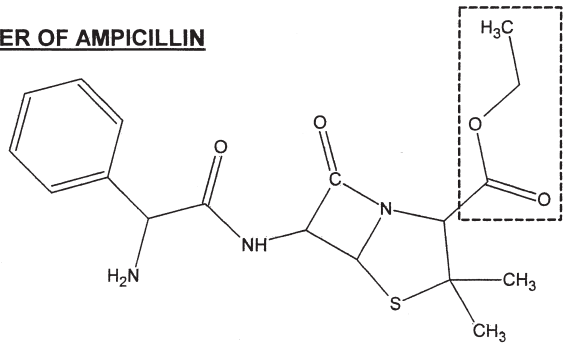

ethyl 6-{[amino(phenyl)acetyl]amino}-3,3-dimethyl-7-oxo-4-thia-1-azabicyclo[3.2.0]heptane-2-carboxylate

FIGURE 1. Molecular structures of ampicillin, methyl, and ethyl ester derivatives are shown here having the ester functional group designated. The methyl ester functional group is indicated by inset circle and ethyl ester group by inset rectangle. The primary amine group and β-lactam ring remain intact.

boxyl groups to form ester moieties (21–24). Diazoalkanes react only with acidic hydrogens; see Figure 2 where an example carboxyl group structure is shown reacting with diazomethane CH_2N_2 (the synthesis of the ethyl ester is similar). The diazomethane obtains a hydrogen from the acidic carboxyl group, which has a pKa = 4. Diazoalkane reactions are specific for acidic groups (note that the pKa of a primary amine is ≥ 10) and rapidly form species that quickly progress to the methyl ester derivative. The carboxyl group is approximately 106 times more acidic than the primary amine group. Final products of the reaction are the ester derivative and nitrogen gas. Ester formation utilizing diazoakanes is highly favorable energetically, because of the greater stability of N_2. Diazoalkanes are highly useful for forming simple esters when only small quantities of carboxylic acids are available. Yields of essentially 100% are obtained with repeated passage through the diazoalkane.

Molecular properties of the ester derivatives are presented in Table I for comparison to properties of the parent ampicillin. As the number of carbons increase within the ester group a consistent numerical increase in these properties occurs: formula weight, molar refractivity, molar volulme, parachor, Ghose-Crippen molar refractivity, I. Moriguchi Log P, Clog P, miLog P, and Log BB. Notably, a decrease is seen in the index of refraction and polarizability. The lipophilic substituent constant π indicates a lipophilic nature for the new substituents of the derivatives (π=Log P_{ester} – Log P_{parent}) giving $\pi = 0.234$ and 0.481, for the methyl and ethyl ester, respectively (utilizing the values of I. Moriguchi method).

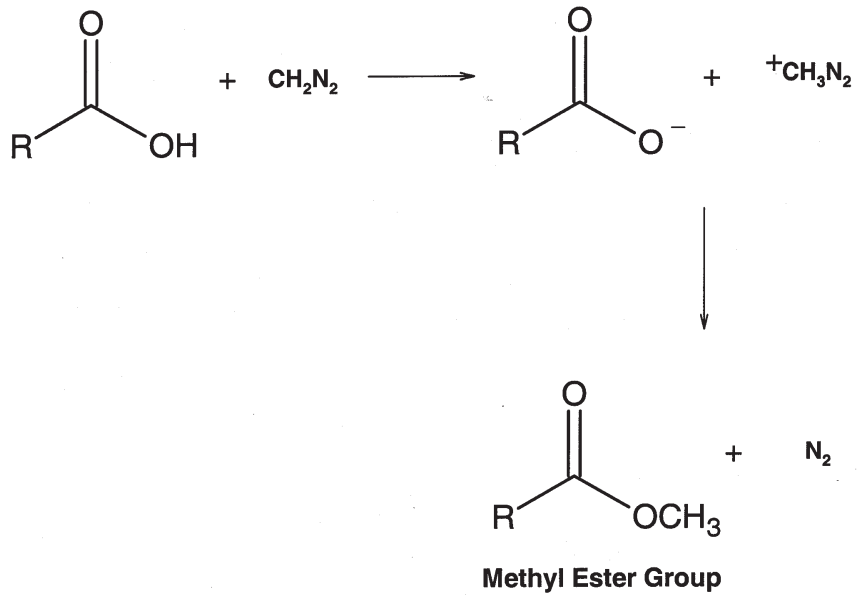

FIGURE 2. The synthesis of the ester derivatives of ampicillin is represented here in two major steps. First step, the diazoalkane (diazomethane shown here) encounters the acidic hydrogen from the carboxyl group (-COOH) of ampicillin and is protonated, producing a charged species. Second step, methylation occurs with the result being the ester derivative and nitrogen gas. The yield obtained after several passes is essentially 100% and high purity.

TABLE I. Molecular Properties of Antibiotics

Properties	Ampicillin	Methyl Ester Ampicillin	Ethyl Ester Ampicillin
[1]Formula Weight	349.41	363.43	377.46
[1]Molar Refractivity (cm^3)	89.94	94.78	99.41
[1]Molar Volume (cm^3)	239.3	264.2	280.4
[1]Parachor (cm^3)	702.7	746.1	786.1
[1]Index of Refraction	1.675	1.636	1.627
[1]Polarizability ($x10^{-4}$ cm^3)	35.65	37.57	39.41
[2]GhoseCrippen Molar Refractivity (cm^3)	87.58	92.35	97.03
[2]Polar Surface Area ($angstroms^2$)	79.75	88.98	88.98
[2]I. Moriguchi Log P	0.289	0.532	0.770
[3]Clog P	–0.04	0.41	0.85
[4]miLog P	–0.215	0.337	0.74
[5]Log BB	–1.535	–1.30	–1.25

[1]Calculated by ChemSketch.
[2]Calculated by Dragon (Milano Chemometrics).
[3]Calculated by Actelion.
[4]Calculated by Molinspiration.
[5]Calculated utilizing miPSA and Actelion Clog P in the equation:
Log BB = –0.0148(miPSA) + 0.152(Clog P) + 0.139

The positive values indicate an increase of lipophilic nature and increased solubility in lipid membranes. Log P values are also indicative of hydrophobic interactions. Parachor, molar refractivity, and molar volume properties are descriptive of polarizability and vander-Waals interactions. An increase in Log BB values as carbon length of the ester group increases indicates a favorable aspect of these derivatives. Log BB is defined as C_{brain}/C_{blood} giving the following values for the equilibrium concentration across the blood-brain-barrier as 0.02917, 0.05012, and 0.0562 for ampicillin, methyl ester, and ethyl ester, respectively. The longer the aliphatic ester substituent the greater the brain penetrating potential. Log BB values for polar molecules are calculated utilizing the following equation:

$$\text{Log BB} = -0.0148\text{PSA} + 0.152\text{CLog P} + 0.139$$

Where, BB = C_{brain}/C_{blood} and PSA = polar surface area. Previous studies have shown that polar surface area as well as Log P can be utilized to determine absorption of drugs (25–27) and penetration of the brain (28, 29).

Molecular properties of ampicillin and two derivatives are presented in Table II. Polar surface area (miPSA) has been effectively applied as a predictor of intestinal absorption (25, 26). The percent of drug absorbed in the intestinal tract is determined to be 27%, 45%, and 45% for ampicillin, methyl ester, and ethyl ester, respectively. Ampicillin parent drug is absorbed at a lower 27%, while the ester derivatives have a higher and mod-

TABLE II. Molecular Properties of Antibiotics

Properties	Ampicillin	Methyl Ester Ampicillin	Ethyl Ester Ampicillin
[1]miPSA (angstroms^2)	112.73	101.74	101.74
Intestinal Absorbance	27%	45%	45%
[1]Number of Atoms	24	25	26
[1]Number of O and N	7	7	7
[1]Number of –OH and –NH	4	3	3
[1]Violations of Rule of 5	0	0	0
[1]Number of Rotatable Bonds	4	5	6

[1]Calculated by Molinspiration method (PSA = polar surface area).

erate absorption of 45% each. This characteristic places more of the antibacterial compound into the blood stream (bioavailability). All three agents show zero violations of Rule of 5 (30), which indicates the drugs will have good bioavailability.

Druglikeness is a measure of similarity of a proposed drug compound to the general population of drugs in use. Druglikeness evaluation by Actelion (see Materials and Methods) calculates a permissible numerical range (incorporates most drugs in use) of approximately −7.0 to +8.5. Druglikeness score for ampicillin, methyl, and ethyl ester of ampicillin are 10.72, 8.14, and 7.16, respectively. Similar evaluation by the method of MolSoft shows an acceptable druglikeness scale of approximately −2.2 to 2.5. Values calculated by MolSoft are 1.22, 1.26, and 1.00 for ampicillin, methyl, and ethyl esters of ampicillin, respectively. By these two evaluations, the methyl and ethyl esters of ampicillin have favorable druglikeness scores which support their potential for application as antibacterial agents.

The methyl and ethyl esters of ampicillin were synthesized here similarly as in previous studies and tested in tissue culture against *Escherichia coli* (31), the results showed their capability of inhibiting the growth of penicillin and streptomycin resistant *E. coli* (31). High similarity of these two ester derivatives to other penicillin antibiotics utilized clinically has been shown using rigorous multivariate techniques (32). Not accomplished previously is the combination of both methyl and ethyl ampicillin esters simultaneously to affect growth of penicillin resistant *E. coli*. A mixture of methyl and ethyl esters at a mole ratio of 1:1 was assembled and placed in tissue culture utilizing LB media and penicillin resistant *E. coli*. The observed growth inhibition bacterial growth is shown graphically in Figure 3. Clearly the mixture of ampicillin ester derivatives inhibit growth of bacteria even at low concentrations which are expressed for each compound at the x-axis as micrograms/milliliter. While the effects of the parent ampicillin maximizes quickly and levels out throughout its concentration range, the two ester derivatives quickly move to greater than 50% growth inhibition and the inhibition of bacterial growth continuous to increase as concentration increases. The ester derivatives strongly inhibit the growth of penicillin resistant *E. coli* when applied simultaneously and in a mole ratio of 1:1.

Additional properties were determined and shown in Table III. The methyl and ethyl esters of ampicillin are solids which have melting points, 211 ± 3.0°C and 217 ± 3.0°C

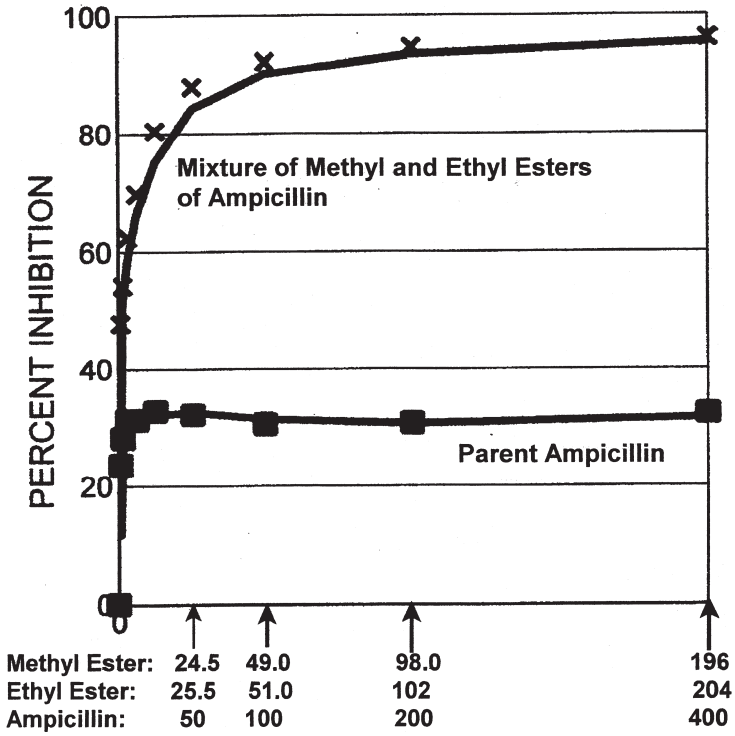

FIGURE 3. Percent growth inhibition of penicillin resistant *Escherichia coli* by combined methyl, ethyl esters of ampicillin compared to parent ampicillin. The mixture containing both ester derivatives of ampicillin greatly inhibits the growth of this penicillin resistant *Escherichia coli* even at concentrations lower than 50 μg/mL for each of the esters. Compared to the parent ampicillin it is clearly seen that the ester derivatives are highly effective in suppressing the bacterial growth. Over 60% growth suppression is observed at concentrations below 24 μg/mL for each ester compound. The concentration values of each antibiotic at the data points shown in this graph is given on the x-axis. Concentration values beginning at zero are as follows in chronological order least to greatest (methyl ester/ethyl ester/ ampicillin) in μg/mL: 1) 0/0/0; 2) 0.766/0.797/1.563; 3) 1.53/1.59/3.125; 4) 3.06/3.19/6.25; 5) 6.125/6.375/12.5; 6) 12.25/12.75/25; 7) 24.5/25.5/50; 8) 48/51/100; 9) 98/102/200; 10) 196/204/400.

TABLE III. Molecular Properties of Antibiotics as Determined by Episuite

Properties	Ampicillin	Methyl Ester Ampicillin	Ethyl Ester Ampicillin
Melting Point (°C)	215	211 ± 3.0	217 ± 3.0
Log Kow	1.45	0.69	1.18
Ester Hydrolysis kp (L/(mole•sec)	—	3.44E-05	3.25E-05
Dermal Absorbance Kp (cm/hr)	0.000128	0.0000357	0.0000654

respectively, compared to that of ampicillin (215°C). Values of Log Kow indicate dispersion between aqueous and organic solvent layers and assume only neutral species are present. Rate constant values for nonenzymatic acid/base hydrolysis of the methyl and ethyl ester groups are presented in Table III and reflect slow reaction. Dermal permeability coefficients (Kp in cm/hr) reflect the greater lipophilic trait of the ester derivatives relative to the parent ampicillin. The decreased values of Kp of the ester derivatives indicate expected entrapment of these drugs within lipid membranes of the skin. Whereas the more hydrophilic ampicillin will penetrate into aqueous layers.

In summation, a methyl ester and ethyl ester of ampicillin were synthesized by use of diazoalkanes and found to be solids at room temperature, soluble in LB media, and when applied as a mixture (mole ratio 1:1) greatly inhibited the growth of a penicillin resistant *Escherichia coli* bacteria at concentrations of less than 25 μg/mL. Both ester derivatives showed zero violations of the Rule of 5, indicating good bioavailability. Favorable values of Log P indicate the ester derivatives will have improved absorption compared to the parent ampicillin. Polar surface area values indicate that both ester derivatives will have moderate intestinal absorption, an improvement compared to the low absorption for the parent ampicillin. Log BB values for the ester derivatives indicate greater penetration of the blood brain barrier than that of the parent ampicillin. Favorable druglikeness scores by two methods support the clinical potential of these two ester derivatives. Alteration of the molecular structures of drugs that are utilized in the clinical environment can provide improvements in therapeutic results and additional insight into the mechanism of bacterial multiple drug resistance.

References

1. Graham, P.L. (2001) *An Introduction to Medicinal Chemistry* (Oxford University Press, Bath).
2. Gringauz, A. (1997) *Medicinal Chemistry* (Wiley-VCH, New York).
3. Gringauz, A. (1997) *Medicinal Chemistry* (Wiley-VCH, New York).
4. King, F.D. (2001) *Medicinal Chemistry* (Royal Society of Chemistry, Cambridge).
5. King, F.D. (2001) *Medicinal Chemistry* (Royal Society of Chemistry, Cambridge).
6. Graham, P. (2002) *An Introduction to Medicinal Chemistry* (Oxford University Press, Oxford).
7. Ehmebo, M., Nisson, S.O., and Boreus, L.O. (1979) *J. Pharmacokine Biopharm. (5):* 429–451.
8. Gan, H.J., Patemotte, I., Vermander, M., Li, K., Beaujean, M., Scorneaux, B., Dumont, P., Osinski, P., Claesen, M., Tulkens, P.M., and Sonveaux, E. (1997) *Bioorg. Med. Chem. Let. 7(24):* 3107–3112.
9. Sjovall, J., Huitfeldt, B., Jagni, L., Nord, C.E. (1988) *Scand. J. Infec. Dis. 49:* 73–84.
10. Bergan, T. (1978) *Antimicrob. Agents Chemother. 13(6):* 971–974.
11. Sakamoto, F., Ikeda, S., and Tsukamoto, G. (1984) *Chem. Pharmac. Bull. 32(6):* 2241–2248.
12. *British National Formulary*. (2003) 5.1.1.2 Penicillinase-resistant penicillins. British Medical Association and Royal Pharmaceutical Society of Great Britain 46 ed. London.
13. Bonten, M., Stobberingh, E., Philips, J., and Houben, A. (1990) *J. Antimicrob. Chemother. 26(4):* 585–592.
14. Wermuth, C. (1996) *The Practice of Medicinal Chemistry* (Academic Press, San Diego).
15. Nathwani, D., and Wood, M.J. (1993) *Drugs 45(6):* 866–894.

16. Iwane, T., Urase, T., and Yamamoto, K. (2001) *Water Sci. Technol. 43(2):* 91–99.
17. Sanguinetti, C.M., De Benedetto, F., and Miragliotta, G: (2000) *Int. J. Antimicrob. Agents 16(4):* 467–471.
18. Li, J., Xiao, Z., Liang, J., Zhong, G.,and Xu, H. (2002) *Zhongguo Kangshingsu Zazhi 27(7):* 401–405.
19. Park, J.C., Lee, J.C., Oh, J.Y., Jeong, Y.W., Cho, J.W., Joo, H.S., Lee, W.K., and Lee, W.B. (2003) *Water Sci. Technol. 47(3):* 249–253.
20. EiKholy, A., Baseem, H., Hall, G.S., Procop, G.W., and Longworth, D.L. (2003) *J. Antimicrob. Chemother. 51(3):* 625–630.
21. Kupchan, S., Britton, R., Ziegler, M., Sigel, C., and Dep, C. (1973) *J. Org. Chem. 38(1):* 178–179.
22. Unterhalt, B. And Moghaddam, S. (1994) *Pharmazie 49(5):* 317–319.
23. Nolte, J., Mayer, H., Khalifa, M., and Linsched, M. (1993) *Sci. Total Environ. 132(2–3):* 141–146.
24. Domino, M., Pepich, B., Munch, D., and Fair, P. (2004) *J. Chromatog. A 1035(1):* 9–16.
25. Palm, K., Stenberg, P., Luthman, K., and Artursson, P. (1997) *Pharm. Res. 14:* 568–571.
26. Clark, D.E. (1999) *J. Pharm. Sci. 88:* 807–814.
27. Ertl, P., Rohde, B., and Selzer, P. (2000) *J. Med. Chem. 43:* 3714–3717.
28. Kelder, J., Grootenhuis,, P.D.J., Bayada, D.M., Delbressine, L.P.C., Ploemen, J.P. (1999) *Pharm. Res. 16:* 1514–1519.
29. Clark, D.E. (1999) *J. Pharm. Sci. 88:* 815–821.
30. Lipinski, C.A., Lombardo, F., Dominy, B.W., and Feeny, P.J. (1997) *Adv. Drug Deliv. Rev. 23:* 3–25.
31. Bartzatt, R., Benish, T., and Koziol, K. and Stoddard, J. (2000) *Physiol. Chem. Phys. & Med. NMR 32:* 49–56.
32. Malesa, C., Stoddard, J., and Bartzatt, R: (2003) *J. Undergrad. Chem. Res. 3:* 127–134.

Received November 18, 2004;
accepted March 8, 2005.

Physiol. Chem. Phys. & Med. NMR (2004) *36*: 95–107

Role of α-Tocopherol in the Regulation of Mitochondrial Permeability Transition

Masae Yorimitsu[1,2], Shikibu Muranaka[1], Eisuke F. Sato[3], Hirofumi Fujita[1], Koichi Abe[4], Tatsuji Yasuda[2], Masayasu Inoue[3] and Kozo Utsumi[1*]

[1]*Institute of Medical Science, Kurashiki Medical Center, Kurashiki 710-8522,* [2]*Department of Cell Chemistry, Okayama University Graduate School, Okayama 700-8558, Japan,* [3]*Department of Biochemistry and Molecular Pathology, Osaka City University Medical School, Osaka 545-8585, Japan,* [4]*Tsukuba Research Laboratories, Eisai Company, Ltd., Ibaraki, Japan.*
**Corresponding author, e-mail: utsumiko@mx3.kct.ne.jp*

Abstract: We previously showed that Ca^{2+}-induced cyclosporin A-sensitive membrane permeability transition (MPT) of mitochondria occurred with concomitant generation of reactive oxygen species (ROS) and release of cytochrome c (Free Rad. Res.38, 29-35, 2004). To elucidate the role of α-tocopherol in MPT, we investigated the effect of α-tocopherol on mitochondrial ROS generation, swelling and cytochrome c release induced by Ca^{2+} or hydroxyl radicals. Biochemical analysis revealed that α-tocopherol suppressed Ca^{2+}-induced ROS generation and oxidation of critical thiol groups of mitochondrial adenine nucleotide translocase (ANT) but not swelling and cytochrome c release. Hydroxyl radicals also induced cyclosporin A-sensitive MPT of mitochondria. α-Tocopherol suppressed the hydroxyl radical-induced lipid peroxidation, swelling and cytochrome c release from mitochondria. These results indicate that α-tocopherol inhibits ROS generation, ANT oxidation, lipid peroxidation and the opening of MPT, thereby playing important roles in the prevention of oxidative cell death.

APOPTOSIS plays important roles in embryonic development, maintenance of tissue homeostasis, and pathogenesis of various diseases (1–3). Accumulated evidences indicate that reactive oxygen species (ROS) and antioxidants play important roles in the regulation

Abbreviations: ANT, adenine nucleotide translocase; CHL, chemiluminescence; CMPT, classic MPT: HRP, Horseradish peroxidase; L-012, 8-amino-5-chloro-7-phenylpyrido[3,4-d]pyridazine-1, 4-(2H,3H)dione; MPT, membrane permeability transition; Pi, inorganic phosphate; NCMPT, non-classic MPT; ROS, reactive oxygen species; SOD, superoxide dismutase; TBARS, thiobarbituric acid reactive substances.

of survival of a wide variety of cells (4–6) and that intracellular ROS increase prior to the onset of DNA fragmentation (7, 8).

Although various organelles including mitochondria (9), Golgi apparatus (10), endoplasmic reticulum (11) and lysosomes (12) underlie the mechanism of apoptosis, mitochondrial membrane permeability transition (MPT) plays a key role in various types of apoptosis. Recent studies revealed that ROS were produced as by-products of oxidative metabolism in mitochondria (13–16). Opening of mitochondrial MPT pores releases apoptosis-related proteins including cytochrome c to cytosol and triggers the activation of caspase cascade (9. 17). Thus, mitochondria pivotally determine the survival and death of cells through energy transduction and release of apoptosis-related proteins, respectively.

Classic type of MPT (CMPT) associated with mitochondrial membrane depolarization and swelling is characterized by its dependency on Ca^{2+} and energy metabolism and high sensitivity to cyclosporin A. In the presence of inorganic phosphate (Pi) and respiratory substrates, Ca^{2+} induces ROS generation and typical CMPT (9, 13–16, 18). Because α-tocopherol is an efficient oxyradical scavenger and enriched in cell membranes, especially in mitochondria (19), it might affect the opening of MPT pore (20). In fact, α-tocopherol has been reported to reduce bile acid-induced liver injury by preventing oxidative stress and subsequent stimulation of mitochondrial MPT and cytochrome c release (21). However, effect of α-tocopherol on MPT in isolated mitochondria remains unknown. The aim of the present work is to elucidate the role of α-tocopherol in mitochondrial MPT.

Materials and Methods

Chemicals

Cyclosporin A, cytochrome c and horseradish peroxidase were obtained from Sigma Co. Ltd (St. Louis, MO). Amplex Red was obtained from Molecular Probes (Eugene, OR). Anti-cytochrome c antibody was obtained from PharMingen (San Jose, CA). 8-Amino-5-chloro-7-phenylpyrido[3,4-d] pyridazine-1,4-(2H,3H)dioene (L-012) was obtained from Wako Pure Chemical Ind. (Osaka, Japan). Anti-ANT antibody was donated by Dr. H. Terada (Tokyo University of Science, Faculty of Pharmaceutical Science, Japan).

Isolation of rat liver mitochondria

Control and α-tocopherol-deficient male Wister rats (4 weeks) were obtained from Funabashi Farma Co. (Chiba, Japan). After fasting the animals overnight, the livers were excised and homogenized in 0.25 M sucrose containing 10 mM Tris-HCl buffer (pH 7.4) and 1 mM EDTA at 4°C. Mitochondria were isolated from these homogenates by the method of Hogeboom as described previously (22).

Assay for mitochondrial functions

Mitochondria (0.1 mg protein/ml) were incubated in a standard medium (10 mM Tris-HCl pH 7.4 containing 0.15 M KCl) at 25°C. Swelling of mitochondria was monitored by a change in the absorbance at 540 nm and recorded with a Shimadzu UV-3000. Cytochrome c release from mitochondria was analyzed by Western blotting using anti-cytochrome c antibody (23).

Assay for mitochondrial ROS generation

Generation of H_2O_2 was assayed at 25°C in a fluorescence spectrophotometer (Hitachi 650–10LC) using Amplex Red/Horseradish peroxidase (HRP) system (24). Mitochondria (0.1 mg protein/ml) were suspended in the standard medium containing 150 mM KCl, 1 mU/ml HRP and 20 μM Amplex Red in the presence or absence of $CaCl_2$. The change in fluorescence intensity was measured at 590 nm with excitation at 550 nm.

Because mitochondria contain high activity of Mn-superoxide dismutase (SOD), generation of ROS was analyzed by using a highly sensitive chemiluminescence (CHL) probe, L-012 (25). Mitochondria (0.1 mg protein/ml) were incubated in a standard medium containing 150 mM KCl, 2.5 mM succinate and 1 mM phosphate buffer (pH 7.4) in the presence of 100 μM L-012 at 25°C. After incubation for 1 min at 25°C, the reaction was started by adding $CaCl_2$. During the incubation, chemiluminescence intensity was recorded continuously for 20 min using an Intracellular Ion Analyzer (CHL mode, Jasco PL-03).

Western blotting

The electrophoresed proteins in an agarose gel were transferred onto an Immobilon membrane (Millipore, Waltham, MA). The membrane was blocked in TBS (0.15 M NaCl, 10 mM Tris-HCl, pH 7.4) containing 5% skim milk, and then incubated with primary antibodies diluted with TBS containing 0.05% Tween 20 (TBST) at 25°C for 1 h. After washing three times in TBST, the membrane was incubated at 25°C for 1 h with peroxidase-conjugated secondary antibody (DAKO, Glostrup, Denmark) diluted in TBST. Immunoreactive bands were visualized using an enhanced CHL system (Amersham Pharmacia Biotech, Uppsala, Sweden) (23).

Binding of ANT to phenylarsine oxide-conjugated agarose

The reduced form of ANT was analyzed as described previously (26). Briefly, mitochondria (2 mg protein) treated with 100 μM $CaCl_2$ in the presence or absence of various reagents were centrifuged at 12,000 x g and 4°C for 5 min. Proteins in the precipitates were solubilized in 100 μl of 50 mM HEPES buffer (pH 7.4) containing 150 mM Na_2SO_4, 1 mM EDTA, 3% Triton X-100, 1 mM PMSF and 1 μM leupeptin. After centrifugation of the lysate at 15,000 x g for 5 min at 4°C, the supernatant fraction was incubated with 4-aminophenylarsine oxide agarose (ThioBond Resin, Invitrogen, Carlsband, CA) equilibrated with 50 mM HEPES buffer (pH 7.4) containing 150 mM Na_2SO_4, 1 mM EDTA, 0.25% Triton X-100, 1 mM PMSF, and 1 μM leupeptin. After incubation at 4°C for 15 min, the agarose was washed three times with 0.5 ml of the buffer by centrifugation at 15,000 x g for 1 min at 4°C. Proteins bound to the agarose were eluted with 50 μl of the buffer containing 10 mM dithiothreitol, and analyzed by SDS-PAGE and Western blotting using anti-ANT antiserum.

Assay for protein and thiobarbituric acid reactive substances

Protein concentrations were determined by the method of Bradford (27) using bovine serum albumin as a standard. Thiobarbituric acid-reactive substances (TBARS) in mitochondria were assayed by the method of Ohkawa (28) before and after incubation with inducers of MPT.

Results

Effect of α-tocopherol on Ca^{2+}-induced generation of ROS and oxidation of ANT-SH in mitochondria

Since Ca^{2+} induces ROS generation and typical MPT in mitochondria in the presence of Pi and respiratory substrates (9, 14, 18), the effect of α-tocopherol on ROS generation by mitochondria was analyzed. In the presence of succinate and Pi, Ca^{2+} enhanced the generation of H_2O_2 by a mechanism that was suppressed by cyclosporin A. The generation of H_2O_2 was also suppressed by α-tocopherol (Figure 1A). Furthermore, in the presence of Pi and Ca^{2+}, mitochondria transiently increased CHL intensity of L-012 by a mechanism that was suppressed by cyclosporin A and α-tocopherol but not by δ-tocopherol (Figure 1B).

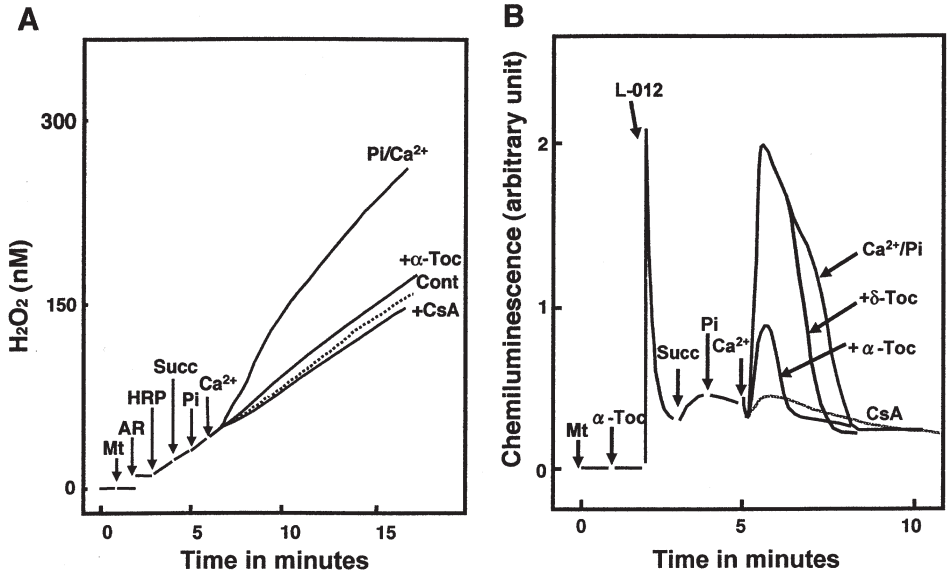

FIGURE 1. Effect of α-tocopherol on Ca^{2+}-induced ROS generation by isolated mitochondria. **A)** Effects of α-tocopherol and cyclosporin A on H_2O_2 generation induced by Ca^{2+}. Mitochondria (0.1 mg protein/ml) were incubated in a standard medium (150 mM KCl, 10 mM Tris-HCl, pH 7.4) containing 1 μM EGTA, 20 μM Amplex Red, 1 mU/ml horseradish peroxidase, 2.5 mM succinate and 1 mM Pi in the presence or absence of 75 μM α-tocopherol or 1 μM cyclosporin A. H_2O_2 generation was induced by adding 20 μM Ca^{2+}. The change in the fluorescence intensity was measured at 590 nm with excitation at 550 nm. Downward deflection shows mitochondrial swelling. Similar results were obtained in three separate experiments. Cont, control; Mt, mitochondria; AR, Amplex Red; HRP, horseradish peroxidase; Succ, succinate; Pi, inorganic phosphate; α-Toc, α-tocopherol; CsA, cyclosporin A. **B)** Effect of tocopherols on ROS generation induced by Ca^{2+}. Mitochondria (0.1 mg protein/ml) were incubated in the standard medium containing 1 μM EGTA, 100 μM L-012, 2.5 mM succinate, 1 mM Pi in the presence or absence of 75 μM tocopherol or 1 μM cyclosporin A. ROS generation was induced by adding 20 μM Ca^{2+} and L-012 CHL was monitored using an Intracellular Ion Analyzer (Jasco CAF-110). Similar results were obtained in three separate experiments. δ-Toc, δ-tocopherol.

ANT, an important component of MPT pore, has three SH groups exposed to mitochondrial matrix. Thus, ROS generated by mitochondria might affect the thiol status of ANT. To test this possibility, the effect of Ca^{2+} on the redox status of the critical cysteine residues in ANT was analyzed by using phenylarsine oxide-agarose, an affinity matrix that interacts selectively with vicinal dithiols in proteins (26, 29). Figure 2 shows that the binding of ANT to the phenylarsine oxide-agarose was strongly suppressed by pretreating mitochondria with Ca^{2+}, suggesting the oxidation of the vicinal dithiols. The presence of either cyclosporin A or α-tocopherol inhibited the Ca^{2+}-induced suppression of the binding of ANT.

Kowaltowski *et al*. (13) reported that Ca^{2+}-induced MPT in mitochondria occurred with concomitant formation of TBARS. However, under the identical conditions for the experiment of swelling, we failed to detect the increase in TBARS in the presence of Ca^{2+} (data not shown).

Effect of α-tocopherol on Ca^{2+}-induced mitochondrial swelling and cytochrome c release

In the presence of Pi and succinate, Ca^{2+} induces cyclosporin A-sensitive MPT. The Ca^{2+}-induced mitochondrial swelling and cytochrome c release is shown in Figure 3. The Ca^{2+}-induced changes of mitochondria were inhibited by cyclosporin A (16). Since

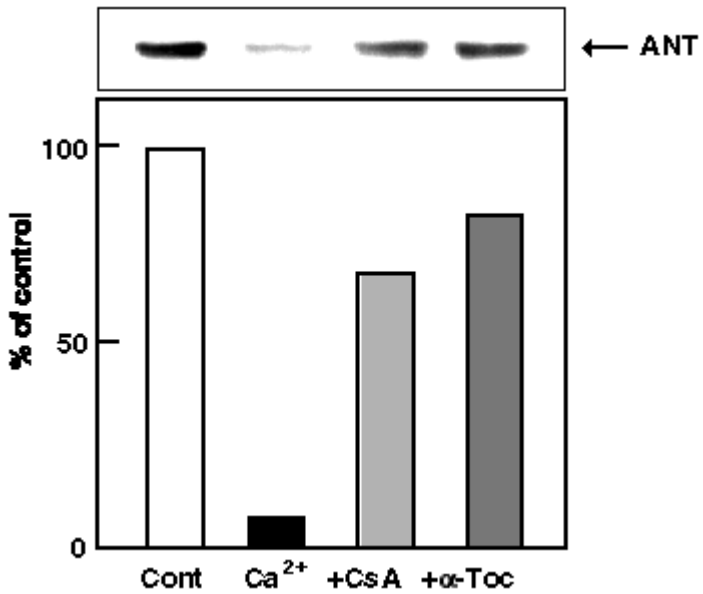

FIGURE 2. Effect of α-tocopherol on the Ca^{2+}-induced changes in the thiol status of ANT. Mitochondria (2 mg/ml) were incubated for 10 min at 25°C in the standard medium containing 2.5 mM succinate, 1 mM Pi and 100 μM Ca^{2+} in the presence or absence of 100 μM α-tocopherol or 1 μM cyclosporin A. The reduced form of ANT was analyzed using phenylarsine oxide-agarose and Western blot analysis with anti-ANT antibody. Similar results were obtained in three separate experiments.

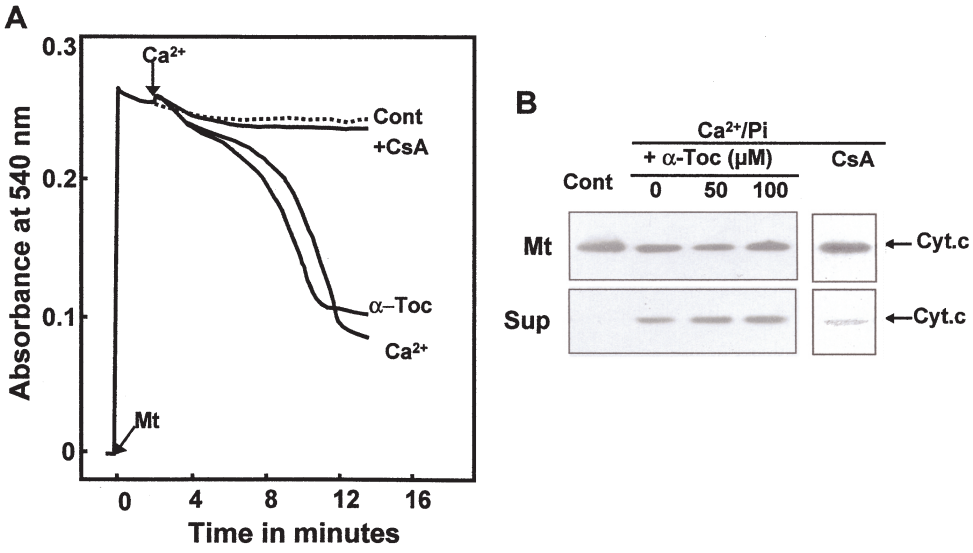

FIGURE 3. Effect of α-tocopherol on Ca^{2+}-induced mitochondrial swelling and cytochrome c release. Mitochondria (0.1 mg protein/ml) were incubated in 2 ml of the standard medium containing 1 μM EGTA, 1 mM phosphate and 2.5 mM succinate at 25°C. **A)** Mitochondrial swelling was induced by adding 20 μM Ca^{2+} in the presence or absence of 100 μM α-tocopherol or 1 μM cyclosporin A. Mitochondrial swelling was monitored by the change in the absorbance at 540 nm. Decrease in the absorbance reflects mitochondrial swelling. Similar results were obtained in three separate experiments. **B)** Cytochrome c release was induced by 20 μM Ca^{2+} in the presence or absence of 1 μM cyclosporin A or 50 ~ 100 μM α-tocopherol and analyzed by Western blotting using anti-cytochrome c antibody. Similar results were obtained in three separate experiments. Mt., mitochondria; Sup., supernatant.

α-tocopherol suppressed the Ca^{2+}-induced ROS generation and oxidation of ANT thiol groups, the effect of α-tocopherol on the swelling of mitochondria was examined. Unexpectedly, mitochondrial swelling and cytochrome c release were not inhibited by α-tocopherol.

Effect of α-tocopherol on hydroxyl radical-induced changes in mitochondrial functions and lipid peroxidation

To obtain further insight into the role of α-tocopherol in MPT, its effect on the hydroxyl radical-induced oxidation of ANT thiol groups was examined. In the presence of Pi and succinate, the hydroxyl radical generated by Fe^{2+} and H_2O_2 oxidized the critical thiol groups of ANT by a mechanism that was suppressed by cyclosporin A. The oxidation of ANT thiol groups was suppressed by α-tocopherol (Figure 4). Under identical conditions, lipid peroxidation was also induced by a mechanism that suppressed by α-tocopherol but not by cyclosporin A as determined by the generation of TBARS (Figure 4B). In the presence of Pi and succinate, the hydroxyl radical also induced mitochondrial swelling and cytochrome c release by a mechanism that was suppressed by cyclosporin A. Mitochondrial swelling and cytochrome c release were also suppressed by α-tocopherol (Figure 5).

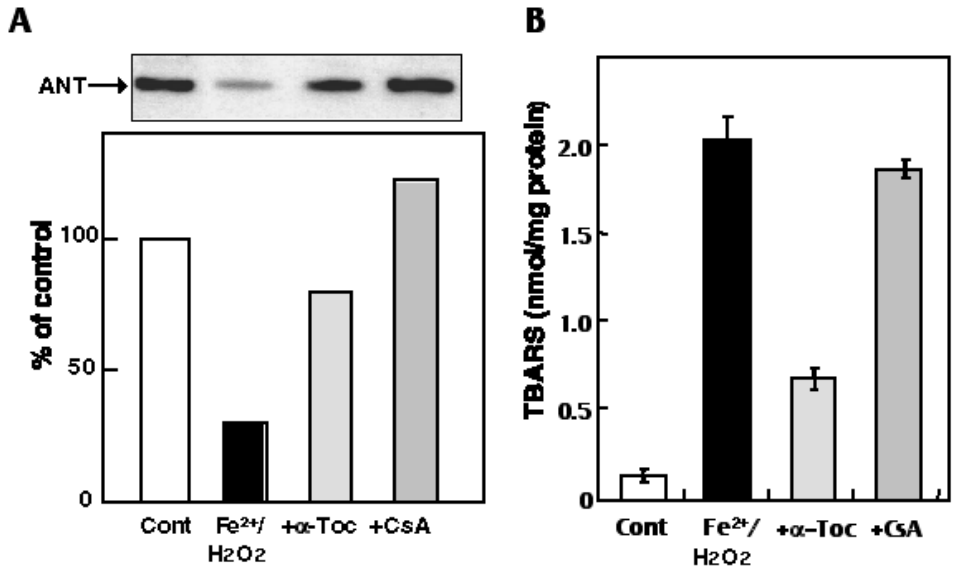

FIGURE 4. Effect of α-tocopherol on Fe^{2+}/H_2O_2-induced lipid peroxidation and oxidation of ANT SH groups. Mitochondria were incubated at 25°C for 10 min in the standard medium containing 2.5 mM succinate in the presence or absence of 100 μM α-tocopherol or 1 μM cyclosporin A. Mitochondrial MPT was induced by 10 μM Fe^{2+} and 100 μM H_2O_2. **A)** The reduced form of ANT was analyzed as described in Figure 2. The concentration of mitochondria used was 2 mg protein/ml. Similar results were obtained in three separate experiments. **B)** TBA reactive substance (TBARS) in mitochondria was measured by the method of Ohkawa *et al.* (28). The concentration of mitochondria used was 0.1 mg protein/ml.

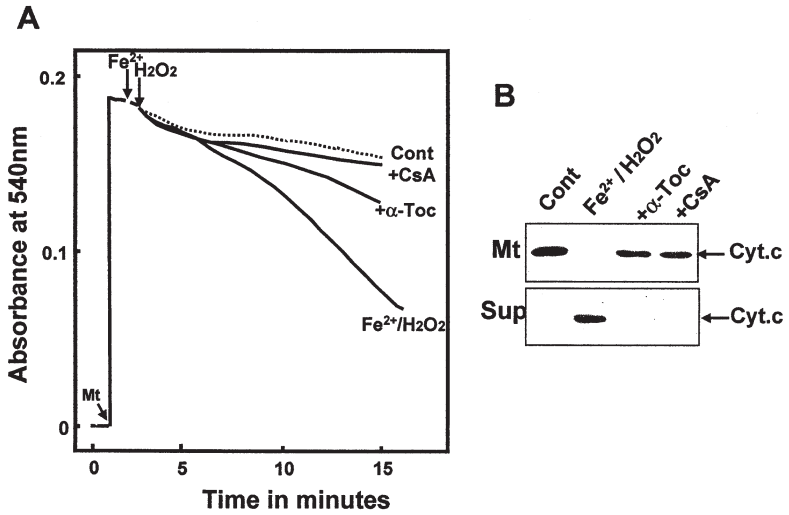

FIGURE 5. Effect of α-tocopherol on Fe^{2+}/H_2O_2-induced mitochondrial swelling and cytochrome c release. Mitochondria (0.1 mg protein/ml) were incubated in 2 ml of the standard medium containing 1 mM phosphate and 2.5 mM succinate at 25ºC. The swelling and cytochrome c release were induced by 10 μM Fe^{2+} and 100 μM H_2O_2 in the presence or absence of 75 μM α-tocopherol or 1 μM cyclosporin A. Mitochondrial swelling **A)** and cytochrome c release **B)** were analyzed as described in Figure 3. Similar results were obtained in three separate experiments.

The effect of Fe^{2+} and ADP on mitochondrial functions was examined to get further insight into the role of α-tocopherol in the hydroxyl radical-induced MPT. In the presence of succinate, Fe^{2+}/ADP increased the CHL intensity of L-012 and TBARS levels. The increased CHL and lipid peroxidation were suppressed by α-tocopherol but not by δ-tocopherol and cyclosporin A (Figure 6). Under identical conditions, Fe^{2+}/ADP also induced mitochondrial swelling and cytochrome c release by a cyclosporin A-inhibitable mechanism. The Fe^{2+}/ADP-induced swelling and cytochrome c release were also suppressed by α-tocopherol in a concentration dependent manner (Figure 7).

Discussion

Mitochondrial MPT plays an important role in the mechanism of apoptosis (9). Mitochondrial CMPT is characterized by membrane depolarization, swelling, energy- and Ca^{2+}-dependency and sensitivity to cyclosporin A. In the presence of Pi and succinate, Ca^{2+} induced typical CMPT in isolated mitochondria with concomitant generation of ROS (9, 13–16, 18). The present work shows that α-tocopherol suppressed the Ca^{2+}-induced ROS generation and oxidation of critical thiol groups in ANT. α-Tocopherol also suppressed the hydroxyl radical-induced and cyclosporin A-sensitive mitochondrial swelling, oxidation of ANT thiols and cytochrome c release.

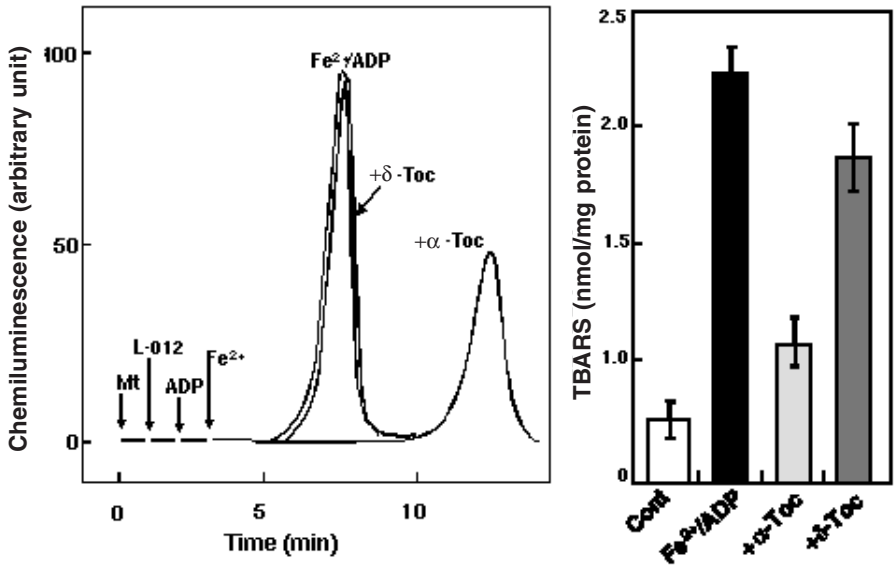

FIGURE 6. Effect of α-tocopherol on Fe^{2+}/ADP-induced development of L-012 CHL and lipid peroxidation of mitochondria. Mitochondria (0.1 mg protein/ml) were incubated at 25°C in the standard medium containing 2.5 mM succinate and 100 μM L-012 in the presence or absence of 100 μM α- or δ-tocopherol. Mitochondrial MPT was induced by 10 μM Fe^{2+} and 100 μM ADP. (A) L-012 CHL was developed by Fe^{2+}/ADP and CHL was measured as described in Figure 1B. Similar results were obtained in three separate experiments. (B) After incubation with Fe^{2+}/ADP for 10 min, values of TBARS in mitochondria were measured as described in Figure 4B.

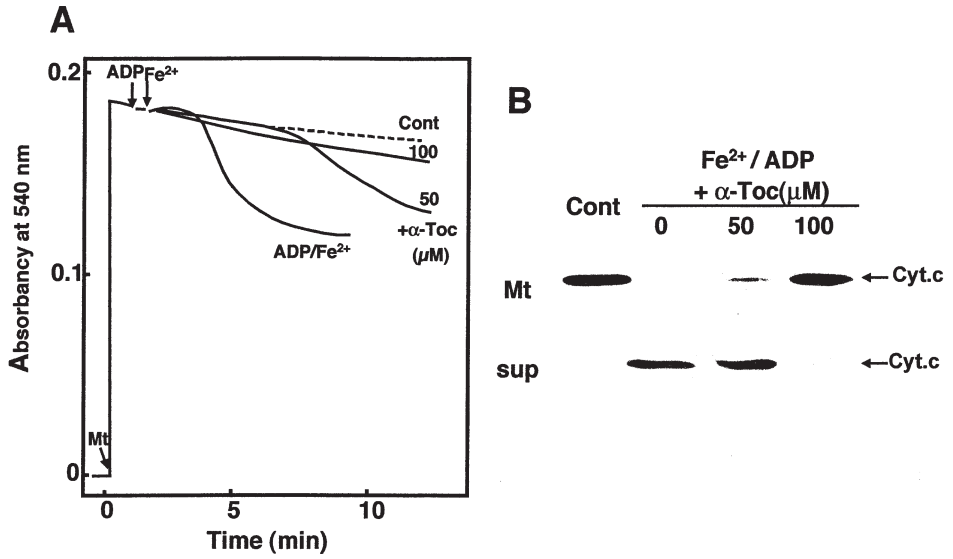

FIGURE 7. Effect of α–tocopherol on Fe^{2+}/ADP-induced mitochondrial swelling and cytochrome c release. Experimental conditions were the same as described in Figure 6. Swelling and cytochrome c release were induced by 10 μM Fe^{2+} and 100 μM ADP in the presence or absence of 50 ~ 100 μM α-tocopherol. Mitochondrial swelling **A)** and cytochrome c release **B)** were analyzed as described in Figure 4. Similar results were obtained in three separate experiments.

Several lines of evidence indicate that Ca^{2+}/Pi stimulates mitochondrial generation of ROS through electron transport system and oxidatively impairs their membranes to release cytochrome c, a prerequisite to the activation caspase cascade (13–16, 30–33). Using electron spin resonance technique, Grijalba *et al.* (30) reported that Ca^{2+} interacted with the anionic head of cardiolipin in the inner mitochondrial membranes, thereby altering their organization. Such alterations in membrane organization of mitochondria may affect functions of their respiratory chain and favor the generation of superoxide (14). In fact, the present work shows that Ca^{2+} increased CHL intensity of L-012, H_2O_2 generation, and oxidation of ANT thiol groups by a α-tocopherol-inhibitable mechanism.

Kinetic analysis revealed that L-012 developed CHL predominantly by reacting with hydroxyl radical and hypochlorite more strongly than did luminol (25). Preliminary experiments in this laboratory showed that α-tocopherol suppressed the xanthine oxidase-enhanced CHL in a concentration dependent manner. Analysis by ESR spectroscopy revealed that α-tocopherol reacted with superoxide radicals (34, 35). These results suggested that the suppression of Ca^{2+}-induced mitochondrial ROS generation by α-tocopherol might reflect its scavenging activity towards oxygen radicals.

Cardiolipin contains polyunsaturated fatty acids and binds to cytochrome c at the outer surface of mitochondrial inner membranes (31, 32). Peroxidation of their unsaturated fatty acids allows cytochrome c to dissociate from cardiolipin localized bound to mitochondrial membranes (33). These observations suggested that Ca^{2+}, ROS and mitochondrial swelling might cooperate in releasing cytochrome c from membrane-associated cardiolipin. Present work shows that Ca^{2+}-induced TBARS had undetectable values under iden-

tical conditions of mitochondrial swelling. This might be due to the low concentration of mitochondria, used 0.1 mg protein /ml. Present work also shows that α-tocopherol failed to suppress the Ca^{2+}-induced swelling and cytochrome c release despite its inhibitory effect on ROS generation. These results suggest that inhibition of ROS generation and oxidation of ANT thiols *per se* are not sufficient for the induction of cyclospolin A-sensitive MPT. It has been known that Ca^{2+} accumulated in mitochondria alter the membranous organization of phospholipids and nonspecifically increases the permeability of the inner membranes (12). The mechanism by which Ca^{2+}-induced swelling and cytochrome c release were unaffected by α-tocopherol remains unknown. In this context, similar effect of ubiquinone on Ca^{2+}-induced MPT was reported. Minor modifications of the isoprenoid side chain of ubiquinone converted its activity as an inhibitor to that of an activator of mitochondrial MPT (36). This observation suggests that the isoprenoid chain of α-tocopherol is responsible for the inhibition of MPT pore opening. Analysis of Ca^{2+}-induced swelling using α-tocopherol-deficient rat mitochondria is under our current investigations.

Sakurai *et al*. (37) reported that the Fenton reaction induced mitochondrial swelling by a cyclosporin A-sensitive mechanism. Present work shows that, in the presence of succinate, hydroxyl radical generated by Fe^{2+}/H_2O_2 or Fe^{2+}/ADP increased the amount of TBARS with concomitant occurrence of mitochondrial swelling by a cyclosporin A-sensitive mechanism (data not shown). Taken together, lipid peroxidation-coupled mechanism seems to underlie the mechanism for the cyclosporin A- and α–tocopherol-sensitive MPT.

Lipid peroxidation has been shown to generate 4-hydroxynonenal (4-HNE) (38) that triggers the signaling pathway leading to apoptosis (39). Among various mitochondrial proteins, ANT has been shown to react rapidly with 4-HNE (40) that increases the permeability of mitochondrial membranes and ANT containing liposomes by a cyclosporin A-inhibitable mechanism (41, 42). These observations suggest that the occurrence of lipid peroxidation and 4-HNE that interacts with mitochondrial proteins including ANT play important roles in the induction of MPT (39). Thus, hydroxyl radical-induced MPT might occur through oxidative modulation of mitochondrial membranes and ANT SH groups. α-Tocopherol seems to inhibit lipid peroxidation and/or oxidation of ANT, thereby suppressing the sequence of events leading to MPT pore opening and oxidative cell death**.**

It has been reported that cyclosporin A-insensitive and Ca^{2+}-independent NCMPT (nonclassical membrane permeability transition) occur in some apoptotic cells (33, 43–47). In this context, Ca^{2+}-induced mitochondrial MPT has been shown to occur independently from the accumulation of lipid peroxidation products (30). Thus, NCMPT can be induced either with or without induction of lipid peroxidation coupled with cyclosporin A-sensitive or insensitive mechanisms.

Although α-tocopherol suppressed the ROS generation coupled with CMPT, it suppressed the cyclosporin A-sensitive MPT induced by hydroxyl radicals but not by Ca^{2+}. Thus, α-tocopherol seems to play an important role in the mechanism of apoptosis through the regulation of peroxidation-coupled mitochondrial MPT.

This work was supported in part by grants from the Ministry of Education, Science and Culture of Japan, Grant from the Eisai Co. and the Japan Keirin Association.

References

1. Shi, L., Kraut, R.P., Aebersold, R. and Greenberg, A.H. (1992a) A natural killer cell granule protein that induces DNA fragmentation and apoptosis. *J. Exp. Med. 175:* 553–566.
2. Shi, L., Kam, C. M., Powers, J. C., Aebersold, R. and Greenberg, A. H. (1992) Purification of three cytotoxic lymphocyte granule serine proteases that induce apoptosis through distinct substrate and target cell interactions. *J. Exp. Med. 176:* 1521–1529.
3. Shi, L., Mai, S., Israels, S., Browne, K., Trapani, J.A. and Greenberg, A.H. (1997) Granzyme B (GraB) autonomously crosses the cell membrane and perforin initiates apoptosis and GraB nuclear localization. *J. Exp. Med. 185:* 855–866.
4. Jacobson, M.D. (1996) Reactive oxygen species and programmed cell death. *Trends Biochem. Sci. 21:* 83–86.
5. Carmody, R.J. and Cotter, T.G. (2001) Signalling apoptosis: a radical approach. *Redox Rep. 6:* 77–90.
6. Nordberg, J. and Arner, E.S. (2001) Reactive oxygen species, antioxidants, and the mammalian thioredoxin system. *Free Radic. Biol. Med. 31:* 1287–1312.
7. Chakraborti, T., Das, S., Mondal, M., Roychoudhury, S. and Chakraborti, S. (1999) Oxidant, mitochondria and calcium: an overview. *Cell Signal. 11:* 77–85.
8. Lenaz, G., Bovina, C., D'Aurelio, M., Fato, R., Formiggini, G., Genova, M.L., Giuliano, G., Pich, M., Paolucci, U., Castelli, G. and Ventura, B. (2002) Role of mitochondria in oxidative stress and aging. *Ann. N. Y. Acad. Sci. 959:* 199–213.
9. Zoratti, M. and Szabo, I. (1995) The mitochondrial permeability transition. *Biochim. Biophys. Acta. 1241:* 139–176.
10. Kristal, B.S. and Brown, A.M. (1999) Apoptogenic ganglioside GD3 directly induces the mitochondrial permeability transition. *J. Biol. Chem. 274:* 23169–23175.
11. Oyadomari, S., Araki, E. and Mori, M. (2002) Endoplasmic reticulum stress-mediated apoptosis in pancreatic beta-cells. *Apoptosis 7:* 335–345.
12. Ishisaka, R., Utsumi, T., Yabuki, M., Kanno, T., Furuno, T., Inoue, M. and Utsumi, K. (1998) Activation of caspase-3-like protease by digitonin-treated lysosomes. *FEBS Lett. 435:* 233–236.
13. Kowaltowski, A.J., Castilho, R.F., Grijalba, M.T., Bechara, E.J. and Vercesi, A.E. (1996) Effect of inorganic phosphate concentration on the nature of inner mitochondrial membrane alterations mediated by Ca^{2+} ions. A proposed model for phosphate-stimulated lipid peroxidation. *J. Biol. Chem. 271:* 2929–2934.
14. Kowaltowski, A.J., Naia-da-Silva, E.S., Castilho, R.F. and Vercesi, A.E. (1998) Ca^{2+}-stimulated mitochondrial reactive oxygen species generation and permeability transition are inhibited by dibucaine or Mg^{2+}. *Arch. Biochem. Biophys. 359:* 77–81.
15. Kowaltowski, A.J., Castilho, R.F. and Vercesi, A.E. (2001) Mitochondrial permeability transition and oxidative stress. *FEBS Lett. 495:* 12–15.
16. Kanno, T., Sato, E.F., Utsumi, T., Yoshioka, T., Inoue, M. and Utsumi, K. (2004) Oxidative stress underlies the mechanism for Ca^{2+}-induced permeability transition of mitochondria. *Free Rad. Res. 38:* 27–35.
17. Mancini, M., Nicholson, D.W., Roy, S., Thornberry, N.A., Peterson, E.P., Casciola- Rosen, L.A. and Rosen, A. (1998) The caspase-3 precursor has a cytosolic and mitochondrial distribution: implications for apoptotic signaling. *J. Cell Biol. 140:* 1485–1495.?
18. Kushnareva, Y., Haley, L. and Sokolove, P. (1999) The role of low (< or = 1 mM) phosphate concentrations in regulation of mitochondrial permeability: modulation of matrix free Ca2+ concentration. *Arch. Biochem. Biophys. 363:* 155–162.
19. Taylor, S., Lamden, M.P. and Tappel, A.L. (1976) Sensitive fluorometric method for tissue tocopherol analysis. *Lipid 11:* 530–538.
20. Tsuruga, M., Dang, Y., Shiono, Y., Oka, S. and Yamazaki, Y. (2003) Differential effects of vitamin E and three hydrophilic antioxidants on the actinomycin D-induced an colcemid-accelerated apoptosis in human leukemia CMK-7 cell line. *Mol. Cell Biochem. 250:* 131–137.

21. Yerushalmi, B., Dahl, R., Devereaux, M.W., Gumpricht, E., Sokol, R.J. (2001) Bile acid-induced rat hepatocyte apoptosis is inhibited by antioxidants and blockers of the mitochondrial permeability transition. *Hepatology 33:* 616–626.
22. Hogeboom, G.H. (1995) Fractionation cell components and animal tissues. In: *Methods Enzymol,* vol. 1 Colowick, S. P., Kaplan, N. O., eds, Academic Press, New York, pp. 16–19.
23. Ishisaka, R., Kanno, T., Akiyama, J., Yoshioka, T., Utsumi, K. and Utsumi, T. (2001) Activation of caspase-3 by lysosomal cysteine proteases and its role in 2,2'-azobis-(2- amidinopropane) dihydrochloride (AAPH)-induced apoptosis in HL-60 cells. *J. Biochem. 129:* 35–41.
24. Mohanty, J.G., Jaffe, J.S., Schulman, E.S. and Raible, D.G. (1997) A highly sensitive fluorescencnt micro-assay of H_2O_2 release from activated human leukocytes using a dihydroxyphenoxazine derivative. *J. Immuno. Methods 202:* 133–141.
25. Imada, I., Sato, E.F., Miyamoto, M., Ichimori, Y., Minamiyama, Y., Konaka, R. and Inoue, M. (1999) Analysis of reactive oxygen species generated by neutrophils using a chemiluminescence prove L-012. *Analy. Biochemi. 271:* 53–58.
26. Nishikimi, A., Kira, Y., Kasahara, E., Sato, E.F., Kanno, T., Utsumi, K. and Inoue, M. (2001) Tributyltin interacts with mitochondria and induces cytochrome c release. *Biochem. J. 356:* 621–626.
27. Bradford, M.M. (1976) A rapid and sensitive method for the quantitation of microgram quantities of protein utilizing the principle of protein-dye binding. *Anal. Biochem. 72:* 248–254.
28. Ohkawa, H., Ohnishi, N. and Yagi, K. (1979) Assay for lipid peroxides in animal tissues by thiobarbituric acid reaction. *Anal. Biochem. 95:* 351–358.
29. McStay G.P., Clarke S.J., Halestrap A.P. (2002) Role of critical thiol groups on the matrix surface of the adenine nucleotide translocase in the mechanism of the mitochondrial permeability transition pore. *Biochem J. 367:* 541–548.
30. Grijalba, M.T., Vercesi, A.E., Schreier, S. (1999) Ca^{2+}-induced increased lipid packing and domain formation in submitochondrial particles. A possible early step in the mechanism of Ca^{2+}-stimulated generation of reactive oxygen species by the respiratory chain. *Biochemistry 38:* 13279–13287.
31. Soussi, B., Bylund-Fellenius, A.C., Schersten, T., Angstrom, J. (1990) 1H-n.m.r. evaluation of the ferricytochrome c-cardiolipin interaction. Effect of superoxide radicals. *Biochem. J. 265:* 227–232.
32. Touminen, E.K., Wallace, C.J., kinnunen, P.K. (2002) Phospholipid-cytochrome c interaction: evidence for the extended lipid anchorage. *J. Biol. Chem. 277:* 8822–8826.
33. Petrosillo, G., Ruggiero, F.M., Pistolese, M., Paradies, G. (2004) Ca^{2+}-induced reactive oxygen species production promotes cytochrome c release from rat liver mitochondria via mitochondrial permeability transition (MPT)-dependent and MPT-independent mechanisms: role of cardiolipin. *J. Biol. Chem. 279:* 53103–53108.
34. Ozawa, T., Hanaki, A., Matsumoto, S., Matsuo, M. (1978) Electron spin resonance studies of radicals obtained by the reaction of alpha-tocopherol and its model compound with superoxide ion. *Biochim. Biophy. Acta. 531:* 72–78.
35. Ozawa, T., Hanaki, A., Matsuo, M. (1983) Reactions of superoxide ion with tocopherol and its model compounds: correlation between the physiological activities of tocopherols and the concentration of chromanoxyl-type radicals. *Biochem. Int. 6:* 685–92.
36. Walter, L., Nogueira, V., Leverve, X., Heitz, M.P., Bernardi, P., Fontaine, E. (2000) Three classes of ubiquinone analogs regulate the mitochondrial permeability transition pore through a common site. *J Biol Chem. 275:* 29521–29527.
37. Sakurai, K., Stoyanovsky, D.A., Fujimoto, Y., Cederbaum, A.I. (2000) Mitochondrial permeability transition induced by 1-hydroxyethyl radical. *Free Radic. Biol. Med. 28:* 273–280.
38. Giron-Calle, J. and Schmid, H.H., Peroxidative modification of a membrane protein. Conformation-dependent chemical modification of adenine nucleotide translocase in Cu^{2+}/tert-butyl hydroperoxide treated mitochondria. *Biochemistry 35:* 15440–15446 (1995).

39. Petersen, D.R., Doorn, J.A. (2004) Reactions of 4-hydroxynonenal with proteins and cellular targets. *Free Rad. Biol. Med. 37:* 937–945.
40. Chen, J.J., Bertrand, H. and Yu, B.P. (1995) Inhibition of adenine nucleotide translocator by lipid peroxidation products. *Free Radic. Biol. Med. 19:* 583–590.
41. Yan, L.J. and Sohal, R.S. (1998) Mitochondrial adenine nucleotide translocase is modified oxidatively during aging. *Proc. Natl. Acad. Sci. 95:* 12896–12901.
42. Vieira, H.L., Belzacq, A.S., Haouzi, D., Bernassola, F., Cohen, I., Jacotot, E., Ferri, K.F., El Hamel, C., Bartle, L.M., Melino, G., Brenner, C., Goldmacher, V. and Kroemer, G. (2001) The adenine nucleotide translocator: a target of nitric oxide, peroxynitrite, and 4-hydroxynonenal. *Oncogene 20:* 4305–4316.
43. Gogvadze, V., Robertson, J.D., Zhivotovsky, B. and Orrenius, S. (2001) Cytochrome c release occurs via Ca^{2+}-dependent and Ca^{2+}-independent mechanisms that are regulate by Bax. *J. Biol. Chem. 276:* 19066–19071.
44. Gogvadze, V., Walter, P.B. and Ames, B.N. (2003) The role of Fe^{2+}-induced lipid peroxidation in the initiation of the mitochondrial permeability transition. *Arch. Biochem. Biophys. 414:* 255–260.
45. Sultan, A. and Sokolove, P.M. (2001) Palmitic acid opens a novel cyclosporin A-insensitive pore in the inner mitochondrial membrane. *Arch. Biochem. Biophys. 386:* 37–51.
46. Sultan, A. and Sokolove, P.M. (2001) Free fatty acid effects on mitochondrial permeability: an overview. *Arch. Biochem. Biophys. 386:* 52–61.
47. Kanno, T., Fujita, H., Muranaka, S., Yano, H., Utsumi, T., Yoshioka, T., Inoue, M. and Utsumi, K. (2002) Mitochondrial swelling and cytochrome c release: sensitivity to cyclosporin A and calcium. *Physio.l Chem. Phys. Med. NMR 34:* 91–102.

Received June 15, 2004;
accepted February 17, 2005.

Physiol. Chem. Phys. & Med. NMR (2004) *36*: 109–121

Phosphate Deposition During and After Hypokinesia in Phosphate Supplemented and Unsupplemented Rats

Vassilis J. Kakuris[1*], Costas B. Tsiamis[2], Victor A. Deogenov[3] and John G. Peskaratos[3]

[1]*European Foundation of Environmental Sciences, Athens GR-16232, Greece*
[2]*Department of Medicine, School of Medicine, Athens GR-11527, Greece*
[3]*Higher Institute of Biochemistry, Gomelo, Belarus*
**Author for correspondence*

Abstract: The objective of this study was to show that prolonged restriction of motor activity (hypokinesia) could reduce phosphate (P) deposition and contribute to P loss with tissue P depletion. To this end, measurements were made of tissue P content, P absorption, plasma P levels, urinary and fecal P excretion of rats during and after hypokinesia (HK) and daily phosphate supplementation.

Studies were conducted on male Wistar rats during a pre-hypokinetic period, a hypokinetic period and a post-hypokinetic period. All rats were equally divided into four groups: unsupplemented vivarium control rats (UVCR), unsupplemented hypokinetic rats (UHKR), supplemented vivarium control rats (SVCR) and supplemented hypokinetic rats (SHKR).

Bone and muscle P content, plasma intact parathyroid hormone (iPTH) levels, P absorption, plasma P levels and urinary and fecal P excretion did not change in SVCR and UVCR compared with their pre-HK values. During HK, plasma P levels, urinary and fecal P excretion increased significantly ($p<0.05$) while muscle and bone P content, P absorption and plasma iPTH levels decreased significantly ($p<0.05$) in SHKR and UHKR compared with their pre-HK values and the values in their respective vivarium controls (SVCR and UVCR). During the initial 9-days of post-HK, plasma, urinary and fecal P levels decreased significantly ($p<0.05$), and plasma iPTH levels, muscle and bone P levels remained significantly ($p<0.05$) depressed in hypokinetic rats compared with their pre-HK values and the values in their respective vivarium control rats. By the 15th day, these values approached the control values. During HK and post-HK, changes in P absorption, plasma iPTH levels, and P levels in muscle, bone, plasma, urine and feces were significantly ($p<0.05$) greater in SHKR than in UHKR.

Decreased tissue P content with increased P loss in animals receiving and not receiving P supplementation demonstrates decreased P deposition during HK. Higher P excretion with lower tissue content in SHKR and UHKR demonstrates that P deposition is decreased more with P supplementation than without. Because SHKR with a lower tissue P content showed higher P excretion than UHKR it was concluded that the risk of decreased P deposition with greater tissue P depletion is

inversely related to P intake, that is, the higher the P intake the greater the risk for decreased P deposition and the greater tissue P depletion. It was shown that P (regardless of the intensity of its tissue depletion) is lost during HK unless factors contributing to the decreased P deposition are partially or totally reversed. It was concluded that dissociation between (decreased) tissue P content and (increased) P uptake indicates decreased P (absorption and) deposition as the main mechanisms of tissue P depletion during prolonged HK.

MUSCULAR ACTIVITY is regarded as an important factor in normal regulation of mineral deposition in animals and humans. The mechanism by which muscular activity affects electrolyte deposition is not known, but the absence of activity, such as during hypokinesia (HK), results in a mineral loss from the body with tissue electrolyte depletion (1–5). While a limited number of studies have been conducted to establish the effects of prolonged HK on electrolyte deposition in animals or humans, the mechanisms of excessive electrolyte losses with tissue electrolyte depletion during prolonged HK remain unclear (1–5).

It is known that the coefficient of distribution of electrolytes in muscle and plasma, and between muscle and plasma is an integral characteristic of the functional status of skeletal muscles. Being involved in the finely regulated processes of active membrane transport and intracellular phases, electrolytes are distributed in muscles according to the functional condition of the system of the membranomyo-fibril conjugation (6), the levels of metabolic activity of cells (7), and the chemical state of the cytoplasmic template that carries fixed charges (8). Consequently, any condition that could affect the level of muscular activity, would inevitably contribute to the electrolyte redistribution in tissue resulting in an increase of plasma electrolyte levels (3–6); this in turn could potentially contribute to an increase of electrolyte loss from the body and consequently to the decrease of total electrolyte content of the body (4, 5, 9–11).

During HK, increase of mineral loss occurs in animals while at the same time there is a decrease of tissue mineral content (4, 5, 9–11). Increase of mineral loss with tissue mineral depletion shows decreased electrolyte deposition (4, 5, 9–11). Because of the presence of decreased electrolyte deposition excessive electrolyte losses with tissue mineral depletion may be seen in hypokinetic rats (4, 5, 9–11). The decreased electrolyte deposition may be attributed to several factors and primarily to the decreased cell mass (4, 5). During post-HK, electrolyte excretion may fall dramatically, similar to the tissue electrolyte depletion during HK (1–5). Electrolyte tissue depletion during HK is most likely the result of increased electrolyte loss, secondary to decreased mineral deposition. Moreover, tissue mineral depletion has not been seen to inhibit mineral loss, while mineral supplementation failed to restore a tissue mineral depletion during HK (12–14) indicating intensity of decreased mineral deposition. Previous studies have shown strong relation between decreased mineral deposition and increased electrolyte losses (4, 5, 9–11).

Although the effect of HK on mineral deposition has yet to be firmly established, the hypokinetic mineral changes in tissue, plasma, urine and feces have been clearly established (1–5, 9–11). Excessive mineral loss with tissue mineral depletion is a typical reaction of reduced mineral deposition (4, 5, 9–11). However, the impact of HK on phosphate (P) deposition and thus on P losses has not yet been thoroughly studied. Moreover, little is known about the effect of HK on P deposition and it is still not known by what mechanisms HK could lead to the increased P losses with tissue P depletion (15–17). It is important, therefore, to determine what mechanisms are involved in decreased P deposition

with tissue P depletion that could contribute to the significant P losses from the body and consequently to tissue P depletion. For this reason, the determination of P absorption and tissue P levels during prolonged HK and P supplementation is very important.

The aim of this study was to show that HK could contribute to decreased P deposition, and thus P loss with tissue P depletion. Measurements of P absorption, tissue P levels, and P levels in plasma, urine and feces during HK and post-HK with or without P supplementation were made.

Materials and Methods

Four hundred eight 13-week-old Wistar male rats were obtained from a Local Research Laboratory. On arrival they were given an adaptational dietary period of 10-days during which they were fed a commercial laboratory diet. At the start of the study, all rats were about 90-days old and weighted 370 to 390 g. All rats were housed in individual metabolic cages where light (07:00 to 19:00 h), temperature (25±1°C) and relative humidity (65%) was automatically controlled. Cages were cleaned daily in the morning before feeding. Studies were approved by the Institute's Ethical Committee for the Protection of Animals.

Hypokinetic studies were preceded by a pre-HK period of 10-days that involved a series of biochemical examinations, training, testing and conditioning of animals to their laboratory conditions. The preparation period was used for collecting baseline (pre-HK) values for the variables being examined during the study. This adaptation period also aimed at minimizing hypokinetic stress due to diminished muscular activity (18, 19).

Assignment of the animals into four groups was performed randomly and their conditions were:

Group one: one hundred-two unrestrained rats were housed in individual cages for 98-days under vivarium control conditions. They served as unsupplemented vivarium control rats (UVCR).

Group two: one hundred-two restrained rats were kept in small individual cages for 98-days. They served as unsupplemented hypokinetic rats (UHKR).

Group three: one hundred-two unrestrained rats were housed in individual cages for 98-days under vivarium control conditions. They were supplemented with P and served as supplemented vivarium control rats (SVCR).

Group four: one hundred-two restrained rats were kept in small individual cages for 98-days. They were supplemented with P and served as supplemented hypokinetic rats (SHKR).

Simulation of hypokinesia

Hypokinesia was effected, by keeping hypokinetic rats in small individual wooden cages. The cages dimensions of 195 x 80 x 95 cm allowed movements to be restricted in all directions without hindering food and water consumption. However, hypokinetic rats could still assume a natural position that allowed them to groom different parts of their body. The cages were constructed in such a way that, using special wood inserts, their size could be changed in accordance with size of each rat so that the degree of restriction of motor activity could be maintained at a relatively constant level throughout HK.

Food and fluid consumption

The daily food consumption was measured and 90% of a daily amount (12 g) was mixed with deionized distilled water (1:2 wt/vol) to form a slurry which was divided into two meals. Rats were pair-fed and daily food consumption measured during pre-HK, HK and post-HK periods. Control rats were allowed to eat approximately the same amount of food as hypokinetic rats. The dietary amount of food was placed in individual feeders formed by the little trough and wood partitions. Food for the entire study was from the same production lot and contained all essential nutrients: vitamins, A, D, E, 4% fat, 19% protein, 38% carbohydrates, 16% cellulose, 0.6% sodium chloride, 0.76% calcium, 0.66% phosphorus, 0.5% magnesium and 0.9% potassium per one g food and kept in a cold chamber (4°C). Food consumption was measured daily by weighing the slurry food containers. Rats received daily deionized-distilled water *ad libitum*. Water dispensers (120 to 150 mL) were secured onto a wooden plate installed on the front cage panels and filled daily. All animals were weighed daily between 9 and 10 a.m.

Phosphate supplementation and phosphate absorption measurements

During pre-HK, HK and post-HK periods, supplemented rats took 85 mg dicalcium phosphate per day. This P amount was designed to facilitate the maximal absorption of P supplementation by remaining just below the renal tubular maximum for P absorption (4, 5). To minimize diurnal variations, blood samples for each rat were drawn at identical times of the day and after the P was consumed. The P amount in the diet was calculated directly by keeping an exact duplicate of the consumed food of each rat and the total P loss in 24 h urinary and fecal samples were measured. Measuring P absorption [(intake-losses)/intake], with and without P supplementation, required the consumption of a calculated phosphate amount, followed by 24 h urinary and fecal collection, with calculation of the percentage of P retained in the body. That is, absorption of P is equal to [(phosphate intake-phosphate excretion in urine and feces)/intake] and expressed as percent. The phosphate amounts in the 24 h urinary and fecal collections during the pre-HK period were considered to be each rat's pre-HK values of urinary and fecal excretion. These phosphate values were then subtracted from P in the 24 h urine and fecal collections during HK and post-HK and after phosphate consumption. The differences were compared with the total amount of phosphate consumed and then expressed as a percentage of P absorption 24 h after P consumption.

Plasma, urine and fecal sample collection

Urine and feces were collected from each rat every day and pooled to form 6-days composites while plasma samples were collected every 6-days during pre-HK, HK and post-HK. A 6-day (consecutive day) pooled samples were collected. Blood samples of 1 to 2 mL were obtained *via* a cardiac puncture from ether-anaesthetized rats. To obtain plasma, blood samples, transferred into polypropylene tubes containing heparin, were centrifuged immediately at 10,000 x g for 2 min at room temperature and separated using glass capillary pipets that had been washed in hydrochloric acid and deionized-distilled water. Aliquots for plasma phosphate (P) and intact parathyroid hormone (iPTH) analyses were kept frozen at −20°C. 24-h urine samples uncontaminated by stool were obtained. Stainless steel urine-feces separating funnels (Hoeltge, model HB/SS, Hoeltge Inc., Cincinnati, OH) were placed beneath each rat to collect uncontaminated 24 h urine samples. Urine was collected in a beaker with a layer of mineral oil to prevent evaporation. Beakers were

replaced daily. Urine for each 24-h period was collected in acidified acid-wash containers and refrigerated at –4°C until needed for P analyses. Creatinine excretion was measured to ensure 24 hr urine collections. Fecal samples were dried, wet ashed with nitric and perchloric acid and diluted as necessary with deionized distilled water and analyzed for P. A marker was used for complete feces recovery.

Muscle and bone sample collection

Six hypokinetic and control rats from each group were sacrificed by decapitation on the 1st, 7th and 9th day of the pre-HK period, on the 3rd, 7th, 15th, 30th, 50th, 70th and 98th of HK period and on the 1st, 3rd, 5th 7th, 9th, 11th and 15th day of post-HK period. Muscle (gastrocnemius) and bone (right femur) data are represented as the average of six rats. The femur bones were cleaned of soft tissues, dried to a constant weight, weighed, reduced to ash in a muffle furnace at 600 degrees for 144 minute, then the ash was weighed and dissolved in 0.05 N HCl and, as a chloride solution, analyzed for P. The gastrocnemius muscles were excised immediately after sacrificing the animals. Muscles were thoroughly cleaned of connective tissues, fatty inclusions and large vessels, weighed on Teflon liners and placed in a drying chamber at 110°C. After drying to a constant weight muscles were transferred to quartz tubes for mineralization by means of concentrated HNO_3, distilled off in a quartz apparatus. After ashing, the residue was dissolved in 0.05 M HCl and, as chloride solution, analyzed for P content in muscle and bone of rats.

Phosphate and parathyroid hormone measurements

Samples were analyzed in duplicate and adequate standards were used for measurements: Plasma iPTH levels were measured using immunoradiometric assay test kits (Nichols Inst., San Juan Capistrano, CA). Muscle (gastrocnemius) and bone (femur) P content, plasma, fecal and urinary P levels were measured by spectrophotometry on a Perkin-Elmer 330 model (Perkin-Elmer Corp., Norwalk, CT). Urine and fecal samples, were aspirated directly into a spectrophotometer and diluted as necessary.

Statistical analyses

The results were analyzed with a 2 (hypokinetic *vs.* active controls) X 2 (supplemented *vs.* unsupplemented) X 2 (pre-intervention *vs.* post-intervention) ANOVA with repeated measures on the last factor. The Tukey-Kramer post-hoc test was applied to establish which means were significantly different from each other. A format analysis was conducted to establish the shape of changes. A correlation coefficient was used to examine the correlation between P absorption with tissue P content, P excretion and plasma P levels. The predetermined levels of significance was set at alpha <0.05. The obtained results were reported as mean ± SD (standard deviation).

Results

Pre-hypokinetic phosphate values with and without phosphate supplementation

Phosphate absorption, and P levels in muscle, bone, plasma, urine and feces (Table IA) and iPTH levels (Table IB) were not different between hypokinetic and control groups of rats. With the daily P supplementation, P absorption and P levels in muscle, bone, plasma,

TABLE IA. Absorption, plasma, urine, feces, gastrocnemius muscle and femur bone phosphate levels measured in rats at pre-hypokinesia and during vivarium control, and hypokinesia.

Days	Absorption (%)	Plasma (mmol/L)	Urine (mmol/day)	Feces (mmol/day)	Gastrocnemius Muscle (mEq/kg dry tissue)	Femur Bone (mg/100 g ash)
			Unsupplemented Vivarium Control Rats (UVCR), n = 6			
Pre-HK	65 ± 3	2.04 ± 0.05	2.17 ± 0.5	4.54 ± 0.22	4.05 ± 0.4	20.2 ± 0.7
3rd	66 ± 2	2.03 ± 0.03	2.16 ± 0.2	4.52 ± 0.24	4.07 ± 0.3	20.3 ± 0.4
7th	65 ± 4	2.04 ± 0.04	2.17 ± 0.3	4.50 ± 0.30	4.06 ± 0.5	20.5 ± 0.6
15th	66 ± 3	2.02 ± 0.05	2.15 ± 0.2	4.51 ± 0.27	4.07 ± 0.3	20.3 ± 0.7
30th	65 ± 4	2.03 ± 0.06	2.16 ± 0.7	4.50 ± 0.30	4.06 ± 0.4	20.5 ± 0.4
50th	66 ± 5	2.02 ± 0.03	2.15 ± 0.4	4.53 ± 0.24	4.07 ± 0.4	20.6 ± 0.8
70th	66 ± 2	2.03 ± 0.05	2.16 ± 0.3	4.50 ± 0.25	4.06 ± 0.5	20.7 ± 0.6
98th	65 ± 3	2.04 ± 0.03	2.15 ± 0.2	4.52 ± 0.27	4.07 ± 0.4	20.7 ± 0.4
			Unsupplemented Hypokinetic Rats (UHKR), n = 6			
Pre-HK	65 ± 4	2.04 ± 0.03	2.16 ± 0.2	4.53 ± 0.34	4.06 ± 0.3	20.1 ± 0.6
3rd	19 ± 2*	2.27 ± 0.05*	2.85 ± 0.3*	6.66 ± 0.33*	3.66 ± 0.4*	18.2 ± 0.4*
7th	23 ± 3*	2.25 ± 0.04*	2.78 ± 0.4*	6.41 ± 0.34*	3.70 ± 0.5*	18.4 ± 0.5*
15th	17 ± 4*	2.29 ± 0.06*	2.93 ± 0.6*	7.15 ± 0.28*	3.57 ± 0.4*	17.7 ± 0.4*
30th	19 ± 3*	2.27 ± 0.03*	2.85 ± 0.3*	6.82 ± 0.35*	3.63 ± 0.5*	17.9 ± 0.7*
50th	15 ± 2*	2.33 ± 0.05*	3.00 ± 0.5*	7.48 ± 0.27*	3.47 ± 0.6*	17.1 ± 0.5*
70th	17 ± 3*	2.30 ± 0.03*	2.93 ± 0.4*	7.23 ± 0.35*	3.55 ± 0.4*	17.5 ± 0.4*
98th	13 ± 2*	2.36 ± 0.04*	3.13 ± 0.3*	7.72 ± 0.30*	3.43 ± 0.5*	16.8 ± 0.5*
			Supplemented Vivarium Control Rats (SVCR), n = 6			
Pre-HK	66 ± 2	2.09 ± 0.05	2.27 ± 0.4	4.76 ± 0.33	4.18 ± 0.3	20.7 ± 0.4
3rd	45 ± 4	2.11 ± 0.03	2.30 ± 0.3	5.20 ± 0.25	4.20 ± 0.4	20.8 ± 0.5
7th	46 ± 3	2.08 ± 0.04	2.27 ± 0.6	5.12 ± 0.34	4.19 ± 0.3	20.9 ± 0.4
15th	47 ± 2	2.12 ± 0.05	2.34 ± 0.3	5.23 ± 0.26	4.21 ± 0.4	20.9 ± 0.5
30th	46 ± 4	2.09 ± 0.03	2.30 ± 0.5	5.14 ± 0.35	4.20 ± 3.3	21.0 ± 0.6
50th	47 ± 5	2.13 ± 0.04	2.41 ± 0.4	5.25 ± 0.25	4.22 ± 0.5	21.2 ± 0.5
70th	46 ± 3	2.10 ± 0.03	2.37 ± 0.5	5.16 ± 0.27	4.21 ± 0.4	21.3 ± 0.4
98th	47 ± 4	2.13 ± 0.05	2.45 ± 0.3	5.22 ± 0.25	4.22 ± 0.3	21.4 ± 0.5
			Supplemented Hypokinetic Rats (SHKR), n = 6			
Pre-HK	67 ± 4	2.09 ± 0.05	2.26 ± 0.5	4.77 ± 0.33	4.18 ± 0.4	20.7 ± 0.7
3rd	13 ± 3*+	2.55 ± 0.04*+	3.87 ± 0.42*+	8.97 ± 0.24*+	3.27 ± 0.5*+	16.7 ± 0.5*+
7th	15 ± 2*+	2.53 ± 0.03*+	3.71 ± 0.38*+	8.76 ± 0.33*+	3.30 ± 0.4*+	16.9 ± 0.7*+
15th	11 ± 4*+	2.57 ± 0.04*+	3.93 ± 0.46*+	9.55 ± 0.34*+	3.21 ± 0.5*+	16.2 ± 0.4*+
30th	13 ± 3*+	2.55 ± 0.05*+	3.87 ± 0.35*+	9.31 ± 0.25*+	3.25 ± 0.3*+	16.4 ± 0.5*+
50th	07 ± 2*+	2.59 ± 0.03*+	3.99 ± 0.42*+	9.88 ± 0.34*+	3.15 ± 0.5*+	15.7 ± 0.8*+
70th	09 ± 3*+	2.57 ± 0.04*+	3.93 ± 0.40*+	9.66 ± 0.35*+	3.20 ± 0.3*+	15.9 ± 0.6*+
98th	05 ± 2*+	2.63 ± 0.05*+	4.07 ± 0.39*+	10.23 ± 0.23*+	3.12 ± 0.4*+	15.3 ± 0.5*+

All values are expressed as mean ± SD.

*$p < 0.05$ significant differences between vivarium control and hypokinetic groups of rats. Each of the hypokinetic groups was compared with their respective controls (UVCR *vs* UHKR and SVCR *vs* SHKR).

+$p < 0.05$ significant difference between supplemented and unsupplemented hypokinetic groups.

TABLE IB. Parathyroid hormone levels (ng/dL) measured in rats at pre-hypokinesia and during vivarium control and hypokinetic conditions

Days	Unsupplemented Vivarium Control Rats (UVCR)	Unsupplemented Hypokinetic Rats (UHKR)	Supplemented Vivarium Control Rats (SVCR)	Supplemented Hypokinetic Rats (SHKR)
Pre-HK	0.45 ± 0.03	0.45 ± 0.04	0.46 ± 0.02	0.46 ± 0.04
3rd	0.46 ± 0.02	0.38 ± 0.05*	0.47 ± 0.03	0.33 ± 0.05*+
7th	0.47 ± 0.04	0.40 ± 0.02*	0.46 ± 0.05	0.31 ± 0-03*
15th	0.46 ± 0.07	0.35 ± 0.05*	0.48 ± 0.04	0.30 ± 0.04*
30th	0.47 ± 0.03	0.37 ± 0.03*	0.47 ± 0.03	0.34 ± 0.05*+
50th	0.46 ± 0.04	0.33 ± 0.04*	0.48 ± 0.05	0.28 ± 0.03*+
70th	0.47 ± 0.03	0.34 ± 0.03*	0.47 ± 0.03	0.30 ± 0.05*+
98th	0.46 ± 0.04	0.32 ± 0.05*	0.48 ± 0.05	0.26 ± 0.04*+

*, +, S.D., as in Table I.

urine and feces and plasma iPTH levels were not different between hypokinetic and control groups of rats (Tables IA, IB).

Hypokinetic phosphate changes with and without supplementation

Muscle and bone P content, P absorption, plasma iPTH levels, plasma P levels, fecal and urinary P excretion did not change in UVCR and SVCR compared with their pre-HK values (Tables IA, IB). Muscle and bone P content, P absorption and plasma iPTH concentration decreased significantly ($p<0.05$) while plasma P levels, fecal and urinary P excretion increased significantly ($p<0.05$) in SHKR and UHKR compared with their pre-HK values and values in their respective vivarium controls (SVCR and UVCR) (Tables IA, IB). However, muscle and bone P content, P absorption, and plasma iPTH levels decreased significantly ($p<0.05$) more while plasma P levels, and fecal and urinary P excretion increased significantly ($p<0.05$) more in SHKR than in UHKR (Tables IA, IB). A significant correlation, $r = 0.93$, was present between decreased P absorption and decreased tissue P level, and increased plasma P levels and P excretion. Tissue P content, P absorption, plasma iPTH levels, plasma P levels, and P losses fluctuated during HK, but at no time did the measured parameters revert back to the control values (Tables IA, IB).

Post-hypokinetic phosphate changes with and without supplementation

Bone and muscle P content, P absorption, plasma iPTH levels, plasma P levels, fecal and urinary P excretion did not change in SVCR and UVCR compared with their pre-HK values (Tables IIA, IIB). Phosphate absorption increased significantly ($p<0.05$), and plasma P levels, fecal and urinary P excretion decreased significantly ($p<0.05$), while iPTH level, bone and muscle P levels remained significantly ($p<0.05$) depressed in SHKR and UHKR compared with their respective vivarium controls (SVCR and UHKR) (Tables IIa, IIb). However, P absorption increased significantly more, and plasma P levels, fecal and urinary P excretion decreased significantly more, while iPTH levels, bone and muscle P levels remained significantly more depressed in SHKR than in UHKR (Tables IIA, IIB). A significant correlation $r = 0.93$ was present between increased P absorption and decreased tissue P content, plasma P level and P loss. Bone and muscle P content, P absorption, plasma iPTH levels, plasma P levels, fecal and urinary P excretion in SHKR and UHKR fluctuated throughout the initial 9-days of post-HK but at no time did these values

TABLE IIA. Absorption, plasma, urine, feces, gastrocnemius muscle and femur bone phosphate levels measured in rats during vivarium control and post-hypokinesia.

Days	Absorption (%)	Plasma (mmol/L)	Urine (mmol/day)	Feces (mmol/day)	Gastrocnemius Muscle (mEq/kg dry tissue)	Femur Bone (mg/100 g ash)
			Unsupplemented Vivarium Control Rats (UVCR), n = 6			
2nd	65 ± 3	2.05 ± 0.05	2.17 ± 0.2	4.54 ± 0.24	4.05 ± 0.2	20.7 ± 0.4
3rd	64 ± 3	2.04 ± 0.03	2.16 ± 0.3	4.55 ± 0.22	4.06 ± 0.5	20.6 ± 0.2
5th	65 ± 4	2.05 ± 0.04	2.17 ± 0.4	4.54 ± 0.23	4.07 ± 0.6	20.7 ± 0.5
7th	63 ± 2	2.04 ± 0.03	2.16 ± 0.3	4.55 ± 0.20	4.06 ± 0.3	20.5 ± 0.6
9th	65 ± 3	2.05 ± 0.04	2.17 ± 0.2	4.54 ± 0.24	4.05 ± 0.4	20.7 ± 0.4
11th	63 ± 3	2.04 ± 0.05	2.16 ± 0.3	4.55 ± 0.21	4.06 ± 0.5	20.5 ± 0.3
15th	65 ± 2	2.05 ± 0.04	2.17 ± 0.2	4.54 ± 0.23	4.07 ± 0.4	20.6 ± 0.5
			Unsupplemented Hypokinetic Rats (UHKR), n = 6			
2nd	80 ± 5*	1.42 ± 0.03*	1.51 ± 0.7*	3.16 ± 0.23*	3.44 ± 0.6*	16.9 ± 0.5*
3rd	77 ± 4*	1.44 ± 0.04*	1.53 ± 0.5*	3.17 ± 0.23*	3.45 ± 0.4*	17.0 ± 0.3*
5th	82 ± 6*	1.40 ± 0.05*	1.48 ± 0.7*	3.11 ± 0.22*	3.43 ± 0.7*	16.7 ± 0.4*
7th	78 ± 3*	1.44 ± 0.04*	1.54 ± 0.4*	3.15 ± 0.24*	3.44 ± 0.4*	17.2 ± 0.5*
9th	81 ± 4*	1.41 ± 0.03*	1.50 ± 0.5*	3.13 ± 0.23*	3.42 ± 0.5*	16.8 ± 0.3*
11th	56 ± 3	1.89 ± 0.05	1.91 ± 0.6	3.84 ± 0.24	3.86 ± 0.3	18.8 ± 0.5
15th	48 ± 2	2.05 ± 0.03	1.18 ± 0.4	4.57 ± 0.22	3.98 ± 0.2	19.7 ± 0.4
			Supplemented Vivarium Control Rats (SVCR), n = 6			
2nd	66 ± 4	2.16 ± 0.04	2.45 ± 0.5	5.20 ± 0.23	4.22 ± 0.4	21.4 ± 0.6
3rd	64 ± 3	2.15 ± 0.05	2.41 ± 0.3	5.17 ± 0.21	4.21 ± 0.5	21.3 ± 0.4
5th	65 ± 3	2.16 ± 0.03	2.38 ± 0.6	5.20 ± 0.22	4.22 ± 0.3	21.4 ± 0.5
7th	65 ± 2	2.14 ± 0.04	2.41 ± 0.5	5.25 ± 0.24	4.23 ± 0.6	21.0 ± 0.4
9th	64 ± 4	2.15 ± 0.03	2.36 ± 0.4	5.17 ± 0.21	4.20 ± 0.2	20.8 ± 0.6
11th	65 ± 3	2.14 ± 0.05	2.40 ± 0.3	5.24 ± 0.22	4.18 ± 0.4	20.6 ± 0.3
15th	66 ± 2	2.13 ± 0.03	2.38 ± 0.5	5.18 ± 0.23	4.19 ± 0.3	20.3 ± 0.4
			Supplemented Hypokinetic Rats (SHKR), n = 6			
2nd	95 ± 5*+	1.25 ± 0.03*+	1.05 ± 0.5*+	2.17 ± 0.24*+	3.13 ± 0.5*+	15.2 ± 0.4*+
3rd	93 ± 4*+	1.26 ± 0.04*+	1.09 ± 0.4*+	2.23 ± 0.22*+	3.14 ± 0.6*+	15.4 ± 0.5*+
5th	97 ± 6*+	1.23 ± 0.05*+	1.03 ± 0.6*+	2.10 ± 0.20*+	3.10 ± 0.5*+	14.8 ± 0.3*+
7th	95 ± 4*+	1.25 ± 0.04*+	1.06 ± 0.5*+	2.15 ± 0.21*+	3.13 ± 0.4*+	15.0 ± 0.5*+
9th	96 ± 5*+	1.22 ± 0.03*+	1.04 ± 0.4*+	2.12 ± 0.26*+	3.11 ± 0.5*+	14.9 ± 0.3*+
11th	59 ± 3	1.84 ± 0.05	1.85 ± 0.5	3.66 ± 0.03	3.84 ± 0.3	18.4 ± 0.5
15th	51 ± 3	2.05 ± 0.03	2.30 ± 0.5	5.04 ± 0.04	4.03 ± 0.3	19.7 ± 0.4

All values are expressed as mean ± SD.

*$p < 0.05$ significant differences between vivarium control and hypokinetic groups of rats. Each of the hypokinetic groups was compared with their respective controls (UVCR *vs* UHKR and SVCR *vs* SHKR).

+$p < 0.05$ significant difference between supplemented and unsupplemented hypokinetic groups.

TABLE IIB. Parathyroid hormone levels (ng/dL) measured in rats during vivarium control and post-hypokinetic conditions

	Unsupplemented		Supplemented	
Days	Vivarium Control Rats (UVCR)	Hypokinetic Rats (UHKR)	Vivarium Control Rats (SVCR)	Hypokinetic Rats (SHKR)
Pre-HK	0.45 ± 0.03	0.45 ± 0.04	0.46 ± 0.02	0.46 ± 0.04
2nd	0.46 ± 0.03	0.32 ± 0.05*	0.43 ± 0.03	0.22 ± 0.02*$^{+}$
3rd	0.45 ± 0.04	0.33 ± 0.03*	0.44 ± 0.04	0.23 ± 0.03*$^{+}$
5th	0.46 ± 0.03	0.30 ± 0.04*	0.43 ± 0.03	0.20 ± 0.05*$^{+}$
7th	0.45 ± 0.05	0.33 ± 0.03*	0.44 ± 0.05	0.24 ± 0.03*$^{+}$
9th	0.46 ± 0.03	0.31 ± 0.02*	0.45 ± 0.03	0.21 ± 0.04*$^{+}$
11th	0.45 ± 0.04	0.39 ± 0.05	0.43 ± 0.02	0.37 ± 0.05
15th	0.46 ± 0.05	0.44 ± 0.04	0.44 ± 0.04	0.39 ± 0.04

*, $^{+}$, S.D., as in Table I.

revert back to the control values (Tables IIA, IIB). However, as the duration of post-HK increased muscle and bone P content, plasma iPTH levels, plasma P levels, fecal and urinary P excretion increased, and P absorption decreased progressively and by the15th day of post-HK approached the control values (Tables IIA, IIB).

Discussion

Phosphate deposition with and without phosphate supplementation during pre-hypokinesia

Plasma P levels in supplemented and unsupplemented hypokinetic and control groups of rats did not show any increase; this is because the ingested P amount was retained by the body and was taken up for deposition in tissue (4, 5, 15–17). Stable plasma P level shows that P as a consequence of normal motor activity is readily bound to tissue, which means that P is deposited in tissues (4, 5, 15–17). Intake of P supplementation shows that when animals receive large P amounts, while their motor activity is normal, plasma P concentration does not increase, because a significantly greater P amount is deposited in tissues.

Parathyroid hormone changes with and without phosphate supplementation during hypokinesia

With tissue P depletion plasma iPTH levels decreased while significant differences from control values in renal tubular maximum for P were observed. PTH favor the translocation of P in plasma and responds to a plasma P change, so that a constant plasma P level is maintained (4, 5), however, during HK and tissue P depletion the role of PTH still remains confusing. With tissue P depletion iPTH levels should have increased, because it is known that a modest decrease in tissue P content is rapidly followed by significant secretion and/or synthesis of PTH. However, tissue P depletion in hypokinetic rats suppressed iPTH secretion, although the effect of lower plasma iPTH on renal handling of P is char-

acterized by the ability of renal tubules to reabsorb P (4, 5). If iPTH had played any part in the renal handling of P, a similar effect in the renal handling of P would be expected with tissue P depletion. However, findings show that with tissue P depletion iPTH did not play any important role in renal handling of P. Increase of P loss could not have been attributable to the decreased plasma iPTH levels because no clear-cut relation was present between decreased plasma iPTH levels and increased P loss. This means that the increase of P loss was primarily attributable to decreased P deposition inherent to HK (4, 5, 9–11).

Phosphate deposition with and without phosphate supplementation during hypokinesia

During normal muscular activity P consumption in large amounts usually contributes to over absorption and uptake of P, while during HK no matter if animals or humans ingest large or small P amounts, absorption and uptake of P is depressed (15–17). Tissue P depletion during normal muscular activity is normally accompanied by an increase of P absorption and uptake, however, tissue P depletion during HK, is associated with a decrease of P absorption and uptake (15–17). During pre-HK, P supplementation was deposited to a significant extent in bone and muscle that protected plasma P from any increase.

It is interesting that hypokinetic rats have shown a decrease of P content in bone and muscle regardless of their type of functional activity and morphological characteristics. Generally minerals are decreased most in muscle and bone that have a support function (4, 5). The severity of decreased muscle and bone P content was different in gastrocnemius muscle and right femur with different function and morphology, and P level decreased most in gastrocnemius muscle and least in right femur. The mechanism of decreased P content in bone and muscle with different function and morphology is not clear; there are grounds to conclude that decreased tissue mineral content is attributable to many factors (4, 5, 9–11). Decreased tissue mineral content is probably attributable to increased mineral losses due to decreased mineral deposition (4, 5, 9–11). This is possibly ensured by the new level of endocrine mineral control mechanisms, decreased tissue mineral utilization and decreased bone and muscle cell mass (4, 5). Thus, decreased tissue P content is attributable to higher P losses primarily due to decreased bone and muscle P deposition regardless the type of their function and morphology. The severity of decreased tissue P content shows the magnitude of diminished muscular activity and decreased mechanical load in right femur and gastrocnemius muscle and thus intensity of decreased P deposition (4, 5, 9–11).

The significant increase of P excretion in the face of a significant decrease of tissue P content is a striking abnormality. Hypokinetic rats showed excessive P loss with decrease in bone and muscle P level compared with their pre-HK values and the values in control rats. This shows that hypokinetic rats experienced a decrease of P deposition (4, 5). Evidently, P intake regardless of its amount, cannot be deposited in the body unless factors contributing to decreased P deposition are totally reversed. Measuring the 24 h P intake and P losses, it was shown that the lower P deposition, the higher P loss and the lower tissue P content. Failure of P to be deposited in the body with tissue P depletion made it possible to show that tissue P depletion is not so much a matter of P shortage and P imbalance in the diet as decreased ability of the body to utilize P (15–17). Although there is convincing evidence of the role of HK in the genesis of the decrease of P deposition the mechanism for this remains unclear. However, it is clearly established

that prolonged HK is a factor of higher risk for decreased P deposition and excessive P losses with tissue P depletion.

A higher P loss with lower tissue P content has been shown with P supplementation than without supplementation. The higher P intake with lower tissue P content intensified P losses compared with lower P intake and lower tissue P content. This resembles a vicious circle, that is, the higher P intake, the lower tissue P content and the higher P loss in SHKR than in UHKR. Because SHKR experienced higher P loss with lower tissue P content than UHKR it was concluded that the more P consumed the more efficiently P is cleared from the blood stream and the more readily P is lost, thus the less likely it is to normalize tissue P level. It is unknown why SHKR with lower tissue P content would have shown greater P losses than UHKR. However, there is published evidence which suggest that regardless of the intensity of P imbalance, a higher as opposed to a lower P intake contributes to higher P loss (15–17). Moreover, a high P intake has increasingly been recognized as an important determinant of a higher P excretion with P imbalance (15–17). Because of decreased P utilization a higher P intake may place severe stress on the body contributing to impaired P deposition and excessive P losses (15–17). The higher P losses with lower tissue P content is more likely to be attributable to the lower P deposition with P supplementation than without supplementation.

Phosphate absorption with and without phosphate supplementation during post-hypokinesia

Decrease of P excretion during post-HK is indicative of tissue P depletion during HK because decreased P excretion develops with tissue P depletion unless other overriding factors coexist (9–11). Measuring the 24 hour P intake and P excretion during post-HK, it was shown that the higher P absorption, the lower P loss and the greater tissue P depletion. Continuing P absorption during post-HK shows the intensity of tissue P depletion during HK. During the initial 9-days of post-HK, the decrease of P excretion was probably directed towards counteracting tissue P depletion, while increased P absorption during the subsequent days could have resulted from decreased tissue P content and/or resumption of motor activity (9–11). If hypokinetic rats had not experienced tissue P depletion they could not have shown a decrease of P excretion during post-HK. Continuing decrease of bone and muscle P content and decrease of P excretion during post-HK shows the magnitude of tissue P depletion during HK. When tissue P content started to increase, as the duration of post-HK period increased, tissue P content increased progressively and by the end of the post-HK period approached the control values.

Because P supplementation failed to affect tissue P depletion during HK and muscle and bone started to be repleted with P only during post-HK, it was concluded that tissue P depletion cannot be normalized with daily P supplementation unless P deposition and motor activity are restored (9–11). In favor of this are many facts available, for instance, the intake of a daily P supplementation did not normalize bone and muscle P content during HK until P deposition and motor activity were restored during post-HK. During post-HK, P absorption increased, while tissue P content remained significantly depressed. This shows that during HK tissue P content could not reach a certain degree of normalcy with P supplementation and P could not be deposited in the body. Significant increase of P absorption during post-HK could certainly have been attributable to the tissue P depletion during HK, because increase of mineral absorption is associated with tissue mineral depletion

(4, 5, 9–11). Increase of P absorption during post-HK and P supplementation evidently had been attributable to decrease of tissue P level during HK. However, because of the presence of several biochemical and hormonal factors known to affect bone and muscle P content, it is difficult to prove the unequivocal causal role of HK and P supplementation in the genesis of tissue P depletion in such highly complex settings.

In contrast to other non-hypokinetic and P supplementation studies with animals, P supplementation did not affect tissue P content during HK. Differences between P deposition and level of motor activity could have inhibited the effect of P supplementation on tissue P content (4, 5, 9–11). Thus, P supplementation would fail to prevent tissue P depletion in animals forced to restrict their motor activity, allowing cell mass and P deposition to decrease further (4, 5). Several other potential factors could have been present which could have inhibited the effect of P supplementation on tissue P content (4, 5). However, the mechanisms by which SHKR and UHKR experienced higher P loss with lower tissue P content than SVCR and UVCR remains unclear. Many mechanisms have been proposed to explain the cause of increased mineral losses with tissue mineral depletion during prolonged HK (4, 5, 9–11). Chief among these is 1) diminished size of ion pool of cells, 2) decreased bone cell mass (decreased bone matrix), and change in mineral level of cells, 3) injury of skeletal muscle cells that changes the integrity of sarcolemma and leads to release of intracellular electrolytes in plasma and 4) decreased tissue cell mass that results in diminished holding capacity for minerals (4, 5). Studies have shown that decreased tissue cell mass is probably the main contributor for decreased deposition and the main factor of electrolyte loss with tissue electrolyte depletion during prolonged HK (4, 5). Thus, the biological mechanisms and the potential effects of decreased P deposition on tissue P depletion may be found at the cell level.

Conclusion

The increase of P excretion with decrease of tissue P content demonstrates decreased P deposition. Significantly higher P excretion with significantly lower tissue P content in SHKR than in UHKR demonstrates that P deposition is decreased more with than without P supplementation. Because SHKR with a lower tissue P content showed higher P excretion than UHKR it was concluded that the risk of decreased P deposition with greater tissue P depletion is inversely related to P intake, that is, the higher P intake the greater the risk for decreased P deposition and the greater tissue P depletion. It was shown that P, regardless the intensity of its tissue depletion, is lost during HK unless factors contributing to the decreased P deposition are partially or totally reversed as was demonstrated in this study. It was concluded that dissociation between decreased tissue P content and increased P losses from the body indicates decreased P (absorption and) deposition as the main mechanism of tissue P depletion during prolonged HK.

References

1. Zorbas, Y.G., Ivanov, A.L. and Fujiyama, Y. N. (1990) Electrolyte content in organs and tissues of rats during and after hypokinesia. *Materia Medica Polona 22:* 263–266.
2. Zorbas, Y.G., Verentsov, G.E., Bobylev, V.R., Yaroshenko, Y.N. and Federenko, Y.F.

(1996) Electrolyte metabolic changes in rats during and after exposure to hypokinesia. *Physiol. Chem. Phys. Med. NMR 28:* 267–277.
3. Zorbas, Y.G., Kakurin, V.J., Kuznetsov, N.A. and. Deogenov, V.A (2004) Electrolyte content determination in skeletal bone of rat for disclosing mineral depletion during prolonged hypokinesia. *Trace Elements and Electrolytes 21:* 220–228.
4. Krotov, V. P. (1978) Kinetics and regulation of fluid and electrolytes metabolism in animals and human beings during prolonged hypokinesia. PhD thesis, Interkosmos Council, Academy of Sciences USSR and Directorate of Kosmic Biology and Medicine, Ministry of Health USSR, Moscow, Russia.
5. Volozhin, A.V. (1987) Pathogenesis of disturbances of calcium metabolism in mineralized tissues during long-term hypokinesia. PhD thesis, Interkosmos Council, Academy of Sciences USSR and Directorate of Kosmic Biology and Medicine, Ministry of Health USSR, Moscow, Russia.
6. Katz, B. (1968) *Nerves, Muscles and Synapses.* Meditsina Press, Moscow, Russia.
7. Dee, E. and Kerman, R. P. (1963) Energetics of sodium transport in ram puppies. *J. Physiol.* (London) *165:* 550–558.
8. Ling, G. N. (1997) Debunking the alleged resurrection of the sodium pump hypothesis. *Physiol. Chem. Phys. Med. NMR 29:* 123–198.
9. Zorbas, Y.G., Kakurin, V.J., Afonin, V.B., Denogradov, S.D. and Neofitov, A.C. (2002) Muscle electrolyte measurements during and after hypokinesia in determining muscle electrolyte depletion during hypokinesia in rat. *Biological Trace Element Research 90:* 155–1743.
10. Zorbas, Y.G., Yaroshenko, Y.Y., Kuznetsov, N.K., Madvedev, S.N. and Federenko, Y.F. (1997) Electrolyte concentration in skeletal muscles and plasma of rats during and after exposure to hypokinesia and hyperhydration. *Physiol. Chem. Phys. Med. NMR 29:* 243–259.
11. Zorbas, Y.G., Ivanov, A.L. and Federenko, Y.F. (1995) Electrolyte and water content in organs and tissues of rats during and after exposure to prolonged restriction of motor activity. *Rev. Esp. Fisiol 51:* 155–162.
12. Zorbas, Y.G., Kakurin, V.J., Afonin, V.B., Charapakhin, K.P., Yarullin, V.L. and Deogenov, V.A. (2000) Calcium measurements in calcium supplemented primates during and after hypokinesia in establishing calcium deficiency during prolonged hypokinesia. *Biological Trace Element Research 75:* 113–131.
13. Zorbas, Y.G., Federenko, Y.F. and Togawa, M.N. (1990) Effect of fluid and salt supplements in preventing the development of osteopenia in hypokinetic rats. *Acta Astronautica. 25:* 111–116.
14. Zorbas, Y.G., Federenko, Y. F. and Naexu, K. A. (1994) Renal excretion of magnesium in rats subjected to prolonged restriction of motor activity and magnesium supplementation. *Magnesium-Bulletin 16:* 64–70.
15. Zorbas, Y.G., Kakurin, V.J., Kuznetsov, N.A., Yarullin, V.L., Andreyev I.D. and Charapakhin, K.P. (2002) Phosphate deposition capacity of athletes during hypokinesia, phosphate loading, and ambulation. *Biological Trace Element Research 85:* 211–226.
16. Zorbas, Y.G., Andreyev, V.G. and Federenko, Y.F. (1991) Morphological changes in rat kidney after hypokinesia and phosphorus supplement. *Urologia 39:* 254–260.
17. Zorbas, Y.G., Kakurin, V.J., Kuznetsov, N.A., Yarullin, V. L., Andreyev, I.D. and Charapakhin, K.P. (2002) Phosphate measurements during hypokinesia and phosphate supplements in disclosing phosphate changes in hypokinetic subjects. *Panminerva Med 44:* 243–251.
18. Fedorov, I.V. (1980) Biochemical basis of pathogenesis of hypokinesia. *Kosmicheskaya Biol 3:* 3–10.
19. Zorbas, Y.G., Verentsov, G.E. and Federenko, Y.F. (1995) Renal excretion of end products of protein metabolism in urine of endurance trained subjects during restriction of muscular activity. *Panminerva Med 37:* 109–114.

Received April 27, 2004;
accepted October 18, 2004.

Physiol. Chem. Phys. & Med. NMR (2004) *36*: 123–131

Temperature Distribution and Electrical Properties Along the Oriental Hornet Body

Dmitry V. Galushko[1,2,], Natalya Y. Ermakov[1], David J. Bergman[2], Jacob S. Ishay[1*]**

[1]*Department of Physiology and Pharmacology, Sackler Faculty of Medicine, Tel Aviv University, Tel Aviv 69978, Israel,* [2]*School of Physics and Astronomy, Raymond and Beverly Sackler Faculty of Exact Sciences, Tel Aviv University, Tel Aviv 69978, Israel*
**Author for correspondence, e-mail: physio7@post.tau.ac.il*
***Part of a PhD thesis to be submitted by D.V. Galushko to the Tel-Aviv University Senate*

Abstract: The hornet is an endothermic insect. Daily variations in hornet surface temperature were measured. Three peaks were found between 9: 30 and 10: 30 a.m., 11 and 12 a.m. and between 2 and 3 p.m. Electrical current and voltage values were highest along the head. Electrical current along the gaster and the head flowed towards the thorax, i.e., from body parts with minimal temperature towards the body part with maximal temperature. Current and voltage values measured *across* the cuticle of the gaster were about 5nA and 100 mV, respectively, and these were of the same order of magnitude as the current and voltage values *along* the cuticle. It was found that: 1) temperature regulation most probably originates in the thorax and 2) there is a correlation between the temperature distribution along the hornet body surface and levels of the cuticular electrical signals.

THE TEMPERATURE in nests of the Oriental hornet (*Vespa orientalis* L., Hymenoptera, Vespinae) is almost constant and not influenced by changes in the ambient temperature (Ishay and Ruttner, 1971; Guiglia, 1972; Spradbery, 1973; Edwards, 1980; Matsuura and Yamane, 1990). The temperature of the individual hornet outside the nest, however, changes in accordance with the ambient air temperature (Heinrich, 1981). Thermal photographs of isolated hornets taken with infrared camera by Litinetsky *et al*. (2001) showed that the temperature of hornet body parts was higher than the ambient temperature. Subsequently, however Ishay *et al*. (2003) found that the temperature of certain parts of the vespan cuticle may be below the ambient temperature, which suggested that a natural thermoelectric heat pump was the mechanism that cooled the hornet body. The electrical properties of hornet cuticle have been previously investigated (Ishay *et al*., 1991; 1992; 1993; 1995; Ishay and Litinetsky, 1996; Kristianpoller *et al*., 1997) and it has been shown, that these properties were similar to those of some organic semiconductors (Aschcroft and Mermin, 1976; Gutmann *et al*., 1983; Rowe, 1995; Tritt, 1997).

In the present study we measured the temperature distribution along the body parts of the hornet at different hours of the day. This was done in an attempt to detect a prime organ for thermoregulation and a possible correlation between the temperature distribution along the hornet body surface and the distribution of spontaneous voltage and current values.

Materials and Methods

All measurements were carried out on live adult hornets (workers, males and young queens, all together 89 specimens were used) originally collected from nests in the field in the Tel-Aviv area during the hornet active season (July–November) by the method described by Ishay (1964). The Oriental hornet is a colorful insect: most of its body is brown in color but two segments of its gaster are yellow and so also some plates on its head. In the brown body parts the pigment is melanin but in the yellow stripes on the gaster there are yellow granules under the transparent cuticle and these are composed of purines and pteridines (Becker, 1937; Ishay *et al*., 1991; Kristianpoller *et al*., 1997).

Test specimens were picked up by a thin rubber holder from among a group of hornets and placed on a heat-insulating (foamed plastic) holder. Measurements were made under laboratory conditions, in the shade, but with open windows so the hornet could sense the solar radiation, at an ambient temperature of 24°C (imposed by air conditioning of the animal house). A digital thermometer (Neutron TM-5007) with two thermocouples (accuracy of 0.1°C) was used for temperature measurements on the surface of the insect body.

In order to ascertain the origin of the thermoregulation control signal the head of three queens was separated from the rest of the body by a silk thread ligature made between the head and the rest of the body. The temperature along the body was measured before and after the ligature as well as after removal of the ligature. Temperature was recorded along the body surface on the head, thorax and gaster of 13 males. This was done first on the intact insects, and next they were dissected, their wounds blocked by liquid (warmed) beeswax and the temperature then measured on each of the separate sections (head, thorax and gaster).

In order to measure voltage and current, alligator clips were fastened onto the points of the cuticle surface to be measured. The clips, in turn, were connected to an electrometer (Keithley 617, accuracy 0.1%). Electrometer data were recorded by a computer (Pentium-IV, communication Protocol IEEE 488 GPIB). Special plane and point probes were used for electrical measurements *across* the cuticle (instead of the alligator clips). Electrical measurements were made in the dark, whereas all other measurements were carried out under illumination by fluorescent white light of app. 700 Lux. Statistical analyses were made using the program Origin 6.1 (Microcal). The average value was calculated as a geometric mean.

Results

Temperature distribution along the hornet body surface was investigated in 29 hornet specimens and all the recorded temperatures were found to be higher than the temperature of the surrounding air. Mean temperature distribution is given in Figure 1A ($n = 29, SD = 0.41$). As can be seen in the figure, the thorax temperature was highest while the head temperature was usually the lowest. The difference between body temperature

(T_{body}) and ambient temperature (T_{air}) (i.e., ΔT) was about 3.5°C on the average, but occasionally differences as high as 7°C were recorded (usually on the thorax).

The daily variation differences between T_{body} and T_{air} for head, thorax and gaster were also measured [Figures 1B–1D, n = 30; Figure 1B (head) SD = 0.70; Figure 1C (thorax) SD = 0.44; Figure 1D (gaster) SD = 0.54]. In this regard, three variance sinusoid-like curves were recorded. In every curve there are three peaks, the first and second of which were noted in the morning and near noon, while the third occurred between 1 and 3 p.m. As can be seen, throughout the range of temperatures recorded the hornet body temperature was invariably higher than the ambient temperature.

The possible connection between body temperature and spontaneous voltage and current was investigated *along* the hornet body surface. Histograms of mean values of spontaneous voltage and current along the cuticle are given in the Figure 1E. Voltage (n = 15, SD = 0.34) and current (n = 12, SD = 0.25) levels were highest on the head. Note, that both the current along the gaster and that along the head flows toward the respective juncture with the thorax. Current and voltage in a direction perpendicular to the cuticle surface were also measured in the gaster, and as seen in Table I, they were of the same order of magnitude as those along the surface of the cuticle. The interior of the cuticle was usually electrically positive i.e., in these specimens the current (electrons) flows from the outer

TABLE I. Values of spontaneous voltage and current in cross section of cuticle in the gaster region of the hornet body

Sample N	Caste	Interior electrode on the stripe	Exterior electrode on the stripe	Sign of signals at the interior electrode	Voltage† mV	Current† nA
1	queen	yellow*	yellow	–	180	0.1
2	worker	brown	yellow	+	85	5
3	male	yellow	brown	+	80	4
4	worker	yellow	brown	-	50	1.4
5	male	yellow	yellow	+	150	12
6	queen	yellow	yellow	+	55	6
7	male	yellow	yellow	+	70	1.3
8	male	yellow	yellow	+	100	
9	male	brown	brown	+	60	0.7
10	male	brown	brown	–	75	0.02
11	male	brown	brown	+	50	0.4
12	male	brown	brown	+	90	0.1
13	male	brown	brown	+	45	0.25
14	male	brown	brown	+	140	5
15	male	brown	yellow	–	80	
16	male	yellow	yellow	–	70	
Mean					*86*	*2.8*
SD					*39*	*2.4*

†Maximal recorded voltage was 180mV and maximal current was 12nA, which means that the voltage the current *across* the cuticle may be of the same order of magnitude as the voltage and current *along* the cuticle (see Figure 1E).

* The hornet cuticle is largely brown in color with the responsible pigment being melanin , but there are also yellow-colored stripes on the gaster in which the contributory yellow pigments are purines and pteridines.

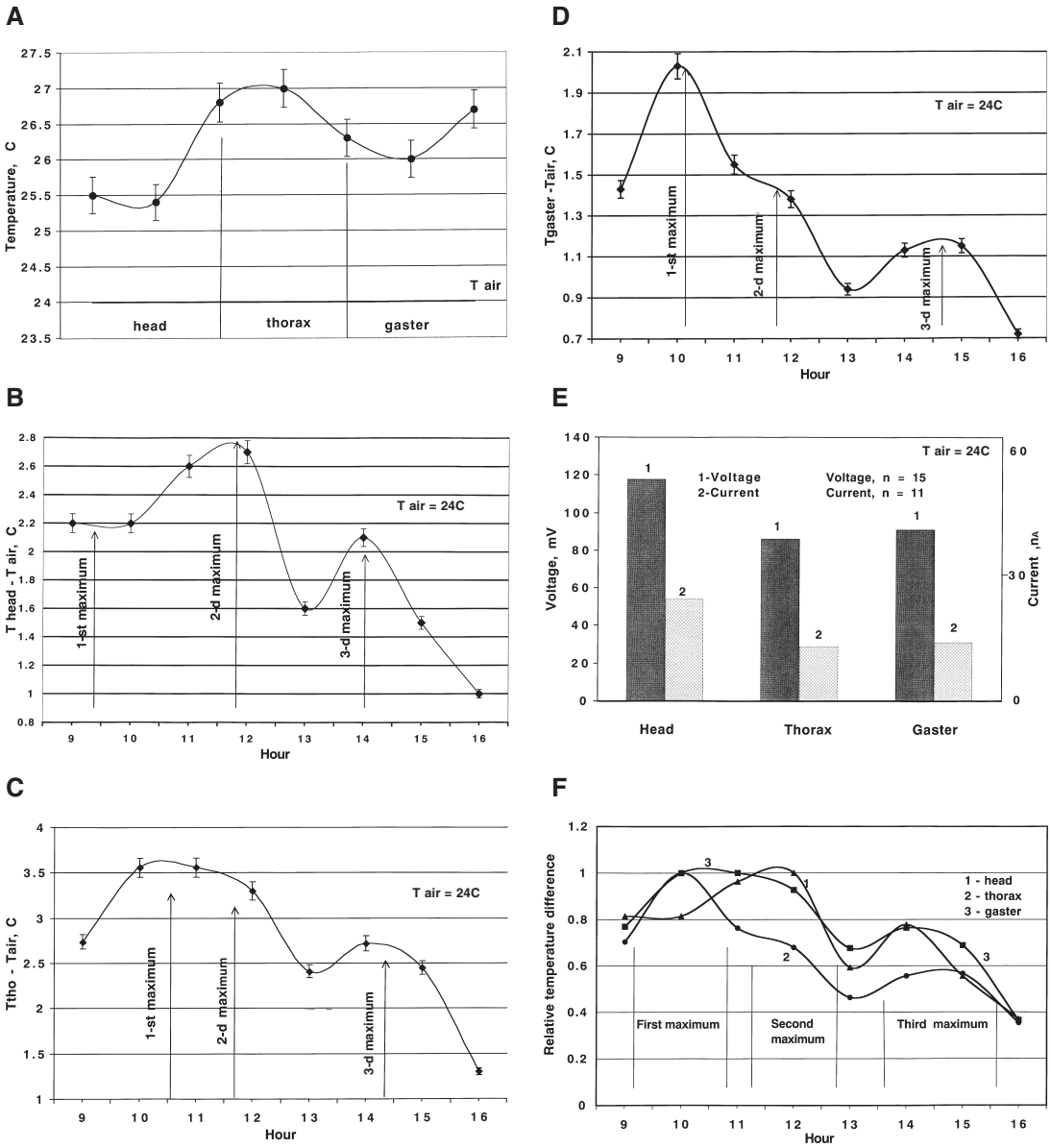

FIGURE 1. **A**) Average temperature distribution along the hornet body. Note that the thorax is the warmest area, the head is the coldest and the gaster temperature is intermediary between the T_{thorax} and T_{head}; n = 29, SD = 0.41. **B**) Mean head temperature as a function of the time of day. The first maximum is not distinct; the main (second) maximum corresponds with the peak solar UV-radiation; and the third maximum occurs at maximum ambient air temperature. n = 30, SD = 0.70. **C**) Average thorax temperature as a function of the time of day. The main (first) maximum is at about 10:30 a.m., the second is at 11:30 a.m. and the third is at about 2:30 p.m. n = 30, SD = 0.44. **D**) Average gaster temperature as a function of the time of day. The main (first) maximum is at about 10:15 a.m., the second is at about 11:30 a.m. and the third is at about 2:30 p.m. n = 30, SD = 0.54. **E**) Average values of spontaneous voltage and current along the cuticle for different parts of the hornet body (head, thorax and gaster). Spontaneous voltage and current were maximum on the head, while values on the thorax and gaster were lower and approximately equal. **F**) Superposition of the graphs of daily variations of temperature for different parts of the hornet body. The curves numbered 1–3 show relative variations of temperature difference for hornet bodily parts. As can be seen there are three maxima on every curve, but the first maximum from the head area is not prominent and is rather very close to the first maximum from the thorax area. The ratio of values of the second and third maxima for curves ($T_{tho} - T_{air}$) and ($T_{gaster} - T_{air}$) was about 1.3/1, i.e. the same as for curve ($T_{head} - T_{air}$). Measurements were performed in September and October 2003.

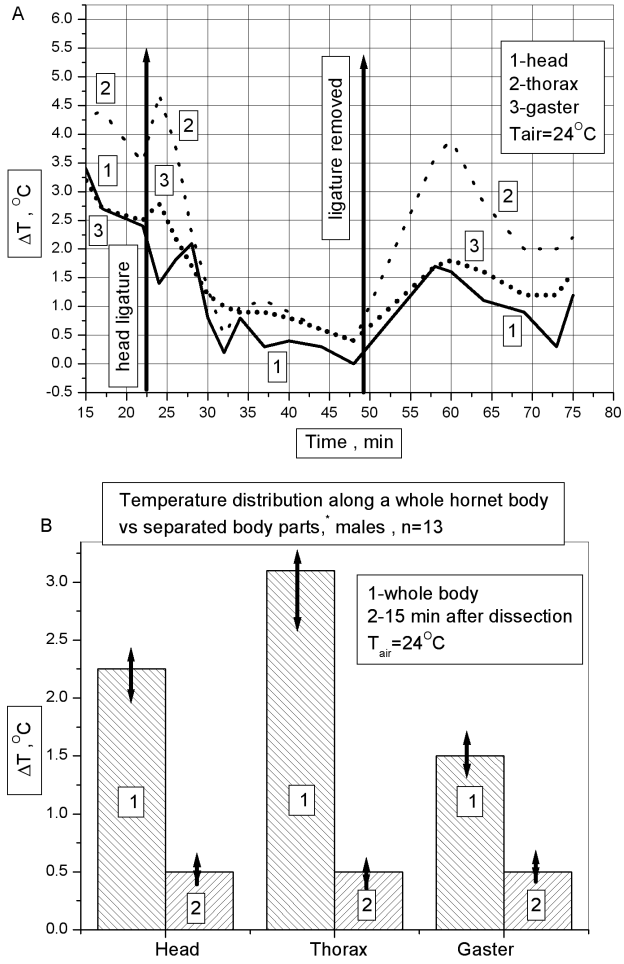

FIGURE 2. **A**) Temperature difference between hornet body parts and ambient air (ΔT) before and after ligature. Ligature *via* silk wire was made between head and rest of the hornet body. Prior to ligating, the ΔT for head, thorax and gaster were 3.5°C, 4.5°C and 3.2°C respectively, after ligating the ΔT decreased to a mere 0.2–0.5 °C for all parts and following removal of the ligature the ΔT increased again to 1.3–2.0°C. **B)** Temperature distribution along the entire body in an intact hornet and in separated body parts. ΔT is the difference between the temperature of the hornet body and the ambient temperature. The body temperature before dissection was higher by 1.5–3.0°C than the surrounding temperature, but within in 15 min after sectioning the ΔT dropped to about 0.5°C. Experiment performed during November 2003.

site to the inner site, but in some specimens it was negative. We were puzzled by these temperature differences between the various body parts of the hornet and also those between the body as a whole and the environment. In an attempt to unravel this puzzle, two experiments were undertaken. In the first, a ligature of silk wire was made between the head and the rest of the body in three young queens and their temperature was measured: a) 20 minutes before ligating their head; b) 25 minutes after ligating the head and c) 25 minutes after removing the ligature. The results are presented in Figure 2A. As can be seen, prior to ligating the head the temperature difference of the head (ΔT) was 3.5°C, after ligating the ΔT decreased to a mere 0.5°C and after removing the ligature the ΔT rose again to about 1.3°C.The similar procedure done with the gaster did not produce significant temperature difference before and after legation.

From this experiment it would seem that the origin of the signal for body thermoregulation is in the thorax.

In the second experiment, the body temperature of 13 males was measured before and after dissection and their ΔT was measured. Results are presented in Figure 2B. As can be seen, the body temperature before dissection was higher by 1.5–3.0°C than the surrounding temperature and 15 min after sectioning the ΔT dropped to about 0.5°C.

The electrical values recorded from the entire hornet body before and after sectioning have been measured and we found that 15 min after sectioning the voltage level in every sectioned part was not significantly different from that of the entire body; however, the current values were lower, namely: on the entire body they averaged 35nA, while in the sectioned parts they averaged only 12nA.

Discussion

Perusal of the curves of daily variation of the body temperature (Figures 1B–1D) reveals three sinusoidal maxima. However, in the curve for head temperature (Figure 1B) only two maxima of differing values are evident. The occurrence of the main maximum (at 11:30 a.m.) is congruent with the peak solar UVB ground radiation recorded in the Tel-Aviv area during August–October (Lubansky, 2003). The lesser maximum on the graph coincides with the daily maximum of ambient temperature (Riabinin *et al*., 2004). Increase of the ambient temperature may possibly boost hornet body temperature (and the temperature difference). The values of spontaneous voltage in hornet cuticle are proportional to values of the UVB irradiation (Ishay *et al*., 1991), and that finding suggests a connection between body temperature and spontaneous electrical voltage in Oriental hornet cuticle. We did not, however, expose hornets to direct UVB-radiation in the course of the present study, so it is conceivable that our specimens retained a prior memory of the daily rhythm of solar radiation, as a biological clock. The main maximum exceeded the afternoon maximum by a ratio of 1.3/1, suggesting that the temperature difference ($T_{head} - T_{air}$) is apparently more dependent on solar UVB-radiation than on the ambient temperature .

In the analogous curves for $T_{\mathbf{tho}}$ (Figure 1C) and $T_{\mathbf{gaster}}$ (Figure 1D) we observed an additional maximum at about 10 a.m., which was the highest in these body parts. If we superpose all the mentioned three graphs of daily variation in temperature (Figures 1B–1D) the following picture evolves (Figure 1F), to wit: there are three maxima on every curve, but the first maximum in the head area is not prominent and is in close proximity to the first maximum in the thorax area. It can be seen that the relative value of the first maximum rises when proceeding from the head to the gaster (i.e., $\Delta T_{\mathbf{relative}} = 0.81$, 0.95 and

1.00 for head, thorax and gaster respectively). The reason for that is not yet clear. It is noteworthy that the ratio between the values of the second and third maxima in Figure 1C ($T_{tho} - T_{air}$) and Figure 1D ($T_{gaster} - T_{air}$) was about 1.3 to 1.0 , i.e., the same as in Figure 1B ($T_{head} - T_{air}$).

The distribution of spontaneous voltage and current along the cuticular surface (Figure 1E) reveals that the maxima of voltage and current are recorded from the head cuticle, followed by lower levels measured in the gaster and thorax areas. We assume that the higher levels of electrical activity measured in the head area stem from two reasons: 1) because in the hornet the head is generating most of the electrical activity, some of which is transferred to the other body parts; and 2) the hornet head houses most of the sensory and motor systems of the body, which intercommunicate *via* electrical means. By ligating the head, the temperature difference (ΔT) in all body parts including the head decreases to about 0.5°C. If we assume that the head is signaling in some fashion (chemical or electrical) why is the head temperature dropping as well after the ligation procedure? Possibly because the other body parts, most probably the thorax, are also signaling to the head, whether intact or separated (feedback mechanism).

Note that the spontaneous voltage and current *across* and *along* the cuticle surface are approximately of the same order of magnitude, but in fact, perpendicular electrical fields are much greater .The electrical field is proportional to $1/\boldsymbol{l}$, where $\boldsymbol{l}$ is the distance between the electrodes. At measurements *along* the cuticle the distance is about 2 cm, but the distance *across* the cuticle is about 40 micrometers. Thus the electrical field *across* the cuticle is about 500 times higher than that *along* the hornet body (20.000μm/40μm). Thus the electrical field across the cuticle is in the range of 250V/cm while along the cuticle the value is 0.5V/cm.

It is worth mentioning that similar measurements have previously been performed on honeybees engaged in collecting nectar in the field during the spring and summer months (Kovac and Schmaranzer, 1996). The body temperature of these bees was usually found to be higher than that of the surroundings, with the thorax yielding the highest temperature and the gaster the lowest. Elsewhere (Inglis *et al*., 1996), grasshoppers have been reported to prefer hotter surroundings reminiscent of a behavioral fever response to infection and which was suggested by the authors to indicate that high temperature and thermoregulation could adversely affect mycoses. Cicadas, as well, are endothermic insects (Sanborn, 2000; 2003) that keep their body within a specific range of temperatures in order to promote and coordinate reproductive activity (Heath, 1967; 1972). Interestingly, it has been shown that many insects (both adult and immature) are able to maintain a body temperature higher than the ambient one when subjected to direct solar radiation (Bryant *et al*., 2002).

References

Aschcroft, M.W. and Mermin, N.D. (1976) *Solid State Physics*. Holt Saunders, Philadelphia, USA.

Becker, E. (1937) Über das Pterinpigment bei Insekten und die Färbung und Zeichnung von *Vespa* im Besonderen. *Z. Morph. Ökol. Tiere 32:* 672–751.

Bryant, S.R., Thomas, C.D. and Bale, J.S. (2002) The influence of thermal ecology on the distribution of three nymphalid butterflies. *J. Appl. Ecol. 39:* 43–45.

Edwards, R. (1980) *Social Wasps.* Rentokil Limited, East Grinstead.

Guiglia, D. (1972) *Les Guêpe Sociales*. Masson et Cie Eds, Paris.

Gutmann, F., Keyzer, H., Lyons, L.E. and Somoano, R.B. (1983) *Organic Semiconductors. Part B.* Robert E. Kriger Publishing Company, Malabar, Florida.

Heath, J.E. (1967) Temperature responses of the periodical "17-year" cicada, *Magicicada cassini* (Homoptera , Cicadidae). *Am. Midl. Nat. 77:* 64–67.

Heath, M.S. (1972) Temperature requirements of the cicada *Okanagana striatips beameri*: a study from Flagstaff. *Arizona Plateau 45:* 31–40.

Heinrich, B. (1981) *Insect Thermoregulation.* John Wiley and Sons, New York.

Inglis, G.D., Johnson, D.J. and Goettel, M.S. (1996) Effects of temperature and thermoregulation on mycosis by *Beauveria bassiana* in Grasshoppers. *Biological Control 7:* 131–139.

Ishay, J.S. (1964) Observations sur la biologie de la Guêpe orientale *Vespa orientalis* en Israël. *Insectes Sociaux XI(3):* 193–206.

Ishay, J.S. and Litinetsky, L. (1996) Thermoelectric current in hornet cuticle: morphological and electrical changes induced by temperature and light. *Physiol. Chem. Phys. & Med. NMR 28:* 55–67.

Ishay, J. and Ruttner, F. (1971) Die Thermoregulation im Hornissennest. *Z. v. Physiol. 72:* 423–434.

Ishay, J.S., Abes, A.H., Chernobrov, H.L., Ishay, I.Z. and Ben-Shalom, A. (1991) Electrical properties of the Oriental hornet (*Vespa orientalis*) cuticle. *Comp. Biochem. Physiol. 100A(2):* 233–271.

Ishay, J.S., Benshalom-Shimony, T., Ben-Shalom, A. and Kristianpoller, N. (1992) Photovoltaic effects in the Oriental hornet. *J. Insect. Physiol. 38(1):* 37–48.

Ishay, J.S., Shimony, T.B., Dabah, B., Shuzz, I.S, Shevach, Y., Shalom, A.B. and Paniry, V.B. (1993) Electrical properties of the cuticle, silk caps and comb of Oriental hornet *Vespa orientalis* (Hymenoptera : Vespidae). *Int. J. Insect Morphol. & Embryol. 22(2–4):* 127–144.

Ishay, J.S., Rosenzweig, E. and Fuksman, E. (1995) Thermo and photoelectric current in hornet cuticle. *Physiol. Chem. Phys. & Med. NMR 27(3):* 179–192.

Ishay, J.S., Pertsis, V., Rave, E., Goren, A. and Bergman, D.J. (2003) Natural thermoelectric heat pump in social wasps. *Physical Review Letters 90,(21):* 81021–81024.

Kovac, H., Schmaranzer, S. (1996) Thermoregulation of honeybees *(Apis mellifera*) foraging in spring and summer at different plants. *J. Insect Physiol. 42:* 1071–1076.

Kristianpoller, N., Weiss, D. and Ishay, J.S. (1997) Irradiation effects in the Oriental hornet. *J. Luminescence 74(6):* 591–592.

Litinetsky, L., Rosenberg, E. and Ishay, J.S. (2001) Thermal properties of hornet colonies: thermography of individual hornets and their nests and the role of the pupal silk in thermoregulation. *Physiol. Chem. Phys. & Med. NMR 33:* 103–118.

Lubansky, V. (2003) *Global radiation on the horizontal surface.* Bet Rad Meteorological Station.

Matsuura, M. and Yamane, S. (1990) *Biology of the Vespine Wasps*. Springer Verlag, Berlin.

Riabinin, K., Kozhevnikov, M. and Ishay, J.S. (2004) Ventilating activity at the hornet nest entrance. *J. Ethol. 22(1):* 49–53.

Rowe, D.M. (1995) *C.R.C. Handbook of Thermoelectrics*. CRC Press, Boca Raton, USA.

Sanborn, A.F. (2000) Comparative thermoregulation of sympatric endothermic and ectothermic cicadas (Homoptera: Cicadidae: *Tibicen winnemanna* and *Tibicen chloromerus*). *J. Comp. Physiol. A 186:* 551–556.

Sanborn, A.F., Villet, M.N. and Phillips, P.K. (2003) Hot-blooded singers : endothermy facilitates crepuscular signaling in African platypleurine cicadas (Hemiptera: Cicadidae: *Platypleura* spp.) *Naturwissenschaften 90:* 305–308.

Spradbery, J.P. (1973) *Wasps*. Sidgwick & Jackson, London.

Shimony, T.B. and Ishay, J.S. (1981) Thermolectrical (Seebeck) effect of the cuticle of social wasps. *J. Theor. Biol. 92:* 497–503.

Tritt, T.M. (1997) Thermoelectric materials — new direction and approaches. *Mat. Res. Soc. Symp. Proc*., p. 478.

Received: August 13, 2004;
accepted: January 24, 2005.

Physiol. Chem. Phys. & Med. NMR (2004) *36*: 131–141

Communication by Electrical Means in Social Insects

Dmitry V. Galushko[1,2], Natalya Y. Ermakov[1], David J. Bergman[2] and Jacob S. Ishay[1*]**

[1]*Department of Physiology and Pharmacology, Sackler Faculty of Medicine and*
[2]*School of Physics and Astronomy, Raymond and Beverly Sackler Faculty of Exact Sciences,*
Tel Aviv University, Ramat Aviv, 69978, Israel
** Author for correspondence, e-mail: physio7@post.tau.ac.il*
*** Part of the PhD thesis to be submitted by D.V. Galushko to the Tel-Aviv University Senate.*

Abstract: Social insects, belonging to the order Hymenoptera, maintain a fixed, optimal temperature in their nest. Thus, in social wasps and hornets, the optimal nest temperature is 29°C, despite the fact that they are distributed in regions of varying climates both in the northern and southern hemispheres of the globe. Since hornets and bees are relatively small insects, determination of their own body temperature as well as that of their nest and the brood was made *via* thermometers or by the use of infrared (IR) rays. It has been suggested that thermoregulation in social insect colonies is effected primarily by the adult insects *via* muscle activation, that is, fluttering of their wings, which can raise both their own and the ambient temperature by many degrees centigrade. However, the larval brood can also contribute to the thermoregulation by acting as heat resources and thereby raising the ambient temperature by 1–2°C. To this end, the adult hornets are endowed with a well-developed musculature and their larvae, too, have muscles that enable them to move about. Not so the hornet pupae which are enclosed in a silk envelope (the cocoon), with a rather thick silk cap spun by the pupating larvae, and have rather undeveloped muscles. In the latter instance, it stands to reason that the pupae benefit from the nest warming achieved primarily by the adult hornets, but how is the *information* regarding their thermal needs relayed from them to the adults?

Previously we showed that the adult hornets are attracted to the pupae by pheromones released by the latter, but such chemical compounds can only convey information of a general nature and we are still left with the question as to how the adult hornet can gauge or ascertain the temperature of a single insulated pupa. The present study provides evidence that the hornet pupa can indeed transmit information regarding its body temperature *via* electrical means.

ORIENTAL HORNETS are social insects which live in nest of large colonies numbering up to several hundred adults as well as brood. The temperature in their nests is almost constant and not influenced by the changes of the ambient temperature (Ishay and Ruttner

1971, Guiglia 1972, Spradbery 1973, Edwards 1980, Matsuura and Yamane 1990). The temperature of the individual hornet outside the nest changes in accordance with the ambient air temperature (Heinrich 1981). Thermal photographs of isolated hornets using infrared camera were taken by Litinetsky *et al*. (2001) and it was found that the temperature of the hornet body parts was higher than the ambient temperature. However, later (Ishay *et al.,* 2003) it was found for the first time, that the temperature of certain parts of the cuticle might be below the ambient temperature, and it was supposed that natural thermoelectric heat pump was the mechanism which cooled the hornet body. The electrical properties have been earlier investigated (Ishay *et al*. 1991, 1992, 1993, 1995, Ishay and Litinetsky 1996, Kristianpoller *et al.* 1997) and it has been shown, that these properties were similar to those of some organic semiconductors (Gutmann *et al.* 1983, Rowe 1995, Tritt 1997, Aschcroft and Mermin 1976). Thermoelectric effect was, also, found in the Oriental hornet cuticle (Shimony and Ishay 1981).

In earlier studies (Ishay and Ruttner 1971, Ishay 1973) we obtained visual evidence that adult Oriental hornets warm their own pupae while inside their cocoons (Figure 1a) or outside them by blowing on them warm air from their spiracles (Figure 1b), and even the pupa of another species of Vespinae (Figure 1d); moreover, they also warm a comb containing the egg-stage only (Figure 1c).

Earlier it was reported that the pupae are very sensitive to changes in temperature during the pupal stage and that deviations in their optimal temperature is damaging to their normal development and maturation (Ishay and Ruttner 1971). Pupae kept in conditions of hypothermia or hyperthermia may develop as short living adults or as adults with malformations — their wings and legs are damaged.

In all these instances, we established that the queen and the nursing worker hornets are attracted to the brood (be it egg or pupa) by pheromones released by the latter. But how do the attracted adults "know" how to warm the brood to optimal temperature? In the present paper we will try to answer this question.

Materials and Methods

All measurements were carried out on live adult hornets and their brood combs originally collected from nests in the field in the Tel-Aviv area during July–October by the method used by Ishay (1964). A digital thermometer (Newtron TM-5007) with two thermocouples (accuracy of 0.1°C) was used for temperature measurements. Measurements of voltage and current were made *via* a Keithley 617 electrometer connected to the computer. We used special plane and point probes for measurements of the pupa properties. Electrical and thermodynamic measurements were made in the dark. Thermodynamic recordings were made in the thermostat. The rate of heating was 1°C/min, and that of cooling was about 0.3°C/min. Schematic presentation of the methodology and sites used to measure voltage, current and resistance levels are given in Figure 2.

Results

Various species of Vespinae are afflicted by the parasitoid *Sphecophaga vesparum* that oviposits into vespan comb cells containing a larva about to pupate (Donovan 1991). At

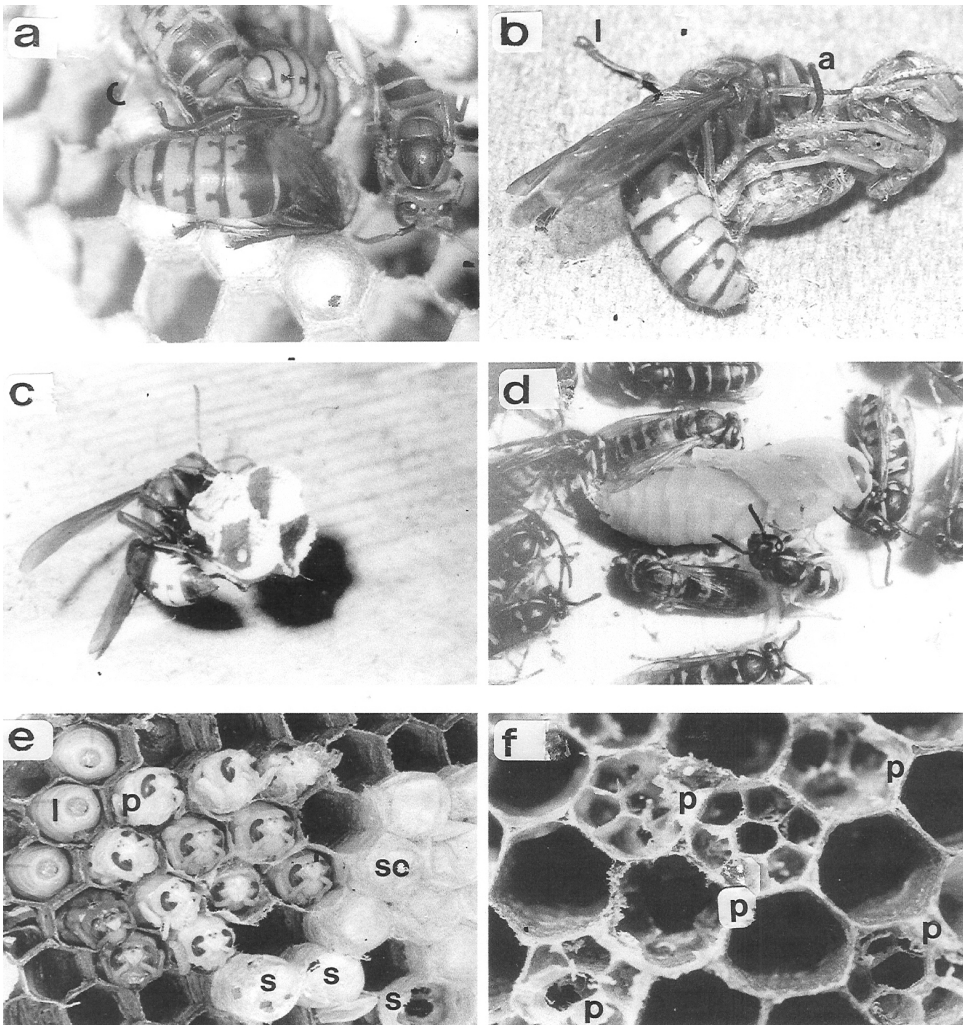

FIGURE 1. Photographs showing moments of interaction between adults and brood of social hornets: **a)** adult hornets (*Vespa crabro*) warming the pupae in a brood comb. **b)** adult hornet (*V. crabro*) warming a pupae extracted from its comb cell; the warming will proceed up to 29°C, which is the optimal temperature in a hornet nest. Note that the adult warming hornet is touching with one leg the head of the pupa (a) while with another leg (1) the ground, as if comparing their temperature. **c)** a hornet queen (*V. orientalis*) warming a brood comb. The open comb cell at center houses an egg. **d)** adult wasps (*Paravespula vulgaris*) warming a pupa of *Vespa crabro* (at center); they will do so till its complete maturation. **e)** part of a large brood comb of *V. orientalis* whose cells are populated by brood prior to metamorphosis (l) as well as by brood post metamorphosis (p) which has been parasitised by the ova of the parasitoid *Specophaga vesparum.* The silk cap has been mechanically removed from some of the puparia (sc), thus revealing only the heads of the developing pupae. In the three cells designated by "s" we see the perforations in the pupal silk cap made by the emerging parasites after their maturation within the pupae. **f)** after mechanical removal of the silk caps from a cluster of brood comb cells, we can see cells harboring 3–6 parasitoids (p) each, without the adult nursing hornets detecting their presence or finding the parasitised pupae defective.

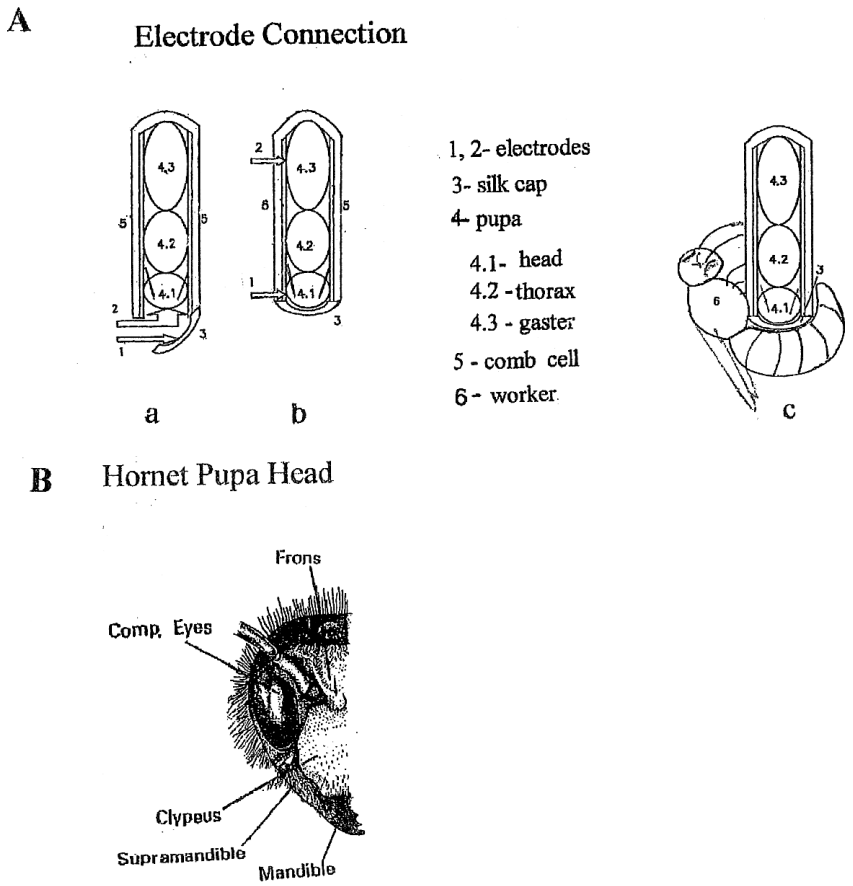

FIGURE 2. Schematic presentation of the methodology and sites used to measure electric parameters in the hornet pupa (A a,b), a schema of an adult hornet warming a pupa (A c) and a drawing of the points measured on a hornet's pupa head (B). **A)** A,a — note that one electrode is affixed to the head of the pupa (large arrow) and the other — to the inside of the silk cap (small arrow). A,b — here one electrode is affixed to the head of the pupa and the other — to its gaster. A,c — the stance assumed by a nursing worker while warming the pupa. **B)** the sites on the head of the pupa to which one of the two electrodes was affixed.

the onset of pupation, when the pupating larva spins its silk weave, the eggs of the parasitoid, now underneath the silk cap, hatch, and the emerging parasitoid larvae feed on the body fluids of the pupated vespan larva, but during this process, the head of the vespan pupa is left intact and apparently continues to transmit (*via* the silk cap) to the nursing worker hornets outside that 'business is as usual'. The reader is referred to Figure 1e (in this picture the cells are upside down relative to their natural position) where, on the left side, one can see a cluster of cells housing larvae prior to pupation and to the immediate right — cells housing pupae at various ages whose silk caps have been mechanically removed. Note that all the pupal heads appear intact, even though in some of the pupae the contents of the body proper (but not the head) have been eaten up (sucked) by the devel-

oping parasitoids, part of which had already ecloded and left the cells, as apparent from the perforations in the silk cap of the original vespan pupa (see Figure 1e(s)). When one removes what remains from the ravaged pupae in the comb-cells effected by the parasitoids, one notices (Figure 1f) that in some of the cells the parasitoids have completed their own pupation — with three to six parasitoid casings of pupae in each vespan comb cell. Yet in each such cell, as mentioned earlier, the head of the vespan pupa remains intact, almost till the complete development of the adult parasitoid, so that the nursing hornets tend to these cells and warm them just as they do to all the other cells (Ishay, unpublished observations). Our assumption here is that the cuticle on the head of the vespan pupa (whose polarity is negative) generates the voltage detected and measured by us (Table I) and it is this voltage, which enables the pupa to communicate *via* the silk cap with the nursing worker hornets outside. The resistance values between various points on the pupal head and the inner side of the silk cocoon are presented in Table II.

TABLE I. Voltage values obtained between various sites on the pupal head and its gaster, (n = 6)

Tair = 24°C

	Points of measurement on the pupal head, Voltage (mV)				
Specimen	Mandible	Supra Mandible	Clypeus	Frons	Comp. Eyes
1	150	265	320	150	220
2	250	215	258	311	220
3	215	221	114	250	136
4	245	225	171	142	143
5	178	215	246	240	210
6	310	268	218	320	142
Mean	225	235	221	236	183
SD	26	23	33	34	42

These data show large variations between different individual specimens. However, in each specimen there is a clearcut positive correlation between electrical measurements at different locations on the head.

TABLE II. Resistance values obtained between various sites on the pupal head and the inner surface of the silk cocoon, (n = 3)

Tair = 24°C

	Points of measurement, Resistance (Mohm)				
Specimen	Mandible	Supra Mandible	Clypeus	Frons	Comp. Eyes
1	3.30	3.57	3.28	3.81	2.80
2	4.20	4.20	5.35	5.45	4.09
3	1.20	1.15	1.15	1.00	1.05
Mean	2.90	2.97	3.26	3.42	2.65
SD	0.75	0.65	0.84	0.68	0.72

In Figure 3 we show that both voltage and current measured in the pupal cuticle are correlated with the temperature. Note that at a temperature lower than optimal (about 20°C), the obtained voltage and current values are lower than those found at 30°C (the optimal temperature in hornet brood combs is 29°C) (Ishay and Ruttner 1971).

As seen in Figure 4, the voltage in the silk cocoon cap increases with the deviation of the temperature from its optimal value in either direction (n = 5). In Figure 5, one sees that at optimal silk temperature, both the resistance and the voltage are minimal, while the current is maximal, and that the farther away is the temperature from this value, the greater are the resistance and voltage and the smaller is the current.

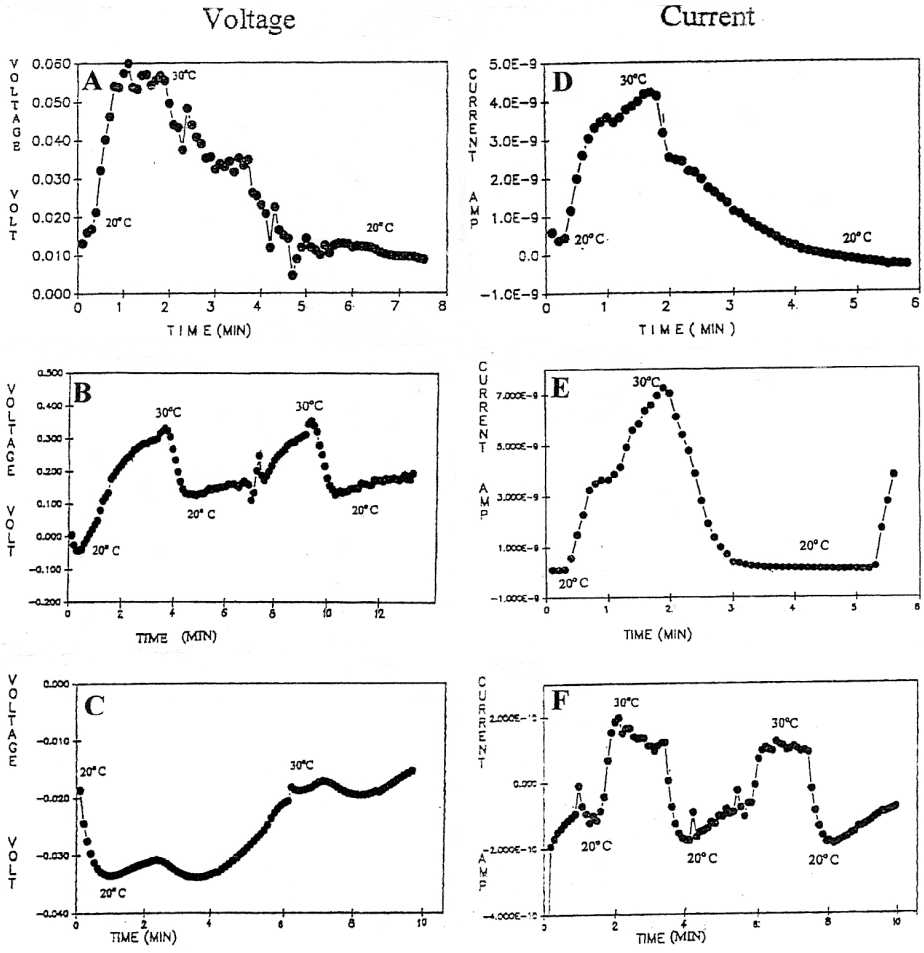

FIGURE 3. Values of electric voltage and current measured between the head and gaster of a pupa (as shown schematically in Figure 2A,b). These measurements were carried out on 3 different pupae. The following three observations merit mention: 1) maximal values are attained in the vicinity of the optimal temperature (in this case ~ 30°C); 2) at lower temperature (20°C), both the voltage and current are lower; 3) the cuticle of the pupa displays temperature dependent electrical behavior that is similar to the behavior displayed by the cuticle of the adult hornet.

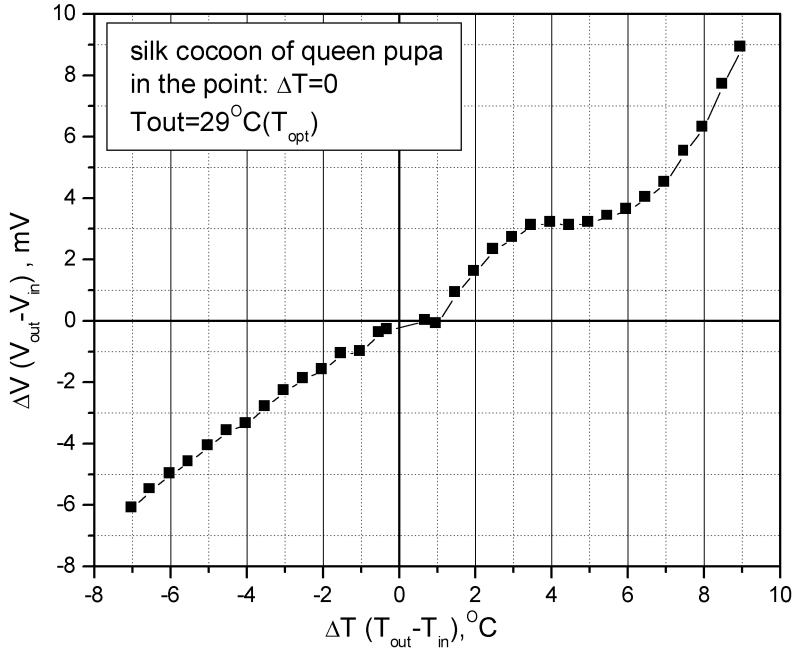

FIGURE 4. Voltage differential between the outer and inner surfaces of the silk puparium as correlated with thermal changes ΔT when the outside temperature is optimal. As can be seen ΔV/ ΔT ≈ 0.8–1.0 mV/ºC. This is a thermoelectric effect.

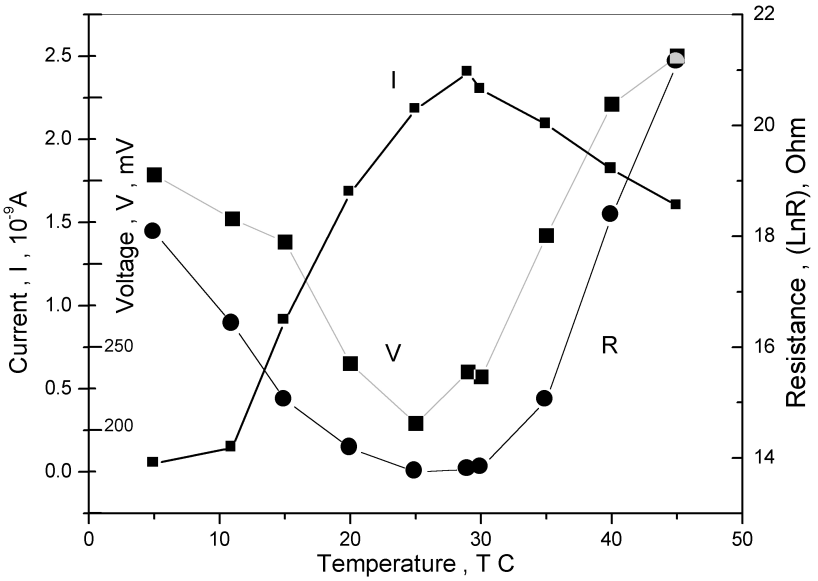

FIGURE 5. The parameters of voltage, current and resistance plotted versus the optimal temperature. Note that at optimal temperature (29ºC) the current is maximal, while the resistance and voltage are minimal.

Discussion

The finding presented herein suggests that it is imperative that the adult hornets, whether in the natural nest or in the laboratory, warm the pupal brood, when this becomes necessary. Pupae that are not warmed to optimal temperature are likely to die or eclode (maturate) with malformations (Ishay and Ruttner 1971). This warming can transpire in two situations. First, when one experimentally removes the pupa from its comb cell (Figure 1b) and there is direct contact between the warming worker and the cuticle of the extracted pupa, and secondly, in all the normal situations when the contact of the nursing worker is rather with the silk cap of the pupa *in situ*. In the latter instance, the warming process is lengthier because the silk cap transmits heat more slowly (Galushko *et al.* unpublished results) than pupal cuticle, but this is what takes place in the intact brood comb cell, whether in the natural nest or in the laboratory (Figure 1a). The phenomenon of extra-nestal warming of the pupae is not strictly intra-specific but can be also inter-specific and even inter-generic. Witness the situation depicted in Figure 1d, where workers of *Paravespula germanica* are seen warming a pupa of *Vespa crabro.* Moreover, the worker hornets may warm not only pupae but also other brood in the comb and even the entire brood comb, as shown in Figure 1c. As for the *Sphecophaga vesparum* parasitoids that invade the pupal cell, these apparently survive because they commence developing by imbibing the body fluids of the pupating hornet larva only after it has completed spinning its silk weave; furthermore, they leave the head of the pupa intact and thereby probably prevent the nursing working hornets from harming them, because the surviving head, we believe, sends the message of 'business as usual' and this *via* electric signals picked up by the workers outside. Indeed on each of five randomly selected sites on the silk cap housing the pupal head, we measured about the same levels of voltage and resistance (Tables I and II).

Upon change in the pupal temperature (from about 30ºC down to 20ºC) there is change in the voltage and current, and apparently this is what the nursing workers detect, whether through a membrane (the silk cap) or through direct contact with the pupal head (Figure 3). Thus, the pupal cuticle displays the properties of a thermoelectric material, just as does adult cuticle and vespan silk (Kirshboim and Ishay 2000, Sverdlov *et al.* 2000). In fact, all of these biological tissues behave like organic semiconductors (Gutmann *et al.* 1983). Measurements of the voltage (ΔV) across the thickness of the silk cap versus the temperature difference (ΔT) across that cap revealed that the further is the temperature from optimal, the greater is the voltage (Figure 4). The sign of ΔV is the same as the sign of ΔT and they are roughly proportional to each other: this is *thermoelectric effect*. Additionally there were in fact changes in the current and resistance as well, all of which could be summed up as follows: at optimal temperature (29ºC) the silk cap current was maximal, while the voltage and resistance were minimal, and this pattern changed with changes of temperature in both directions away from the optimal temperature (Figure 5). Our bottom-line conclusion is that hornets, whether as adults or as pupae, produce in or educe from their cuticle electrical parameters. In the case of the pupa, any thermal change occurring in its head within the silk cap or its cuticle outside the silk weave triggers a 'call for help', alerting any adult hornet in the vicinity, be it of the same or different vespan species. This call for help from afar is probably effected *via* released pupal pheromones, but once help arrives in the form of an adult hornet, electrical parameters on the body of the pupa 'in-

struct' the latter as to what treatment is required, which is usually warming, i.e., electrical parameters produced by the pupae are understood by the adults touching them. This is how they communicate!

The process of warming (or cooling) of the pupa by a worker hornet may be deemed reminiscent of an automatic control system. Variants of such systems, corresponding to two of our situations, are shown in Figure 6. Figure 6a depicts warming of the pupa in the comb achieved *via* the cocoon silk cap, and Figure 6b — warming by direct contact between the hornet and the pupa. In the situation shown in Figure 6a, the operative mechanism is the heat flow achieved by the thermal conductivity of the cocoon silk at nonzero temperature difference (ΔT). Here two informational signals control the process, namely: a temperature difference (ΔT), which affects the rate of warming (i.e., magnitude of the

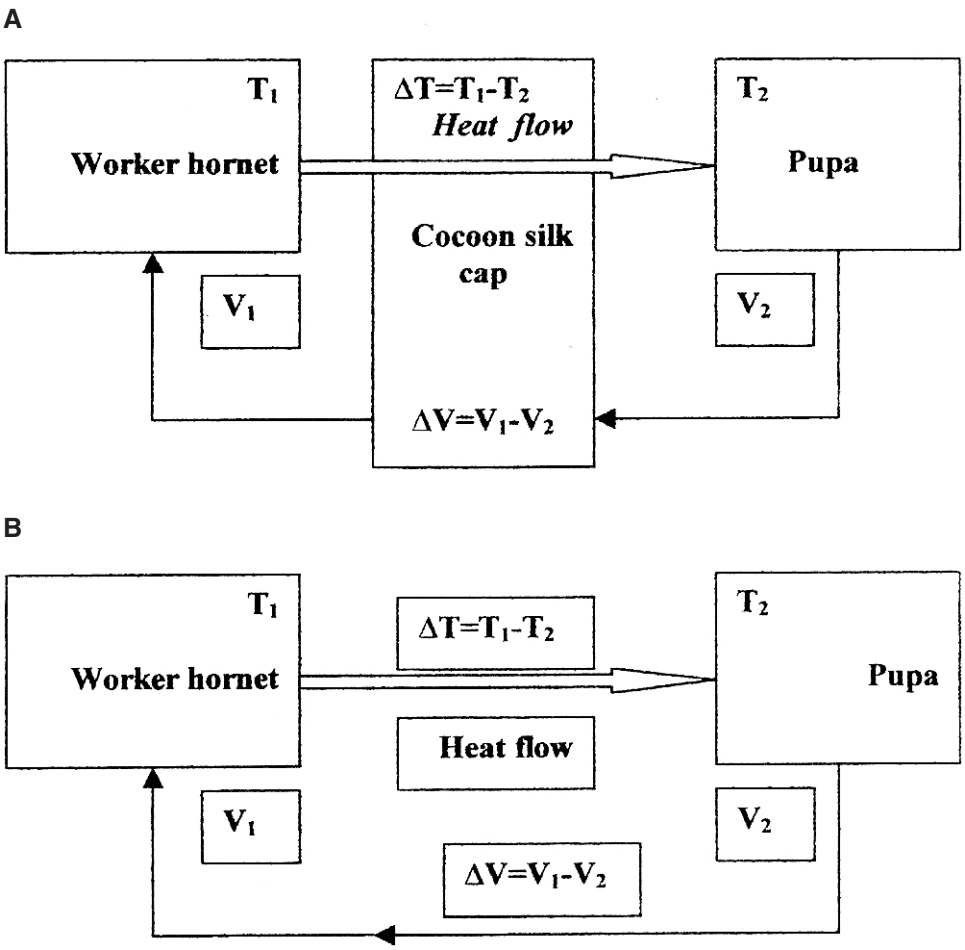

FIGURE 6. Scheme of the interaction between the adult nursing hornet and the pupa during the warming process of the latter.

heat flow), and the voltage across the cocoon silk (ΔV), which determines the duration of the process. Electrophysical properties of the cocoon silk determine the relationship between these two signals. In the case of warming of the pupa outside its comb cell (Figure 6b) the value of the heat flow depends on the temperature difference between the adult hornet and the pupa and on the thermoresistance at the interface of their cuticles. The second information signal is produced here because of the temperature dependence of the spontaneous voltage on the cuticle (see Figure 3 A–F).

In order to sense the electric voltage and/or current produced by the pupa, the worker hornet must make electrical connections with the pupa at two points. We do not know whether this is achieved by using either the legs or the antennae or both as probes. In the case of extracted pupa, it is clear how this can be done — see Figure 1b. In the case of a normally encased pupa, this can be made by one or more probes on the surface of the silk cap, from the one side and the other on a nearly wall of the pupa cell (Figure 7).

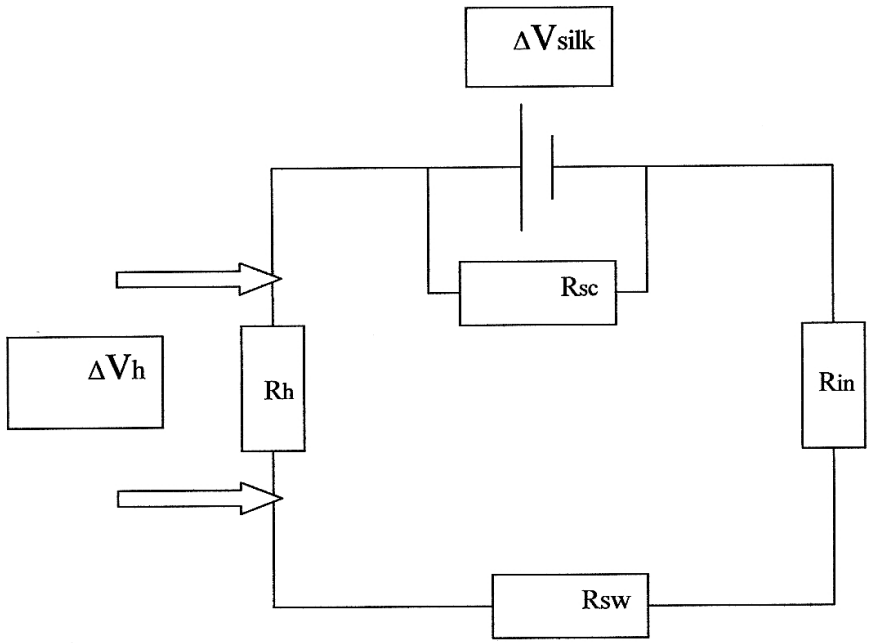

FIGURE 7. Scheme of electrical interaction between hornet and pupa upon warming. When ΔTsilk = 0 then ΔVsilk = 0 (see Fig. 4) and then ΔVh = 0 and "call for help" is not produced.
ΔVh — voltage difference between the legs or the antennae or leg and antennae of the hornet used as probes when it warms the pupa
ΔVsilk — voltage difference across pupal silk which is dependent on temperature difference across the pupal silk
Rsc — resistance of the silk pupa cap
Rin — resistance between inner side of the silk cap and the silk wall
Rsw — resistance of the silk wall
Rh — resistance between "probes of the hornet"

References

Aschcroft, M.W. and Mermin, N.D. (1976) *Solid State Physics.* Holt Saunders, Philadelphia.

Donovan, B.J. (1991) Life cycle of *Sphecophaga vesparum* (Curtis), (Hymenoptera: Ichneumonidae) a parasitoid of some vespid wasps. *New Zealand J. Zool. 18:* 181–192.

Edwards, R. (1980) *Social Wasps.* The Rentokil Library, Rentokil Ltd., East Grinstead.

Guiglia, D. (1972) *Les Guêpes Sociales (Hymenoptera, Vespidae) d'Europe Occidentale et Septentrionale.* Masson et Cie, Eds., Paris.

Gutmann, F., Keyzer, H., Lyons, L.E. and Somoano, R.B. (1983) *Organic Semiconductors,* Part B. Robert E. Kriger Publishing Company, Florida.

Heinrich, B. (1981) *Insect Thermoregulation.* John Wiley & Sons, New York.

Ishay, J. (1964) Observations sur la biologie de la Guêpe orientale *Vespa orientalis* in Israël *Insectes Sociaux XI(3):* 193–206.

Ishay, J. (1973) Thermoregulation by social wasps: behaviour and pheromones. *Trans. New York Acad. Scie. 35(6):* 447–462.

Ishay, J.S. and Barenholz-Paniry, V. (1995) Thermoelectric effect in hornet silk and thermoregulation in hornets nest. *J. Insect Physiol. 41(9):* 753–759.

Ishay, J.S. and Litinetsky, L. (1996) Thermoelectric current in hornet cuticle: morphological and electrical changes induced by temperature and light. *Physiol. Chem. Phys. & Med. NMR 28:* 55–67.

Ishay, J. and Ruttner, F. (1971) Die thermoregulation im Horniensnest (The thermoregulation in a hornet nest). *Z.v. Physiol. 72:* 423–434.

Ishay, J.S., Abes, A.H., Chernobrov, H.L., Ishay, I.Z. and Ben-Shalom, A. (1991) Electrical properties of the Oriental hornet (*Vespa orientalis)* cuticle. *Comp. Biochem. Physiol. 100A(2):* 233–271.

Ishay, J.S., Benshalom-Shimony, T., Ben-Shalom, A. and Kristianpoller, N. (1992) Photovoltaic effects in the Oriental hornet. *J. Insect Physiol. 38(1):* 37–48.

Ishay, J.S., Rosenzweig, E. and Fuksman, E. (1995). Thermo- and Photoelectric current in hornet cuticle. *Physiol. Chem. Phys. & Med. NMR*, *27(3):* 179–192.

Ishay, J.S., Shimony, T.B., Dabah, B., Shuzz, I.S., Shevach, Y., Shalom, A.B.and Paniry, V.B. (1993) Electrical properties of the cuticle, silk caps and comb of Oriental hornet *Vespa orientalis* (Hymenoptera: Vespidae). *Int. J.Insect Morphol. & Embryol. 22(2–4):* 127–144.

Ishay, J.S., Pertsis, V., Rave, E., Goren, A. and Bergman, D.J. (2003) Natural Thermoelectric heat pump in social wasps. *Physical Review Letters 90(21):* 81021–81024.

Kirshboim, S. and Ishay, J.S. (2000) Silk produced by hornets: thermophotovoltaic properties — a review. *Comp. Biochem. Physiol. A 127(1):* 1–20.

Kristianpoller, N., Weis, D. and Ishay, J.S. (1997) Irradiation effects in the Oriental hornet. *J. Luminescence 74(6)*: 591–592.

Litinetsky, L., Rosenzweig, E. and Ishay, J.S. (2001) Thermal properties of hornet colonies: a thermoelectric interpretation of thermoregulation of the entire nest and its individual members. *Physiol. Chem. Phys. & Med. NMR 33:* 103–118.

Matsuura, M. and Yamane, S. (1990) *Biology of the Vespine Wasps.* Springer Verlag, Berlin.

Rowe, D.M. (1995) *C.R.C. Handbook of Thermoelectrics.* Boca Raton, CRC Press.

Shimony, T.B. and Ishay, J.S. (1981) Thermoelectrical (Seebeck) effect of the cuticle of social wasps. *J. Theor. Biol. 92:* 497–503.

Spradbery, J.P. (1973) *Wasps.* Sidgwick & Jackson, London.

Sverdlov, A., Litinetsky, L., Pertsis, V. and Ishay, J.S. (2000) Thermophotovoltaic (TPV) properties of hornet cuticle as dependent on relative humidity *Physiol. Chem. Phys. & Med. NMR 32:* 57–66.

Tritt, T.M. (1997) Thermoelectric materials — new direction and approaches. *Mat. Res. Soc. Symp. Proc*.: 478.

Received October 7, 2004;
accepted January 6, 2005.

Physiol. Chem. Phys. & Med. NMR (2004) *36*: 143–158

How Much Water Is Made "Non-free" by 36% Native Hemoglobin?

Gilbert N. Ling* **and Wei-Xiao Hu****

**Damadian Foundation for Basic and Cancer Research c/o Fonar Corporation, 110 Marcus Drive, Melville, NY 11747 Email: gilbertling@dobar.org*
***9-502 Living Quarter, Zhejiang University of Technology, Hanchow, Zhejiang, 310014,P.R.China*

Abstract: At equilibrium, the concentration ratio of poly(ethylene gycol) (PEG-4000) in a dialysis sac containing a 35.1% solution of *native* bovine hemoglobin over that in the external solution is 0.196 ± 0.028 (mean ± SD). This *apparent equilibrium distribution constant* or ρ-value of 0.196, when viewed side-by-side with the near-equal distribution of sucrose and raffinose in similar native-hemoglobin dominated water suggests *all* (rather than 80%) of the water in this solution has been altered by the native hemoglobin and is no longer free liquid water. Based on Ling's equation for solute exclusion, we found that an excess of water-to-water interaction energy of a mere 4.25 cal/mole could account for both the observed exclusion of PEG-4000 and non-exclusion of sucrose and raffinose. Finally, the long-range action of (even this relatively inactive) native hemoglobin on the dynamic water structure was compared with the exclusion of coated latex microspheres from the altered water 100 μm from the surface of polyvinylalcohol gel (Zheng and Pollack) — in the light of Ling's new theory of *ad infinitum* water polarization-orientation (under idealized conditions) first publicized at the Gordon Research Conference on "Interfacial Water in Cell Biology" on the campus of the Mount Holyoke College in June 2004.

WATER, PROTEINS and K^+ are the primary ingredients of the basic unit of all life — the living cell. As a rule, each living cell spends its life in an aqueous environment rich in Na^+ but poor in K^+. In the traditional membrane-pump theory, this asymmetric distribution of K^+ and Na^+ is maintained by the ceaseless activity of postulated pumps located in the cell membrane. This membrane (Na^+) pump theory is still widely taught as truth at all levels of education, although it has been thoroughly disproved long ago (Ling 2001). Among many contradictory evidence, the simplest and the most unequivocal is that the minimum energy needed to operate the sodium pump far exceeds the total energy available (Ling 1962; 1997).

In an alternative (unifying) theory of the living cell, known as the *association-induction hypothesis* (AI Hypothesis), the segregation of the two ions is the combined consequences

of two causes: (1) low solvency of the bulk of cell water for Na^+ (and K^+); (2) preferential adsorption of K^+ (over Na^+) on the β-, and γ-carboxyl groups of intracellular proteins (Ling 1951; 1952; 1962; 1965; 1969; 1977; 1988; 1992, pp. 160–201; see also Troshin 1966).

The Polarized-Oriented Multilayer Theory of Cell Water, or PM theory, is a subsidiary of the AI Hypothesis (Ling 1965; 1972 pp. 663–700; 1984, pp. 163–181; 1992 pp. 69–110; 2004; 2005). In the PM theory, all or virtually all cell water assumes the dynamic structure of polarized-oriented multilayers — in consequence of direct or indirect interaction with parallel arrays of exposed NHCO groups of fully-extended (segments of) intracellular protein(s) (Ling 1965; 1972).

Instantly, the PM theory has offered a theoretical mechanism for one of the most basic manifestation of life phenomenon. That is, as a rule, a large amount of water exists in living cells. As of today, the PM theory is the only known theory that can explain and/or obeys — indeed, fits like hand and glove (i) the specificity of water content to each cell type, (ii) the law of conservation of energy and (iii) the inextractibility of cell water by centrifugation at 1000 g. after surgical ablation of a part of the cell membrane — which does not regenerate (Ling 2005).

Historically speaking, however, the PM theory was introduced in 1965 with its focus on explaining the low concentration of Na^+ in cell water (Ling 1965). Twenty eight years later, a general and quantitative theory of solute distribution in cell water and model systems was introduced (Ling 1993). An important principle that came from this theory is the "size rule." That is, other things being the same, the larger the solute size, the lower its (true) equilibrium distribution coefficient or q-value.

Aiding greatly in the testing and developing the PM theory of cell water were two classes of experimental models, called respectively **extroverts** and **introverts** (Ling 1992, p. 107). Extroverts include gelatin and various denatured proteins, each containing a major part of its polypeptide chains in the **fully extended conformation.** As a result, their backbone NHCO groups are directly exposed to the bulk-phase water**.** Other extroverts include linear polymers carrying properly spaced oxygen or nitrogen atoms (bearing unshared lone-pair electrons). Examples are poly(ethylene oxide) (PEO), polyvinylpyrrolidone (PVP) and polyvinylmethylether (PVME) (Ling *et al*. 1980; 1980a).

In theory, water under the influence of suitable concentrations of extrovert agents should exhibit properties akin to those of water in living cells. Worldwide testing proved that, within the confines of what has been tested so far, they do (for summary see Ling 1992, Table 5.5, p. 108–109). Introvert models include most of what are conventionally called **native** proteins — usually obtainable from biochemical supply stores in a bottle. The majority of (but not all, see below) the peptide CO and NH groups in these so-called native proteins are locked in α-helical and other macromolecular H-bonds. In these folded or otherwise tethered conformations, these backbone NHCO groups are, in theory, less able or unable to alter the physical properties of the bulk-phase water. Experimental studies support this expectation (Ling *et al*. 1980a; 1980b).

The research presented in this article centers on what is known as the *apparent equilibrium distribution* of the polymer, poly(ethylene glycol). With a molecular weight of 4000 daltons, this large polymer is also known by its short name PEG-4000 (for definition of the ρ-value, see below). Historically, this study began as a part of our broader investigation on the size-dependent solvency of various solutes in the cell water and in model systems (Ling and Hu 1988). However, we did not fully complete our PEG-4000

study until very late. Once completed, we realized that the insight the PEG-4000 study revealed went beyond our original aim. It was then that we decided to write a separate paper. This communication is the result.

Materials and Methods

Bovine hemoglobin (about 75% methemoglobin and 25% oxyhemoglobin) (Lot 112F-9300) was purchased from Sigma Chemical Corp, St. Louis, Mo. So was poly(ethylene glycol) with a molecular weight of 3300 (Catalog No. P-3640, Lot 16F-0477). Labeled polyethylene glycol-4000, ^{3}H-PEG-4000, Lot 2109-295 was obtained from Du Pont (formerly New England Nuclear, Boston). Its average molecular weight given was 4000 daltons.

The basic procedure used was the equilibrium dialysis method earlier described (Ling and Hu 1988). However, instead of following the standard procedure of measuring only the uptake of a radioactively labeled solute by the protein solution inside a dialysis sac, in the present study we did it two ways. In one, the radioactively labeled PEG was added initially to the solution outside the sac; in the other set, the labeled PEG was added to the solution inside the sac. The purpose of this dual approach was to remove any uncertainty on the time it took for diffusion equilibrium of the labeled PEG to be attained. The exact knowledge on the time for the attainment of diffusion equilibrium in turn assures the accuracy of the *apparent equilibrium distribution coefficient* (or ρ-value) of the probe molecule obtained. For the ρ-value of an extraordinarily large and thus slow-moving probe molecule like PEG-4000, this extra effort was essential.

It should be made clear here that the ρ-value of a solute could only be equal to or larger than the true equilibrium distribution coefficient (or q-value). While the q-value refers exclusively to *free* PEG (or other probe solute) in the water of the living cell or the water in the dialysis-sac content, the ρ-value may include PEG bound in one way or another to the macromolecules in the cell or the dialysis sac.

Solution A was a 40% (w/v) solution of bovine hemoglobin dissolved in a solution called Solution B. Solution B contained 0.4 M NaCl; 0.01% penicillin G, sodium; 0.01% streptomycin sulfate; 0.01% thymol and 5% (w/v) polyethylene glycol (approximately 12.5 mM, calculated on the basis of the nominal molecular weight of 4000 for the labeled PEG-4000, see below). In a preceding paper, Ling and Hu (1988) have shown that this combination of antibiotics and thymol was able to check completely the growth of bacteria even at 25°C. The low temperature (0°C) of this study further insured the sterility of the system under study.

To each of four 100-ml screw-cap tubes was added 50-ml aliquots of Solution B and four small sacs of Spectra Por 2 dialysis tubing (diameter 6.4 mm, with molecular cut-off at 12,000 to 14,000) containing 1.2 ml.of Solution A (for details of procedure used in filling and tying these sacs, see Ling and Hu 1988, p. 294). A 0.005-ml aliquot of radioactively labeled H^{3}-poly(ethylene glycol)-4000, containing 500 micro-curie of radioactivity per ml, was added to the solution *outside* the sacs in two of the four screw-cap tubes. Similar 0.005-ml aliquots of the same radioactive solution were added to the *inside* of the dialysis sacs of two other screw-cap tubes. Each capped tube was covered completely in at least one layer of thin paraffin film (Parafilm, Fisher Scientific). The tubes were immersed horizontally in a constant temperature bath kept at 0°C and shaken at the rate of 20 excursions per minute, each excursion covering a distance of one inch.

At various time intervals, ranging from one to four day(s), one dialysis sac from each of the four screw-cap tubes was taken out, and aliquots of its content assayed for their water contents and radioactivity. Briefly, each sample removed was divided into two portions. One portion was weighed, dried in an oven at 105°C for 48 hours and weighted again to determine the water and solid content. The other portion was transferred to a preweighed 15 ml-graduated centrifuge tube and the assembly weighed to determine the sample weight. 2.0 ml of 0.3 M LiOH solution was then added to each of these centrifuge tubes. In this alkaline medium, the dried samples were fully dissolved after overnight incubation. 2.0 ml. of 0.6 M trichloroacetic acid (TCA) was then added to each tube, mixed thoroughly with the LiOH extract before centrifugation. Aliquots of the clear supernatant solution (0.50 ml) were mixed with Bray's scintillation fluid before counting on a Packard γ-Scintillation Counter (Bray 1960). Samples of the initial and final bathing solutions were similarly diluted with LiOH-TCA mixture and Bray's scintillation fluid before assaying for radioactivity.

To achieve the highest accuracy possible, we counted all samples three times before and after the addition with a Hamilton micro-pipet of the same volume of a radioactive ^{3}H-bearing solution — containing at least five times more radioactivity than the experimental sample. The large increments in counts allowed us to determine precisely the counting efficiency of each individual sample and its bathing solution, and to apply the *individual* counting efficiency corrections to each sample set.

Results

Somewhere between the 8th day and 12th day of incubation at 0°C, diffusion equilibrium was reached between labeled PEG-4000 inside and outside the dialysis sacs. This is indicated in Figure 1 and Table I by the attainment of the same levels of radioactivity in the sacs where the radioactivity was initially added to the inside and to the outside of the dialysis sac. The numbers, 0.637, 0.632 etc. in parentheses refer to percentage water content of the sac content in each specific sample.

Now, the ordinate of Figure 1 represents the ratio of the concentration of PEG-4000 in the dialysis sac over that in the bathing fluid. This ratio becomes *the apparent equilibrium distribution coefficient* or ρ-*value* toward the end of the time-course study when diffusion equilibrium of the labeled PEG-4000 has been reached. From the ρ-values obtained on the 12th day from both sets of values, we obtained an average ρ-value for the labeled PEG-4000 of 0.196 ± 0.028 (mean ± S.D).

The water content of the solutions inside the sacs on the 12th day was 63.9% ± 0.36%. By difference, the final concentration of native hemoglobin in the sacs was 36.1%. This percentage is close to the concentration (34%) of hemoglobin in most mammalian red blood cells (Ponder 1971, p. 117; Ling 2005).

Discussion and Conclusion

1. How much bulk-phase water was altered by the 36.1% native hemoglobin?

The study described above shows that the ρ-value of PEG-4000 in the 36.1% hemoglobin solution is 0.196. Since 1.000 – 0.196 = 0.804, 80.4% of the water in the dialysis

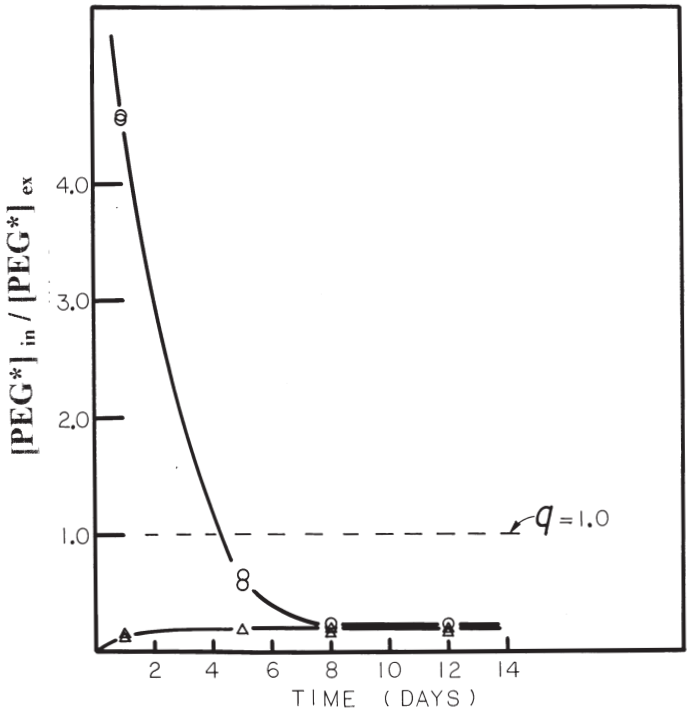

FIGURE 1. The time course of change of the concentration of radioactively labeled poly(ethylene glycol) or PEG-4000 inside a dialysis bag initially containing 40% (w/v) native bovine hemoglobin. The set of data represented by circles came from an experiment in which the radioactively labeled PEG-4000 was added to the inside of the dialysis sac containing the protein. The set of data represented by triangles came from experiments in which the labeled PEG-4000 was added to the outside bathing solution. Dotted line indicates equal concentration of labeled PEG-4000 inside and outside the dialysis bag. Full diffusion equilibrium was attained when the radioactivity of labeled PEG-4000 represented by the circles and that by the triangles reached the same level. The ratio of the labeled PEG-4000 concentration at and after that time represents the apparent equilibrium distribution coefficient or ρ-value of PEG-4000 in the bulk-phase water dominated by the native bovine hemoglobin at 0°C. Numerical data are given in Table I.

TABLE I. Time course of equilibration of labeled PEG-4000 in solution of native hemoglobin.

Incubation time (days)	PEG-Distribution Ratio (Conc. in Sac/External Conc.) 1	5	8	12
Tracer added outside	0.161 (0.637) 0.130 (0.632)	0.202 (0.630)	0.185 (0.628 0.170 (0.629)	0.185 (0.642) 0.176 (0.641)
Tracer added inside	4.599 (0.636) 4.553 (0.632)	0.562 (0.636) 0.661 (0.628)	0.240 (0.634) 0.221 (0.633)	0.238 (0.640) 0.186 (0.634)
Mean ± S.D.			0.196 ± 0.028 (0.639 ± 0.0036)	

Number in parenthesis refers to the water content of the content of the sac yielding the PEG distribution ratio in front of it. Mean and S.D. in the last row is the final ρ-value of PEG-4000 in the hemoglobin solution.

sac appears to have lost its normal solvency for PEG-4000 in consequence of the presence of the hemoglobin. However, this seemingly reasonable quantitative assessment rests upon a rather unlikely assumption. That is, hemoglobin has separated the bulk phase water into two drastically different fractions. One fraction, 80% in quantity, has zero solvency for PEG-4000; the other 20% has 100% full solvency for PEG-4000.

Now, if the 36.1% native hemoglobin has indeed transformed the bulk phase water into these dramatically different fractions, one should be able to confirm their existence with other probe molecules. That, however, is not true.

Ling and Hu have shown earlier that in a solution containing native hemoglobin at an even higher concentration (39%), sucrose (molar volume, 342 cc) and raffinose (molar volume, 504 cc) show q-values of 0.976 and 0. 971 respectively (Ling and Hu 1988). These near-unity q-values indicate a basic homogeneity of the bulk-phase water in the native hemoglobin solution studied. The presence of 36–39% native hemoglobin does not separate the bulk phase water into two diametrically different fractions.

That being the case, the challenging question has shifted. It is now "Why does the same bulk-phase water of a 36 to 39% native hemoglobin solution behave like perfectly normal liquid water to sucrose and raffinose but keeps out PEG-4000 from most of it? To give a meaningful answer, we need a quantitative theory. Ling's PM theory of solute exclusion is the one of choice as we know of no other alternatives.

Very succinctly, the answer lies in the "size rule" mentioned above. Namely, the q-value decreases with increasing molecular size. Sucrose and raffinose exhibit much higher q-values while PEG-4000 exhibits a much lower one, because sucrose and raffinose are roughly ten times smaller than PEG-4000. In the next section, we will go a little deeper into the how's and why's.

2. Ling's quantitative theory of solute distribution — as summarized in his equation of the q-value

In 1993 Ling presented an equation of the q-values of solutes of different size in water polarized-oriented to different levels of intensity (Ling 1993; Ling *et al*. 1993). This equation is reproduced in full in Appendix 1 at the end of this article. In this Equation of solute distribution, the q-value of a solute in (polarized-oriented) water is largely characterized by two parameters: ΔE_v and ΔE_s. For the sake of simplicity, we have omitted from separate consideration the entropy contribution to the q-value. Instead, we consider that the entropy contribution has been incorporated into ΔE_v. (See Equation 26 on p. 157 in Ling 1993).

Now, ΔE_v, the *specific solvent polarization energy* is in units of cal per mole per cm^3; it measures the *difference* in the energy spent in excavating a hole in the polarized-oriented water (to accommodate the probe solute) and the energy recovered in filling up the hole left behind (by the probe solute) in the normal liquid water of the source solution. On the other hand, ΔE_s, the *specific surface polarization energy* is in units of cal per mole per cm^2; it measures the difference between the interaction energy of the surface of the solute with the surrounding polarized-oriented water and that with the normal liquid water of the source solution. At a specific temperature, it is the algebraic sum of the product of molar volume v of the solute and ΔE_v and the product of the surface area of the solute (expressed as a function of v) and ΔE_s that determines the q-value of each solute. For simplicity, Figure 2 shows the q-value due to the action of the volume factor only.

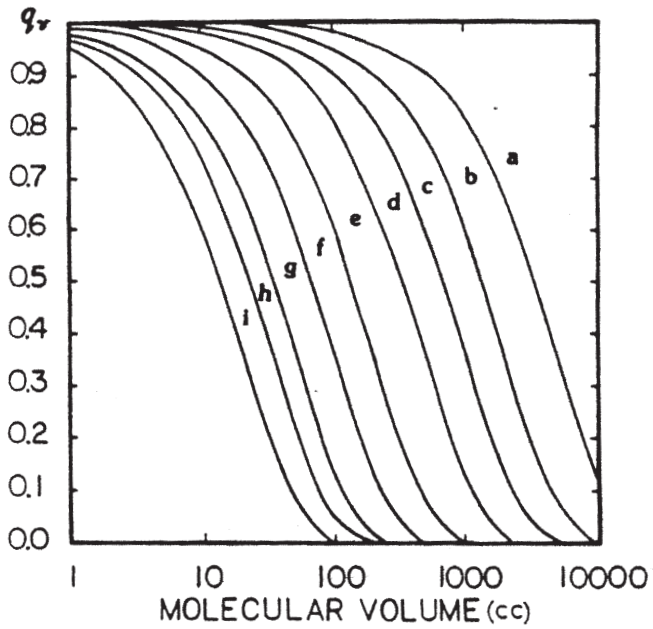

FIGURE 2. The theoretical volume (or solvent) component of the equilibrium distribution coefficient (q_v) for solutes of different molecular volume in water polarized at different intensity (See Equation A3 in Appendix 1.) The intensity of water polarization due to the volume component of the polarization energy is given as the specific solvent polarization energy, ΔE_v. The specific value of ΔE_v in units of RT per cm^3 is indicated by the letter near each curve, where a represents 0.0002; b, 0.0005; c, 0.001; d, 0.002; e, 0.005; f, 0.01; g, 0.02; h, 0.03; i, 0.05. R is the gas constant and T the absolute temperature. At room temperature (25°C), RT is equal to 592 cal./mole. (From Ling 1993)

The ordinate of Figure 2 represents the logarithm of the q-value; the abscissa represents the logarithm of the molecular volumes in units of cm^3 or cc. As examples, the molecular volume of water is 18.02 cc, while that of PEG 4000 is 4000 cc.

The small letters a, b, c etc near each of the curves in Figure 2 indicate the value of ΔE_v used in computing that specific curve and the ΔE_v is given in units of RT, where R is the gas constant and T, the absolute temperature. At room temperature, RT equals 592 cal/mole. Thus, the curve marked with the letter standing for 0.0002 indicates a ΔE_v of $0.0002 \times 592 = 0.118$ cal/mole/cal.

Assuming that the ρ-value of PEG-4000 obtained (0.196) is equal to its q-value, we can draw a horizontal straight line across Figure 2 at that q-value and a vertical straight line at a molecular volume of 4000cc. The point of intersection of these two straight lines gives us an approximate estimate of the ΔE_v of the bulk phase water in the 36.1% hemoglobin solution studied, namely, 0.0004 RT or 0.236 cal/mole/cc. Multiply this figure by the molar volume of water, 18.02 we obtain a volume contribution of the *exclusion intensity*, $\mathcal{U}_{vp}$ (which includes an entropy contribution assumed to be included in the ΔE_v adopted and not explicitly mentioned) of 4.25 cal/mole. The predicted q-value of sucrose and raffinose on the basis of the ΔE_v of 0.236 value and their respective molar volumes are roughly 0.9 and 0.85 to be compared with the experimentally determined values of

0.976 and 0.971 respectively. Because these estimates were made on the basis of the volume contribution only, the agreement must be considered satisfactory.

Thus, Ling's equation of solute distribution in polarized-oriented water can adequately explain at once the low ρ-value of PEG-4000 and high q-values of sucrose and raffinose in an aqueous solution dominated by 36.1% native hemoglobin. And, despite the fact that native hemoglobin like other native proteins in general, is a weak introvert model.

Now, according to the PM theory, (store-bought) native proteins in general fall into the category of weak introverts. (Store-bought) native hemoglobin is no exception. On the other hand, when proteins are made to unfold into a more fully-extended conformation such as by exposure to denaturants like NaOH, they become extroverts. Experimental studies have fully confirmed this.

A parallel study on the q-values of similar family of probe molecules including sucrose and raffinose yielded a $\mathcal{U}_{vp}$ of 16.5 cal/mole of water, which is almost four times higher than the $\mathcal{U}_{vp}$ of 4.25 cal/mole of native hemoglobin (Ling 1993, Table 1 on p. 164) even though the hemoglobin concentration of the NaOH-denatured preparation used was only 20% rather than 36.1% as in the native hemoglobin solution studied here.

3. The much larger amount of water altered than literature values and reconciliation

Hemoglobin makes up 97% of mammalian red cell proteins (Ling *et al*. 1984). There is no known reason to question that this protein plays a correspondingly dominant role in causing the water in red blood cells to exhibit properties different from those of normal liquid water. The fact that even in its folded introvert conformation, it still possess the power to alter all the bulk phase water shows that the difference between the influence of a relatively weak *introvert* model (native hemoglobin) and a much more powerful *extrovert* model (e.g., NaOH denatured hemoglobin) does not lie in the *reach* of the influence of the bulk phase water but in the *intensity* of water-to-water interaction energy of all the water present. This, in fact, is a facet of the PM theory not clearly expressed until 1993 when the quantitative theory of solute exclusion was presented (Ling 1993). Its confirmation coming from the study of the *ineffective* introvert model is at once exciting and intriguing.

However, the present finding that all the water in a 36.1% native hemoglobin solution is altered also tells us that each gram of native hemoglobin has altered the property of all $(1 - 0.361) = 0.639$ grams of water equivalent to 1.77 grams of water altered by one gram of native hemoglobin. How does this compare with figures from other studies on similar native hemoglobin in the literature?

In a review Ling (1972) showed that using a total of six different methods, experts in this field had provided data yielding an average of only 0.25 grams of hydration water per gram of dry native hemoglobin. This is seven times lower than the 1.77 g/g value from the present study. Nonetheless, this divergence does not indicate real conflict.

The explanation we offer for this sharp contrast is this. To begin, we are not dealing with a fixed amount of altered water in a unit volume of total water and accordingly every competent investigator using a competent method would arrive at the same percentage figure of protein-altered water. Rather, each method could have measured a different portion of the protein-altered water. Indeed, as pointed out by Ling recently (Ling 2003) it is possible that a majority of the older methods used to measure hemoglobin hydration in fact measures the fraction of water tightly bound to polar side chains. In contrast, solvency

probes like PEG-4000 measure all, or close to all, water in the protein solution (Ling 2004).

4. What part(s) of the native hemoglobin molecules polarize water weakly but still extensively*?*

The polypeptide chains of store-bought "native" hemoglobin exist largely in the folded α-helical conformation. Yet data shown in Figure 1 and Table I clearly demonstrate that even with most of its backbone NHCO groups locked in intra-macromolecular H bonds, this native hemoglobin at a concentration of 36% still can exercise a long-range water-polarizing power on all the bulk phase water present. What part(s) of the "native" hemoglobin molecule participate in this long-range alteration of the bulk of surrounding water?

The part of a protein molecule that potentially could influence the surrounding water can be put into three categories. They are respectively (i) the α-helically-folded polypeptide backbone; (ii) polar side chains and (iii) segments of fully-extended polypeptide chains with their NHCO groups directly exposed to the bulk phase water. Our best guess at this time is that in the order of decreasing effectivess, the categories fall in the order: (iii) > (ii) > (i).

But before entering into the details, it would be helpful to take a backward glance at a figure that Ling presented in his 1972 review and is reproduced here as Figure 3. The different figures labeled a to f in Figure 3 illustrate how the spatial distribution of negatively charged N sites, positively charged P sites and sites bearing no charges (called O sites) determine the depth of layers of water or other polar molecules. A checkerboard of alternating N and P sites at proper distance apart is called an NP systems (c,d). They and their equivalent checkerboard of P and O sites or N and O sites respectively called PO and NO systems (e,f) are theoretically capable of polarizing and orienting deep layers of water molecules. So are parallel arrays of linear chains carrying alternatingly N and P sites etc. with similar power. In contrast, a checkerboard of all P sites or all N sites (a,b) is not able in theory to achieve multilayer polarization and orientation of water molecules because water dipoles oriented in the same direction strongly repel each other. With these guidelines in mind, we now can proceed to take a deeper look into each of the three types of potential polarizing-orienting sites mentioned above under (i), (ii) and (iii).

Let us begin with a piece of evidence that argues against the idea that α-helically-folded polypeptide chains could polarize and orient multlayers of bulk-phase water. Doty and Gratzer (1962) demonstrated long ago that a block polymer of poly-L-alanine (130 residues) when sandwiched between two water soluble-block polymers of D- and L-glutamic acids (each with 200 residues), remain in the fully folded and water insoluble form even at a temperature as high as 95°C or in the presence of 8 M urea. That total insolubility in water demonstrates that the potentially water-interacting polar NH and CO groups have lost their ability to interact with bulk-phase water when they form α-helical folds.

There are three main types of polar side chains. They are the (1) anionic α-, β- and γ-carboxylate groups, (2) the cationic ε-amino and guanidyl groups and (3) the hydroxyl groups of serine, threonine and histidine. No doubt that some polar side chains can exercise some influences on some surrounding water especially the hydroxyl groups. But there are overwhelming evidence that every α-, β- and γ-carboxylate group as well as every ε-amino and guanidyl group in native hemoglobin are locked in what is known as salt

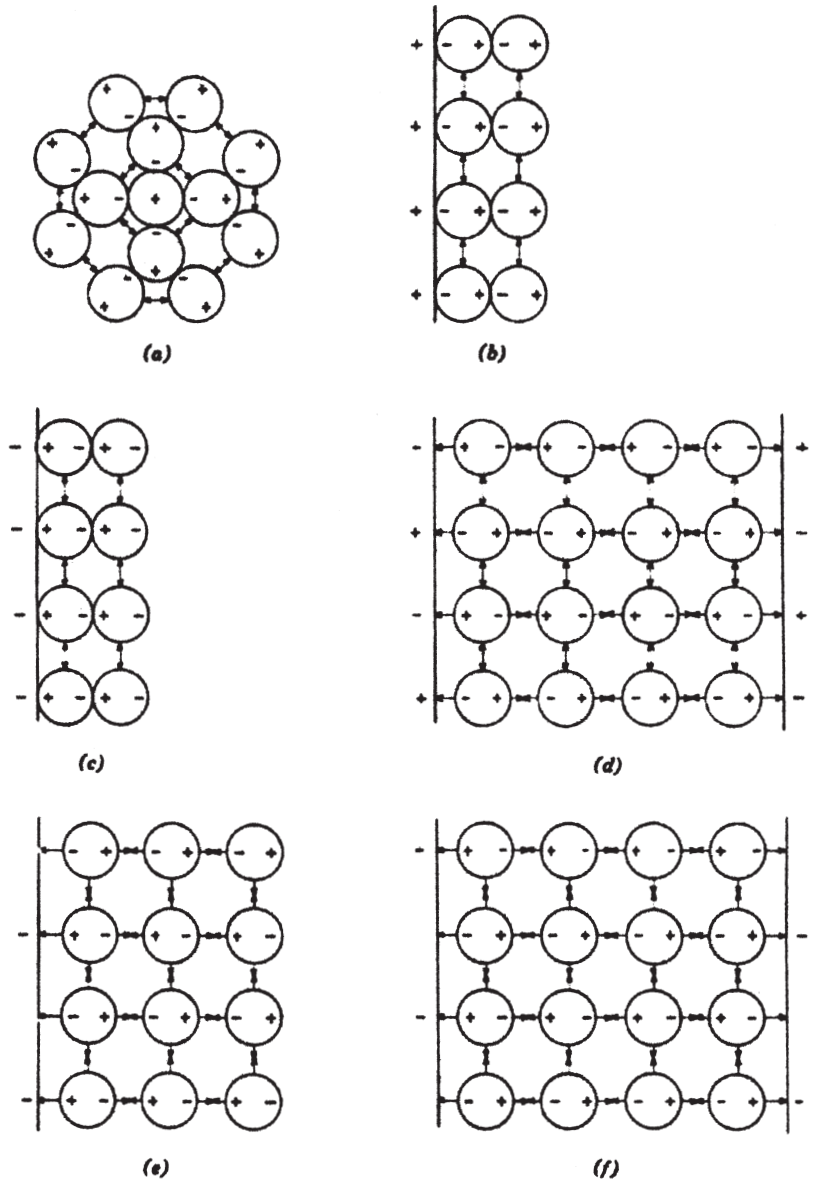

FIGURE. 3. Diagrammatic illustration of the way that individual ions (a) and checkerboards of evenly distributed positively charged P sites alone (b) or negatively charged N sites alone (c) polarize and orient water molecules in immediate contact and farther away. Emphasis was, however, on uniformly distanced bipolar surfaces containing alternatingly positive (P) and negative (N) sites called an NP surface (d). When two juxtaposed NP surfaces are facing one another, the system is called an NP-NP system. If one type of charged sites is replaced with vacant sites, the system would be referred to as PO or NO surface (e). Juxtaposed NO or PO surfaces constitutes respectively an PO-PO system or NO-NO system. Not shown here is the NP-NP-NP system comprising parallel arrays of linear chains carrying properly distanced alternating N and P sites. (From Ling 1972 reprinted with permission of John Wiley & Sons, Inc.)

linkages (See Steinhardt and Zaiser 1955; Edsall and Wyman 1958, p. 539; Ling and Zhang 1984). Being as a whole electrically neutral, polar groups locked in salt linkages are less prone to interact with surrounding water.

Going back to Figure 3, we may say that if these positively charged and negatively charged groups are arranged in an order like that shown in Figure 3c and d, they would end up neutralizing each other by forming salt linkage pairs. Like the NHCO groups locked in α-helices, they are neutral and ineffective. On the other hand, if they stay in groups of all negative or all positive, they would fall into the category of Figure 3a and b, and thus also be ineffective. However, this set of prohibiting rules does not apply to the hydroxyl groups. A hydroxyl group has both a proton accepting site and a proton-donating site. An array of stretches of all OH groups may find itself functioning like chains of the fully extended protein backbone NHCO. And, as such, achieve long-range water polarization and orientation. However, an examination of known primary structure of proteins does not reveal large stretches of hydroxyl bearing serine, threonine and tyrosine in close proximity, so the greatest potentially effective NPNPNP system remains parallel arrays of fully-extended NHCO groups of the polypeptide chains.

Now, many workers in this field of study believe that about 75% of the polypeptide chains of native hemoglobin exist in the α-helical conformation (See Weissbluth 1974, p. 20). To this must be added the other non-water polarizing segments of the hemoglobin chains engaged in the β-pleated sheet conformation. All in all, they set an upper limit to the percentage of fully-extended segments at less than 25%. Next, we would like to take into consideration factors that would raise the percentage of fully extended polypeptide linkages in native hemoglobin to higher than below 25%.

Accurate determination of the fine structures of proteins relies heavily on X-ray studies and X-ray studies can only be carried out on proteins when their constituent atoms remain sufficiently stationary to be photographed, i.e., in a crystalline state. To induce a dissolved hemoglobin (and other proteins) to crystallize, a common procedure is to add a great deal of innocuous salts to a concentrated hemoglobin solution in order to reduce the activity of surrounding water. By the Le Chatelier Principle the protein is driven to adopt the crystalline conformation that X-ray crystallography can investigate with precision. One must remember that it was this type of X-ray investigation that gave us the 75% figure for the percentage in the α-helical conformation.

All this points out that in the 36% native hemoglobin solution, the percentage of the hemoglobin's peptide bonds engaged in α-helical conformation may be less than the widely-accepted 75% figure. And, as a result, the total percentage of coils, turns and other segments of exposed NHCO groups may be equal to or even higher than 25%.

5. Are multilayers of water polarized and oriented in a 36% solution of native hemoglobin*?*

We know that all the bulk-phase water in a 36% native hemoglobin solution has lost on the average 80% of its normal solvency for PEG-4000. We now want to find out if this observed fact is in harmony with the notion that here also multilayers of water had been altered by the *native* hemoglobin.

First, we must find out how many moles of water there are in a 36% hemoglobin solution. To do that, we need to know what is the volume of the hemoglobin in a 36% solution. Most proteins have a *partial specific volume* of 0.70 to 0.75 cc per gram (Edsall

1953, p. 563). For safety, we adopt the larger figure of 0.75 and find out that in a liter of the 36% hemoglobin solution, $360 \times 0.75 = 270$ milliliters are taken up by the protein. The remaining volume of 730 ml is occupied by water. Assuming a specific gravity of unity for the water, 730 ml of water is equivalent to 730 / 18.02 = 40.5 moles of water molecules. Since the ρ-value of PEG-4000 is 0.196, of the 40.5 moles of water in one liter of the protein solution, at a minimum $40.5 \times (1 - 0.196) = 32.6$ moles is altered by the presence of the native hemoglobin.

The average amino acid residue weight in many proteins is estimated to be 112 (Ling 1962, p. 48). Dividing this number into the weight of hemoglobin in a liter of 36% hemoglobin solution would yield the maximum number of amino-acid residues and hence also the approximate number of polypeptide NHCO groups in the 36% hemoglobin solution. And, this equals 360/ 112 = 3.21 moles of NHCO groups per liter of the protein solution.

Now, each free NH group forms a H-bond with one water molecule; each CO groups can form H-bonds with two water molecules. Thus the first layer of water molecules acted on by each NHCO group is three. Each of these three water molecules can in turn form H-bonds with three water molecules, thereby providing a total of nine water-adsorbing "sites."

Let us start out from an exaggerated estimate and assume that 50% of the polypeptide chains exist in the fully-extended conformation. The number of water molecules affected by each of these exposed NHCO groups would be $32.6 / (0.5 \times 3.21) = 20.2$ water molecules. This would be enough to cover the first layer (3), the second layer (9) and still have $20.2 - (3 + 9) = 8.2$ water molecules to fill up a third layer of affected water molecules. There is then no question that our data of PEG-4000 exclusion by a 36% bovine hemoglobin solution has demonstrated that at this concentration, multiple layers of water have lost their normal solvency for PEG-4000.

However, the assumption that 50% of the polypeptide NHCO groups of native hemoglobin exist in the fully-extended conformation is far too high. Half of that, or 25% may be closer to what one may say to be reasonble. With the 25% figure, the number of water molecules affected by each NHCO group would rise to $32.6/ (0.25 \times 3.21) = 40.4$ water molecules. Subtracting 3 molecules in the first layer, 9 in the second layer, and 27 in the third layer, we still have a few left to begin yet another layer.

With fully three or even more layers of water affected by each exposed NHCO groups, the number of layers of affected water molecules between adjacent protein chains would be six or more layers deep.

6. The recent theoretical breakthrough in the long-range dynamical water structuring and its wide significance for both the study of the inanimate world and the living

In 1965 Ling first introduced what is now called the Polarized-Oriented Multilayer (PM) Theory of Cell Water. It is a subsidiary of his unifying theory of cell and subcellular physiology, the association-induction (AI) hypothesis introduced three years earlier (Ling 1962; 1965). Although worldwide experimental confirmation of the AI Hypothesis in general and the PM theory in particular has been uniformly affirmative, its broad acceptance has been unbelievably slow to say the least. The major cause of this is political (See Ling 1997). Nonetheless, there are also some legitimate reasons for the slowness in response. That is, the long range dynamical water structuring, until very recently, lacked a solid theoretical foundation.

That gas and water vapor can gather in deep layers has been known for a long time (See McBain 1932; Henniker 1949). Within a ten year period between 1929 and 1938, no less than four sets of rigorously derived theoretical treatments were presented — by some of the most outstanding physicists of the time (deBoer and Zwikker 1929; Bradley 1936, 1936a; Brunauer, Emmett and Teller 1938). Yet in different ways, each of these theories failed. The overall comment is that the admirable sophisticated methods developed by physicists in studying simple systems encounter great trouble when used to explain natural phenomena like life, which is inextricably complex.

As pointed out by Brunauer *et al*., de Boer and Zwikker's polarization theory as well as Bradley's theory of non-polar gases could not predict more than one layer of adsorbed gas. Brunauer, Emmett and Teller's own theory (known as the BET theory from the first letters of their names) also cannot explain the large quantity of water taken up at near-saturation humidity, nor the altered physiochemical attributes of this water. That leaves only Bradley's theory for gas molecules with permanent dipole moments. And, until 2003, that was the best theoretical foundation for the PM theory. Then there was a lucky break. Ling found a simplying shortcut.

As a result, Ling was able to introduce a new theory with far-reaching consequences. Briefly, under ideal conditions, an idealized checkerboard of alterrningly positively-, and negatively-charged sites of just the right distance apart as illustrated in Figure 4 will polarize and orient multiple layers of water. As one moves farther and farther away from the idealized NP-surface, the water-to-water interaction energy (E_n) does not taper off to zero

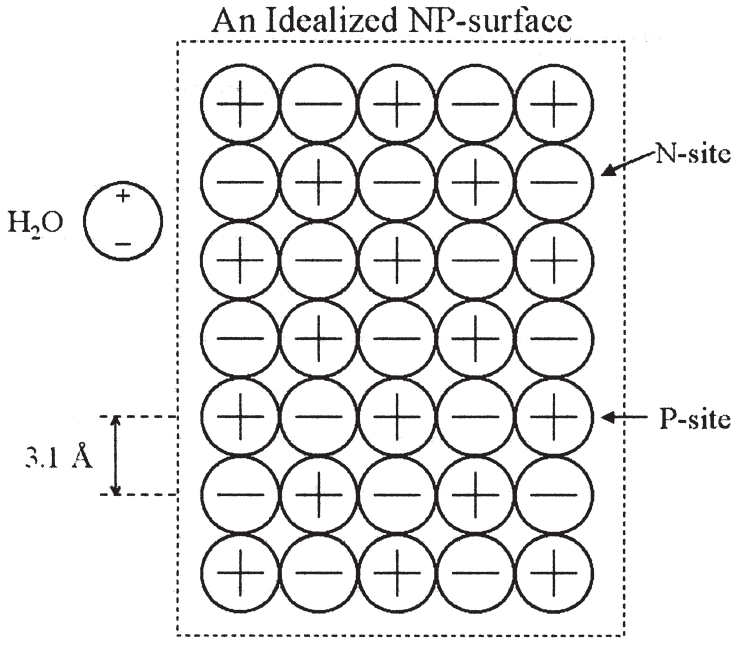

FIGURE 4. An idealized NP surface. The distance between a pair of the nearest-neighboring N and P site is equal to the distance, r, between neighboring water molecules in the normal liquid state and approximately 3.1 Å. (From Ling 2003)

but stays at a constant value *ad infinitum* described by the following equation and illustrated in Figure 5;

$$E_n = (4\mu^2 r^3) / (r^3 - 8\alpha)^2. \quad (1)$$

Based on this finding, three predictions could be made and each had been affirmed retroactively:

1. Thin layer of water held between nearly ideal NP surfaces like that of polished AgCl prisms would not freeze at any attainable temperature. In fact, this was what Canadian chemists, Giguère and Harvey discovered by accident and reported fifty years ago (Giguère and Harvey 1956).
2. Thin layer of water held between near ideal polished NP surfaces would not boil at temperature as high as 400°C. This too was observed and reported fifty years ago by Hori (Hori 1956).
3. Truly long-range (ideally *ad infinitum*) water polarization and orientation under proper conditions (e.g., exposure to NP-, NO-, PO surfaces) was predicted by the new theory and it too was retroactively confirmed but more recently.

   Thus, in 2003 Zheng and Pollack demonstrated exclusion of 10 μm wide, coated latex microspheres at a distance of 100 μm or still farther from the surface of polyvinylalcohol gel (Zheng and Pollack 2003).

Leaving a detailed analysis of Zheng and Pollack's spectacular finding to a later paper, we conclude this communication with a backward look at history, armed with the simple "size rule" of the PM theory.

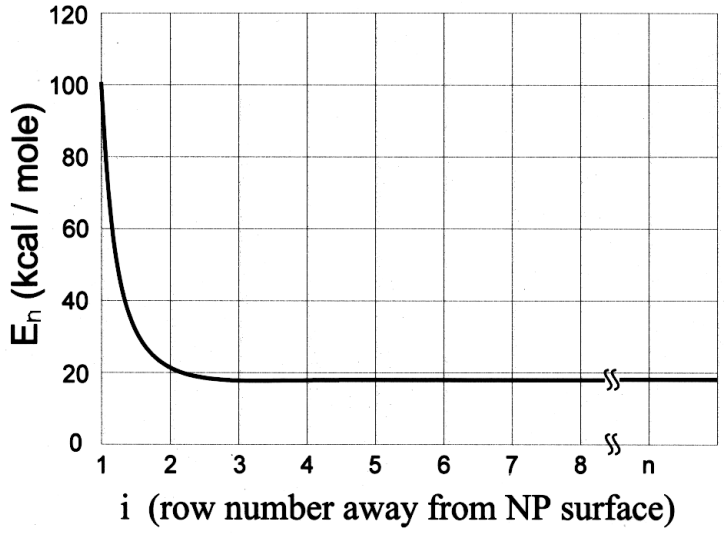

FIGURE 5. The theoretically computed adsorption energy of a water molecule, E_n, in one of successive layers of water molecules away from an idealized NP surface at a temperature very near absolute zero. Note that as the distance between the water molecule and idealized NP surface increases, the adsorption energy does not taper off to zero. Rather, it continues at a constant value described by Equation 1. For details on the makeup of an idealized NP surface, see Figure 4 above. (From Ling 2003)

That is, how the exclusion of PEG 4000, the subject matter of this communication, offers a link between the exclusion from the polarized-oriented water of small particles like hydrated Na^+ and sucrose on one end and the gigantic particles like the coated latex microspheres at the other extreme. In-between are the multitudes of similar exciting findings of deep layers of water altered by special surfaces (or parallel arrays of linear chains) (Henniker 1949) that have been relegated to the ranks of the curious and the forgotten — for the lack of a supportive physical theory. That has finally changed.

We thank Dr. Raymond Damadian and his Fonar Corporation and its many friendly and helpful members for their continued support. We also thank Margaret Ochsenfeld and Dr. Zhen-dong Chen for their dedicated and skillful cooperation, and librarian Tony Colella and Michael Guarino, director of the Media Services and Internet Services, for their patience and tireless assistance.

References

Bradley, S. (1936) *J. Chem. Soc*. 1936: 1467.
Bradley, S. (1936a) *J. Chem. Soc*. 1936: 1799.
Bray. G. (1960) *Analyt. Biochem. 1:* 279.
Brunauer, S., Emmett, P.H. and Teller, E. (1938) *J. Amer. Chem. Soc. 60:* 309.
de Boer, J.H. and Zwikker, C. (1929) *Z. Physik. Chem. B3:* 407.
Doty, P. and Gratzer, W.B. (1962) in *Polyamino Acids, Polypeptides, and Proteins* (M. A. Stahmann, ed.) The University of Wisconsin Press, Madison, pp. 116–117.
Edsall, J.T. (1953) in *The Proteins: Chemistry, Biological Activity, and Methods* (H. Neurath and K. Bailey, eds.), Academic Press, New York Vol. 1, p. 563.
Edsall, J.T. and Wyman, J. (1958) *Biophysical Chemistry* Vol. 1, p. 539.
Giguère, P.A. and Harvey, K.B. (1956) *Canad. J. Chem. 34:* 798.
Henniker, J.C. (1949) *Review Modern Physics 21:* 322.
Hori, T. (1956) *Low Temperature Science A15:* 34 (Teion Kagaku, Butsuri Hen) (English Translation) No 62, US Army Snow, Ice and Permafrost Res., Establishment, Corps of Engineers, Wilmette, Il., USA.
Ling, G.N. (1951) *Amer. J. Physiol. 167:* 806.
Ling, G.N. (1952) in *Phosphorus Metabolism* (Vol. II) (W.D. McElroy and B. Glass, eds.), The Johns Hopkins Univ. Press, Baltimore, p. 748.
Ling, G.N. (1962) *A Physical Theory of the Living State: the Association-Induction Hypothesis*, Blaisdell Publ. Co., Waltham, MA.
Ling. G.N. (1965) *Ann. N.Y. Acad. Sci. 125:* 401.
Ling, G.N. (1969) *Intern. Rev. Cytol. 26:* 1.
Ling, G.N. (1970) *Intern. J. Neuroscience 1:* 129.
Ling, G.N. (1972) in *Water and Aqueous Solutions, Structure, Thermodynamics and Transport Processes* (A. Horne, ed.) Wiley-Interscience, New York, p. 663.
Ling, G.N. (1977) *Physiol. Chem. Phys. 9:* 319.
Ling, G.N. (1980) *Physiol. Chem. Phys. & Med. NMR 12:* 3.
Ling, G.N. (1980a) *Physiol. Chem. Phys. & Med. NMR 12:* 111
Ling, G.N. (1984) *In Search of the Physical Basis of Life*, Plenum Publ. Co, New York.
Ling, G.N. (1988) *Scanning Microscopy 2:* 871.
Ling, G.N. (1992) *A Revolution in the Physiology of the Living Cell,* Krieger Publ. Co. Malabar, FL.
Ling, G.N. (1993) *Physiol. Chem. Phys. & Med. NMR 25:* 145.
Ling, G.N. (1997) *Physiol. Chem. Phys. & Med. NMR 29:* 123. <http://www.physiologicalchemistryphysics.com/pdf/PCP29-2_ling.pdf.>
Ling, G.N. (1997a) <http://www.gilbertling.org>

Ling, G.N. (2001) *Life at the Cell and Below-Cell Level: the Hidden History of a Fundamental Revolution in Biology*, Pacific Press, NY.
Ling, G.N. (2003) *Physiol. Chem. Phys. & Med. NMR 35:* 91. <http://www.physiologicalchemistryphysics.com/pdf/PCP35-2_ling.pdf>
Ling, G.N. (2004) *Physiol. Chem. Phys. & Med. NMR 36:* 1. <http://www.physiologicalchemistryphysics.com/pdf/PCP35-2_ling.pdf>
Ling. G.N. (2005) in *Water in Cell Biology* (G. Pollack, I. Cameron and D. Wheatley, eds.) Springer, New York (in press).
Ling, G.N. and Hu, W. (1988) *Physiol. Chem. Phys. & Med. NMR 20:* 293.
Ling. G.N. and Negendank, W. (1970) *Physiol. Chem Phys. 2:* 15.
Ling, G.N. and Zhang, Z.L. (1984) *Physiol. Chem. Phys. & Med. NMR 16:* 221.
Ling, G.N., Ochsenfeld, M.M., Walton, C. and Bersinger, T.J. (1980) *Physiol. Chem. Phys. 12:* 3.
Ling, G.N., Walton, X. and Bersinger, T.J. (1980a) *Physiol. Chem. Phys. 12:* 111.
Ling, G.N., Zodda, D.A. and Seller, M. (1984) *Physiol. Chem. Phys. & Med. NMR 16:* 381.
Ling, G.N., Niu, Z. and Ochsenfeld, M.M. (1993) *Physiol. Chem. Phys. & Med. NMR 25:* 177.
McBain, J.W. (1932) *Sorption of Gases and Vapors by Solids*, G.Rutledge & Sons, Ltd., London.
Ponder, E. (1948) *Hemolysis and Related Phenomena,* Grune and Stratton, New York, Reissued 1971.
Steinhardt, J. and Zaiser, E.M. (1955) *Adv. Protein Chem. 10:* 151.
Troshin, A.S. (1951) *Byull. Exp. Biol. Med. 31:* 180.
Troshin, A.S. (1958) *Das Problem der Zellpermeabilität,* Gustav Fischer, Jena.
Troshin, A.S. (1966) *Problems of Cell Permeability*, Pergamon, London
Weissbluth, M. (1974) *Hemoglobin: Cooperativity and Electronic Properties,* SpringerVerlag, New York.
Zheng, J.M. and Pollack, G. (2003) *Physical Review E. 68:* 031408.

Appendix 1

$$q = \exp\left\{\frac{1.23v\Delta E_s\left[1-(1-b)\dfrac{(kv)^n}{1+(kv)^n}\right]-(\Delta E_v = 1.23\Delta e^*)v}{RT}\right\} \tag{A3}$$

where q is the equilibrium distribution coefficient of the solute in question — v is the molecular volume (molar volume) of the solute and it is in cm^3. b is a small fractional number describing the probability of (very large) molecules in finding adsorbing sites on the water lattice. k and n are parameters describing the steepness of the declining probability of finding adsorbing sites with increase of molecular volume. ΔE_s is the *specific surface (or solute) polarization energy* per cm^2 in units of $cal.mol^{-1}$ $(cm^2)^{-1}$, when the solute is moved from normal liquid water to the polarized cell water. ΔE_v is the *specific solvent polarization energy*, equal to the difference between the energy spent in excavating a hole 1 cm^3 in size in the polarized (cell) water and the energy recovered in filling up a 1 cm^3 hole left behind in the surrounding normal liquid water; it is in units of $cal.mole^{-1}(cm^3)^{-1}$.Δe^* is the *increment of the activation energy* for overcoming the greater rotational restriction per unit surface area in units of $cal.mole^{-1}(cm^2)^{-1}$, when a solute is transferred from normal liquid water phase to the polarized water phase. R and T are the gas constant and absolute temperature respectively.

Received: September 9, 2004;
accepted: February 21, 2005.

Physiological Chemistry and Physics and Medical NMR
INDEX
Volume 36, 2004